THE DETERMINATION OF THE EQUATION OF STATE OF MOLTEN SILICATES AT HIGH PRESSURES USING SHOCK-WAVE TECHNIQUES

Thesis by

Sally Miranda Rigden

In Partial Fulfillment of the Requirements

of the Degree of

Doctor of Philosophy

California Institute of Technology

Pasadena, California

1986

(submitted 17th February, 1986)

Acknowledgements

I sincerely thank Thomas J. Ahrens and Edward M. Stolper for the support, encouragement and intellectual guidance they have given me during my time as a graduate student. This project could never have been completed without their enthusiasm and confidence and I am immensely grateful to them both. The experimental technique would never have been successfully developed without the tireless efforts of Papo Gelle, Warren Ginn and Mike Long. Their assistance and good humour were truly appreciated.

I wish to thank the numerous people who have provided intellectual and technical support. I particularly wish to acknowledge generous technical assistance from Ellen Bus, Chuck Manning, Sue Yamada and Leon Young and stimulating interactions with fellow members of the Shock Wave Group: Jay Bass, Mark Boslough, Doug Schmitt, Bob Svendsen and Jim Tyburczy.

I also wish to express my appreciation to the many friends and graduate students who have provided personal support in the last two years. I am particularly grateful to Luciana Astiz, Brian Cheetham, Holly Eissler, Barbara Ellenhorn, Dale Furman, Astrid Howard, Richard Kroll, Ann Mori, Carol Prentice, Elma Schonbach, Vicki Silver and David Scott.

I would like to aknowledge financial support from the National Science Foundation and the IBM Corporation and I am most appreciative of the recognition accorded to us by the American Association for the Advancement of Science for the work reported in Chapter 1.

Lastly, I wish to express my heartfelt gratitude to my husband, Robert Hill, for intellectual and personal support from near and far. It is to him and to Berf that I dedicate this thesis.

Abstract

Shock wave (Hugoniot) equation of state experiments have been carried out on molten silicates in the petrologically important system $CaMgSi_2O_6$–$CaAl_2Si_2O_8$ via the projectile impact method. An RF heating technique was developed to heat silicate samples contained in pure Mo containers to the necessary high initial temperatures (up to 1773 K). Thermocouple techniques, a refractory sample holding system and optical shutter systems, were developed to allow utilization of a propellant gun apparatus at impact velocities ranging from 1.0 to 2.5 km sec^{-1} corresponding to shock pressures of 4 to 40 GPa. The methodology for taking into account the effect of the Mo container in measuring the equation of state of the molten silicate is explicitly derived.

Results on molten diopside ($CaMgSi_2O_6$), anorthite ($CaAl_2Si_2O_8$) and an intermediate composition (36 mole % $CaAl_2Si_2O_8$, 64 mole % $CaMgSi_2O_6$: $An_{0.36}Di_{0.64}$) are presented. Reduction of the Hugoniot data for these materials to third-order Birch-Murnaghan isentropes yields 1 atm bulk moduli (K_S) in the range 18-24 GPa which are in good agreement with bulk moduli recently measured by ultrasonic methods at 1 atm and similar temperatures. The pressure derivatives of bulk modulus (K') vary from 5-7. Shock temperature calculations for $An_{0.36}Di_{0.64}$ indicate temperatures of 2400-2600 K at $\sim$ 25 GPa. The Hugoniot states are believed to lie metastably in the liquid field on the basis of measured bulk modulus, calculated Hugoniot density of a solid of the same composition and estimated crystallization times.

The measured equation of state data for molten diopside is used in conjunction with other thermochemical data to constrain the diopside solidus via the Clausius-Clapeyron equation at pressures up to 20 GPa. The present data are consistent with

measured fusion curve data of others to 5 GPa. Above $\sim$ 10 GPa, a marked shallowing of the solidus is predicted as the difference in volume between crystalline and molten diopside in equilibrium approaches zero.

Comparison of the results for molten diopside with those from the intermediate composition indicates that the liquids exhibit ideal mixing behavior with respect to volume to within $\pm 2\%$ up to $\sim$ 40 GPa. Gradual changes in coordination of Al^{3+} and Si^{4+} from tetrahedral at low pressures to octahedral at high pressures are believed to occur during compression of these materials. The integrated compressibility as reflected in the values of K_S and K' is related to the proportion of tetrahedrally coordinated cations at low pressure, and the volume at $\sim$ 40 GPa is from 100-110% of that of a mixture of the dense, high-pressure phases $MgSiO_3$ (perovskite), $CaSiO_3$ (perovskite), Al_2O_3 (corundum) and SiO_2 (stishovite).

Important petrological implications of our results include: (1) basic to ultrabasic melts become denser than olivine- and pyroxene-rich mantle at pressures of 6-10 GPa, and (2) there is a maximum depth from which basaltic melt can rise buoyantly within terrestrial planetary interiors.

Table of Contents

--

INTRODUCTION

There is a pressing need to obtain information about the high-pressure and high-temperature physical properties of silicate materials in order to understand the nature of processes occurring in terrestrial planetary interiors. Experimental determination of the density as a function of pressure and temperature (i.e., the equation of state) has been made for many crystalline earth materials, but the data for molten silicates are sparse and have been limited to relatively low pressures (< 3 GPa). The aim of this work has been to develop a technique for measuring the density of molten silicates at high pressures; to carry out experiments on petrologically and geophysically relevant materials; to use the measured equations of state to constrain processes occurring in planetary interiors, and to gain some insights into how the structure of silicate melts change with increasing pressure.

Measurements of the density of molten silicates at high pressures (up to 40 GPa) were carried out using shock wave techniques. A 40 mm propellant gun was used to accelerate projectiles to high velocities and to impact silicate samples generating high pressure shock waves in the samples. These experiments are carried out routinely at room temperature, but modifications to the apparatus were necessary to do them at the high temperatures required for molten silicates. These experimental details are described briefly in Chapter 1 and in detail in Chapter 2. Because the samples are molten at the time of impact, they are encapsulated in refractory metal (Mo) containers. Calculation of the sample Hugoniot densities requires a correction for the effect of the surrounding container. The method by which this is accomplished is described in Chapter 2.

Preliminary results on a composition which is an analog for natural basalt (36 mole % $CaAl_2Si_2O_8$, 64 mole % $CaMgSi_2O_6$: $An_{0.36}Di_{0.64}$) are reported in Chapter 1, and the complete data set is presented in Chapter 2. Data for molten anorthite ($CaAl_2Si_2O_8$) and diopside ($CaMgSi_2O_6$) are given in Chapter 3. In Chapter 2, evidence is presented that the shock (Hugoniot) states represent metastable liquids throughout the pressure range of the experiments.

Reduction of the Hugoniot states to states directly comparable with high pressure states in the earth's interior is accomplished by constructing Birch-Murnaghan isentropes from the data. The 1 atm bulk modulus (K_S) derived from this analysis is then directly comparable with values that have been measured by others at similar temperatures using ultrasonic techniques.

The analogy of the composition studied in Chapters 1 and 2 with natural basalts allows some inferences to be made about the behavior of natural melts at high pressures. Petrological implications of the density of molten $An_{0.36}Di_{0.64}$ are discussed in Chapter 1.

For materials that melt congruently, the slope of the solidus, given by the Clausius-Clapeyron equation, can be calculated when the volume and entropy of fusion are known. The data presented in Chapter 3 give the first determinations of molten diopside volumes at high pressures, and these have been used in conjunction with thermochemical data to predict the melting curve of diopside to 20 GPa.

The structure of molten silicates at high pressures has been addressed previously by spectroscopic techniques and by molecular dynamics simulations. Spectroscopic studies have been restricted to pressures lower than 8 GPa. The systematic changes in density with composition over the studied composition range allow some insights to

be gained into the structure of molten silicates at high pressures and the role of coordination changes during compression. This is discussed in Chapter 3.

Chapter 1

Densities of Liquid Silicates at High Pressures*

Abstract

Densities of molten silicates at high pressures (up to ~230 kbar) have been measured for the first time using shock wave techniques. For a model basaltic composition (anorthite 36 mole % - diopside 64 mole %), we derived a bulk modulus, K_s ~230 kbar and a pressure derivative $\frac{dK_s}{dP} \sim 4$. Some implications of our results are: (1) basic to ultrabasic melts become denser than olivine- and pyroxene-rich host mantle at pressures of 60-100 kbar, (2) there is a maximum depth from which basaltic melt can rise within terrestrial planetary interiors, (3) the slopes of silicate solidi $\left\{\frac{dT_m}{dP}\right\}$ shallow at high pressures, and (4) enriched mantle reservoirs may have developed by downward segregation of melt early in earth history.

* Published in *Science, 226,* 1071-1074, 1984

Knowledge of the properties of silicate liquids at high pressures and temperatures is fundamental to our understanding of the differentiation processes that occur within planetary interiors. The densities of a variety of silicate liquids have been determined previously at up to 20 kbar in piston cylinder apparatuses using the falling-sphere technique [1]. Calculation of liquid silicate densities at high pressures has also been made by estimation of their elastic properties [2,3]. We report here the first shock wave measurements of silicate liquid densities at high temperatures and pressures extending by more than an order of magnitude (i.e., to 235 kbar) the maximum pressure at which densities of silicate liquids have been determined. Our motivations for this work were the following:

(1) The rates of melt migration and segregation within partially molten source regions in planetary interiors depend on the difference in density between the melt and the coexisting solids. In addition, the sign of the density contrast between melt and the coexisting residual crystals determines whether melt will migrate upwards or downwards [2]. Magma may move from its source by percolation, in cracks, or as diapirs. In each of these cases, the density contrast between melt and solid enters into the velocity with which the magma moves and thus places important constraints on the thermal and chemical evolution of rising (or sinking) magmas.

(2) The slope of the solidus (dT_m/dP), where T_m is temperature and P is pressure, depends upon ΔV_r (the volume change of the reaction defining the solidus). Thus, the pressure dependence of the density contrast between coexisting phases along the solidus is an important factor in the variation of the position of the solidus with pressure and, consequently, of the melting behavior of planetary mantles.

(3) The structures of silicate melts at high pressures and temperatures have been predicted by molecular dynamics simulations. These simulations also model the density and transport properties of silicate melts [4]. Density measurements at high pressures can be compared with those derived from the simulations to place constraints on the interatomic potentials that are critical to the calculations and hence to refine calculated structural models and transport properties.

The composition that we used for our initial experiments is the 1 atm eutectic composition in the system anorthite-diopside ($An_{0.36}Di_{0.64}$, where the subscripts represent molar percentages). This composition is used as an analog for natural basalt and differs from it mainly in the absence of iron and alkalis. Ultrasonic measurements [5] at 1 atm and 1400 ° C yield a bulk modulus of ~230 kbar for this composition.

The pressure (P) and density (ρ) of a material in shock wave experiments are determined from the Rankine-Hugoniot equations [6]. The shock wave is generated in the molten sample encapsulated in molybdenum by impact of a metal flyer plate that has been accelerated to high velocity (1-2.5 km/sec) in a 40 mm propellant gun [7]. A schematic representation of the experimental target, just prior to projectile impact, is shown in Figure 1. During these experiments, the quantities measured are shock velocity (U) and particle velocity (u). The 1 atm density (ρ_o) is calculated using partial molar volumes reported by Nelson and Carmichael [10]. The particle velocity is determined by measurement of projectile velocity and subsequent impedance match with the sample [9]. The shock velocity is obtained by measuring the time difference between the entrance and exit of the shock front through the sample [11].

The results are shown in Table 1 and Figure 2. The U-u data can be fit by a straight line given by U = (2.94 ± 0.05 km/sec) + (1.29 ± 0.06) u. This experimental fit to the Hugoniot is shown in the inset of Figure 2. From the analysis developed by Ruoff [13], we calculated an isentropic, 1 atm bulk modulus, $K_s^0 = \rho \left\{ \frac{\partial P}{\partial \rho} \right\}_s =$ 226 ± 8 kbar and a pressure derivative, $K_s' = dK_s/dP = 4.15 \pm 0.24$. The bulk modulus agrees well with the value calculated from the measured ultrasonic velocity (212 to 243 kbar) [5,14]. For typical mantle minerals K_s° is ~1.2-2.1 Mbar, while K_s' ~4-7 [15].

With increasing pressure, crystalline silicates undergo phase changes leading to abrupt increases in density as the structure transforms to the closer-packing stable at elevated pressures. Waff [16] suggested that similar abrupt increases in density would occur in silicate liquids as coordination changes such as $^{IV}Al^{+4} \rightarrow {}^{VI}Al^{+4}$ and $^{IV}Si^{+4} \rightarrow {}^{VI}Si^{+4}$ occurred. However, silicate liquids could achieve substantial compaction by a continual distortion of the tetrahedral network and/or gradual coordination changes, rather than by the abrupt coordination changes characteristic of solids. Raman spectroscopy carried out on glasses quenched from jadeite melts at pressures up to 40 kbar does indeed suggest that the Al(Si)-O-Al(Si) bond angles in the tetrahedral network decrease continuously and that at this pressure Al and Si are still essentially entirely in tetrahedral coordination [17]. Recent NMR results from albite glasses quenched from melts at high pressures suggest that, when Al^{+3} enters 6-fold coordination in melts, it does so over a wide pressure range [18]. Molecular dynamics simulations have also suggested that structural changes in melts, especially Si and Al coordination numbers, change gradually and continuously as pressure increases to several hundred kilobars [4] rather than abruptly over narrow

pressure intervals [19]. Our results are consistent with gradual and continuous structural changes, since the data can be fit by a single compression curve (a straight line in U-u space). In addition, the unexpectedly low value of K_s' [2,3] can be rationalized by continuous structural changes taking place in the melt with increasing pressure.

The present results have some far-reaching implications for differentiation within terrestrial planetary interiors by igneous processes:

(1) Using the values of K_s and K_s' derived from our experiments [20] we predict that the densities of volatile-poor, basic to ultrabasic melts of the mantle would overtake the bulk density of the residual solid at moderate pressures, 60-100 kbar. Basaltic liquid compression curves fall within the hachured band in Figure 2. The range of 1 atm densities corresponds to that expected for picritic mid-ocean ridge basalt (2.7 g/cm^3) to komatiite (2.8 g/cm^3) at their liquidi [21,22]. The liquids become denser than magnesian olivine and orthopyroxene, which are probable residual phases, at pressures from 40-70 kbar. Furthermore, the liquids become denser than the bulk mantle (derived from whole earth seismological models [24]) between 60 and 100 kbar. We propose that the lack of density contrast between melt and coexisting solid over this pressure range could lead to stabilization of partially molten zones in the region of the low-velocity zone of the present Earth [2].

(2) There is a maximum depth from which volatile-poor basaltic magma produced by partial melting of ultrabasic mantle material can be derived based on the requirement of a positive density contrast to drive upward melt migration [2]. For the Earth and Venus, assuming an average 1 atm basaltic magma density of 2.75 g/cm^3 derived from a mantle where $Mg/(Fe + Mg) \sim 0.9$[26], this depth is about 300

km. For Mars, a much smaller planet, which may have a more iron-rich mantle (Mg/(Fe + Mg) ~0.7-0.8), this depth would be much greater, about 1000 km [27]. Internal pressures within the Moon are not expected to be high enough to lead to a density crossover for a primitive basaltic composition [28].

(3) A decrease in the density contrast between liquid and coexisting solids is expected to lead to a decrease in the slope of the solidus $\left\{\frac{dT_m}{dP}\right\}$, which, in the absence of excess volatiles, is positive for all likely mantle rocks at low pressures. For congruent melting, the slope of the solidus flattens with increasing pressure as $\Delta V_r \rightarrow O$ ($\Delta V_r = V_{liquid} - V_{crystal}$, is the volume change of the reaction defining the solidus). For incongruent melting, melting involving solid solutions, or melting of a polymineralic assemblage, however, dT_m/dP may be positive even though the melt is denser than some or all of the residual solid phases. Thus, care must be taken in using our results to infer the slope of a peridotite solidus at high pressures, since a very dense phase, garnet, is an important participant in likely melting reactions and since the liquid compositions at peridotite solidi are not well known at high pressures. If the slopes of the source rock and basalt solidi remain positive and are greater than the prevailing geothermal gradient, any dense melt percolating downwards will begin to crystallize and presumably may not move very far. However, if the slopes of the solidi do become flat or negative, there could be an increase in the amount of melt with increasing depth, both from concentration of downward percolating liquids and also from the decrease in solidi temperatures.

Our analysis implies that the slopes of the solidi of congruently melting silicates with octahedral Si^{+4} (e.g. $MgSiO_3$ perovskite) at high pressures are less than those of

silicates found in the shallow mantle $\left\{\frac{dT_m}{dP}\right.$ for enstatite at 1 atm is 13 °C/kbar [29]$\left.\right\}$, and that their solidi may indeed become less steep. Recent shock temperature measurements confirm this; for stishovite at 700 kbar and 4200 °C, dT_m/dP was inferred to be 1.1 ± 0.5 °C/kbar [30]. Extrapolating our results, we calculate that the density of liquid $MgSiO_3$ at 3000 °C would increase from 2.31 g/cm^3 at 1 atm to 4.08 g/cm^3 at 400 kbar [31]. At 400 kbar $MgSiO_3$ (perovskite) would have a density of 4.63 g/cm^3 and 4.10 g/cm^3 at room temperature and 3000 °C, respectively [32]. Assuming congruent melting and an entropy of melting of ~R (8.3 g/mole-atom) [33], dT_m/dP = 0.1 °C/kbar. With the melting point estimate of Ohtani [34] for $MgSiO_3$ perovskite of 2900 °C at 230 kbar, we can estimate the melting point at 400 kbar to be ~3500 °C. Despite the substantial extrapolations required for this calculation, we suggest that there may be a maximum in the solidus of perovskite in the vicinity of 400 kbar and that, at the very least, the slope of solidus will be very small. This further implies that the temperature of the lower mantle is constrained to be <3500 °C in the absence of partial melt.

(4) That a silicate liquid may become more dense than its surroundings at high pressure allows not only for the possibility of retaining magma within planetary interiors, but also for concentrating it at depth by downward segregation. Some implications of a laterally extensive, dense, magnesian melt layer for the genesis of komatiites were recently discussed by Nisbet and Walker [22]. Stolper *et al.* [2] and Ohtani [34] also discussed possible implications of dense melts at depth for komatiite genesis. During early Earth history when the heat production from radioactive decay was presumably higher than today [35], it is likely that there was a higher degree of

partial melting globally, and that it extended to greater depths than in the present Earth. Because the likely dominant residual minerals, olivine and orthopyroxene, would be expected to float in basic melts at pressures greater than ~40-70 kbar, stable chemical stratification could occur. If basic to ultrabasic melts could flow downwards in this way, this could lead to the development of a residual olivine-orthopyroxene-rich ("peridotitic") layer underlain by a deep clinopyroxene-garnet-rich ("eclogitic") layer in the upper mantle. Recent fits of elastic models to seismic velocity models lend credence to the idea of a stratified upper mantle having a lower proportion of olivine below ~220 km than was previously thought [36]. The development of such a layer by downward melt migration could have important consequences for the thermal evolution of the early Earth. It would limit the transport of heat towards the surface by magmatic activity, it would interfere with convection patterns that might otherwise develop, and it would allow the segregation of heat-producing incompatible elements (e.g., K, U, Th) into a deep layer.

In summary, initial shock wave experiments on a model basaltic liquid ($An_{0.36}Di_{0.64}$ (molar)) suggest that silicate liquids are far more compressible than their coexisting solids up to pressures of at least 250 kbar. Implications of this phenomenon include:

(1) Basic to ultrabasic melts become denser than coexisting olivines and pyroxenes at pressures of 60-100 kbar.

(2) The maximum depth from which basic magma could segregate upwards on the Earth and Venus is ~300 km; for Mars this depth is ~1000 km.

(3) The slope of the solidus (dT_m/dP) for congruently melting silicate minerals is expected to shallow at high pressures.

(4) Enriched and perhaps partially molten reservoirs might exist deep inside the present Earth, having developed by downward migration of dense magmas during early Earth history.

References

.. T. Fujii, I Kushiro, Carnegie Inst. Washington Y'book, **76**, 419 (1977).

:. E. Stolper, P. Walker, B. H. Hager, J. F. Hays, *J. Geophys. Res.* **86,** 6261 (1981). D. Walker, E. Stolper, J. F. Hays, *J. Geophys. Res.* **83,** 6005 (1978).

:. E. Ohtani, *Earth Planet. Sci. Lett.* **67,** 261 (1984).

C. T. Herzberg, *Earth Planet. Sci. Lett.* **67,** 249 (1984).

:. L. V. Woodcock, C. A. Angell, P. A. Cheeseman, *J. Chem. Phys.* **65,** 1565 (1976). C. A. Angell, P. A. Cheeseman, S. Tamaddon, *Science,* **218,** 885 (1982).

Y. Matsui and K. Kawamura, *Nature (London),* **285,** 648 (1980). Y. Matsui, K. Kawamura, Y. Syono, in *High Pressure Research in Geophysics,* S. Akimoto and M. H. Manghnani, eds. (Center for Academic Publications, Tokyo, 1982) pp. 511-524.

:. M. L. Rivers, I. S. E. Carmichael, *EOS (Transactions AGU),* **62,** 1065 (1981).

M. L. Rivers, I. S. E. Carmichael, *EOS (Transactions AGU),* **63,** 1136 (1982).

:. G. E. Duvall and G. R. Fowles, in *High Pressure Physics and Chemistry,* R. S. Bradley, ed. (Academic Press, New York, 1963), Vol. 2, pp. 209-291.

'. T. J. Ahrens, J. H. Lower, P. L. Lagus, *J. Geophys. Res.* **76,** 518 (1971).

:. The sample is hung and aligned in the impact tank and heated under vacuum to the requisite temperature with a water-cooled copper induction coil powered by a 10kW Lepel High Frequency Induction Heating Generator.

). The impedance match method relies on continuity of stress and particle velocity at the flyer-driver and driver-sample interface [6], R. G. McQueen, S. P. Marsh, J. W. Taylor, J. N. Fritz, and W. J. Carter, in *High Pressure Impact Phenomena,* R. Kinslow, ed. (Academic Press, N. Y., 1970), pp. 293-417.

10. S. A. Nelson and I. S. E. Carmichael, *Contr. Mineral Petrol.* **71,** 117 (1979).

11. Transit time is determined by observing the polished rear surfaces of the Mo capsule on a continuously writing Model 339 Beckman-Whitley streak camera. Because the Mo is polycrystalline, the passage of a shock wave through the free surface results in reorientation of the crystallites and a change in reflectivity. Illumination is accomplished by a 5 kV, 100 μsec duration Xenon flash lamp synchronized with impact. The firing sequence is arranged so that the camera shutter opens $\sim$50 ms prior to impact to prevent fogging of the film by self-illumination of the hot target.

12. Retraction of the ceramic shutter is activated by a double acting Bimba model SSRD-173-DNR-B air cylinder under a pressure of $\sim$1.5 bar controlled via air lines external to the impact chamber.

13. A. L. Ruoff, *J. Appl. Phys.* **38,** 4976 (1967).

14. Relaxation times in liquids are strongly dependent on the liquid viscosity. For an alkali olivine basalt at 1300 ° C, 1 atm relaxation times are inferred to be $<$2 ns [C. S. Rai, M. H. Manghnani, and K. W. Katahara, *Geophys. Res. Lett.* **8,** 1215 (1981)] and viscosity η $\sim$55 Poises (calculated from the data of Bottinga and D. F. Weill, *Am. J. Sci.* **272,** 438, 1972). At 1400 ° C, η $\sim$35 Poises for $An_{0.36}Di_{0.64}$ (molar). Assuming the relaxation time to be $<$2 ns, the ultrasonically measured 1 atm bulk modulus should represent the relaxed value. Good agreement with the shock bulk modulus suggests that we also measure the relaxed value in our experiment.

15. R. Jeanloz and A. B. Thompson, *Rev. Geophys. Space Phys.* **21,** 51 (1983).

16. H. S. Waff, *Geophys. Res. Lett.*, **2,** 193 (1975).

17. S. K. Sharma, D. Virgo, B. Mysen, *Am. Mineral.* **64,** 779 (1979).

18. E. Ohtani, F. Taulelle, C. A. Angell, submitted to *Nature* (1984).

19. A. Boettcher, Q. Guo, S. Bohlen, B. Hanson, *Geology,* **12,** 202 (1984).

20. The application of our results to complex, natural liquid compositions is, we believe, justified in view of the weak dependence of elastic properties of silicate melts on bulk composition observed in ultrasonic experiments [2,5].

21. E. Stolper, *Contrib. Mineral. Petrol.* **74,** 13 (1980).

22. E. G. Nisbet, D. Walker, *Earth Planet. Sci. Lett.* **60,** 105 (1982).

23. The Birch-Murnaghan adiabats shown are for magnesian olivine (Fo_{90}), orthopyroxene (En_{90}) and mantle garnet [density from F. R. Boyd, R. H. McCallister, *Geophys. Res. Lett.* **3,** 509 (1976)] at an initial temperature of 1400 ° C. Elastic properties, density and thermal expansivity for olivine and orthopyroxene are from Jeanloz and Thompson [15]; for garnet, data of N. Soga *J. Geophys. Res.* **72,** 4227 (1967), and B. J. Skinner, *Geol. Soc. Am. Mem.* **97,** 75 (1966) were used.

24. PREM: A. M. Dziewonski, D. L. Anderson, *Phys. Earth Planet. Int.* **25,** 297 (1981). PEM: A. M. Dziewonski, A. L. Hales, and E. R. Lapwood, *Phys. Earth Planet. Int.* **10,** 12 (1973). Density model from free oscillations: T. H. Jordan, D. L. Anderson, *Geophys. J. R. Astr. Soc.* **36,** 411 (1975).

25. Z. N. Zharkov and V. P. Trubitsyn, *Physics of Planetary Interiors,* W. B. Hubbard, ed. (Pachart Publishing House, Tucson, 1979) Vol. 6, 388 pp.

26. Typical values for Mg/(Mg+Fe) (molar) for the Earth are 0.9 [e.g., Basaltic Volcanisn Study Project, *Basaltic Volcanism on the Terrestrial Planets* (Pergamon Press, Inc., New York, 1981), 1286 pp.]. Recent chemical analyses made by Venera 13 and Venera 14 suggest strong similarities between Venusian and terrestrial surface rocks [V. L. Barsukov, Yu A. Surkov, L. P. Moskalera, O. P. Scheylov, V. P. Zharyukora, O. S. Manuelyan, V. G. Perminov, *Geochemistry International,* **19,** N° 4, 1 (1982)] and lead us to use a similar internal composition for Venus.

27. Estimates of Mg/(Mg+Fe) in Mars and the composition of model Mars magma were taken from T. R. McGetchin and J. R. Smyth, *Icarus* **34,** 512 (1978). Initial density of model Mars basalt is slightly higher ($\sim$2.77 g/cm^3) than primitive terrestrial basalt because of higher iron content. However, mantle density is inferred to be on the order of 0.2 g/cm^3 higher on Mars up to a pressure of $\sim$125 kbar because of its higher iron content [Basaltic Volcanism Study Project *op. cit.*]. Thus, the pressure at which $\Delta\rho \rightarrow$ O for Mars would be expected to be higher than on the Earth or Venus.

28. The composition of a primitive lunar magma, a supposed parent to the lunar crust, was taken from A. E. Ringwood, *Origin of the Earth and Moon,* Springer-Verlag, New York, 295 pp. (1979). An inferred lunar density-depth profile is given by Basaltic Volcanism Study Project, *op. cit.*

29. F. R. Boyd, J. L. England, B. T. C. Davis, *J. Geophys. Res.* **69,** 2101 (1964).

30. G. A. Lyzenga and T. J. Ahrens, *J. Geophys. Res.* **83,** 2431 (1983).

31. The 1 atm density of $MgSiO_3$ liquid is calculated by extrapolation of density measurements of J. W. Tomlinson, M. S. R. Haynes, and J. O'M Bockris,

Trans. Faraday Soc. **54,** 1822 (1958).

32. For $MgSiO_3$ perovskite $K_s^0 = 2620$ kbar, $K_s' = 4$ [15]. A third-order Birch-Murnaghan equation-of-state was used in calculating high pressure densities and thermal expansion, $\alpha = 0.2367 \times 10^{-4} + 0.5298 \times 10^{-8} T - 0.5702 T^{-2}$. [H. Watanabe, in *High Pressure Research in Geophysics*, S. Akimoto and M. H. Manghnani, eds. (Center for Academic Publications, Tokyo, 1982) p. 441] was assumed.

33. S. M. Stishov, *Sov. Phys. Usp.* **17,** 625 (1975).

34. E. Ohtani, *Phys. Earth Planet. Int.* **33,** 12 (1983).

35. *e.g.*, N. H. Sleep, *J. Geol.* **87,** 671 (1979).

36. J. D. Bass, D. L. Anderson, *Geophys. Res. Lett.* **11,** 229 (1984). H. Sawamoto, D. J. Weidner, S. Sasaki, M. Kumazawa, *Science* **224,** 751 (1984).

37. Acknowledgments: We are grateful to L. T. Silver for use of the Lepel RF generator and for his continued interest. We have benefited from discussions with and comments from D. L. Anderson, J. D. Bass, A. Boettcher, I. S. E. Carmichael, H. Eissler, R. Hill, M. H. Manghnani, S. A. Morse, O. Navon, R. O'Connell, E. Ohtani, F. Richter, M. L. Rivers, D. R. Scott, D. J. Stevenson, and D. Walker. Supported by NSF grant EAR80-18819. Contribution No. 4112, Division of Geological and Planetary Sciences, California Institute of Technology, Pasadena, CA 91125.

--

Table 1: Molten $An_{0.36}$ $Di_{0.64}$ Hugoniot data

Shot #	Flyer Plate	Impact Velocity (Measured) km/sec	Shock Velocity (Measured) km/sec	Particle Velocity (Calculated) km/sec	Hugoniot Pressure (Calculated) GPa	Hugoniot Density (Calculated) g/cc
592	Al	1.05 ±0.02	3.59 ±0.04	0.44 ±0.01	4.10 ±0.09	2.978 ±0.026
593	Al	1.50 ±0.03	3.65 ±0.04	0.65 ±0.02	6.15 ±0.14	3.176 ±0.030
605	Al	2.00 ±0.04	4.06 ±0.10	0.88 ±0.02	9.30 ±0.29	3.33 ±0.04
607	W	1.80 ±0.03	5.20 ±0.05	1.73 ±0.03	23.54 ±0.50	3.92 ±0.05

Figure Captions

Figure 1: (a) Shock experiment for molten silicate target. Silicate sample is encapsulated between a Mo driver plate and Mo cover plate. The metal capsule is heated via induction [8] and acts as a furnace. Measurement of projectile velocity via double flash (30 nsec) x-ray shadowgraph (12-30 μsec apart) allows determination of the particle velocity by impedance match with the Mo driver plate [9]. The temperature of the molten sample, monitored by a Pt-Rh thermocouple, determines the initial density [10]. The shock velocity is determined by measuring the time difference between the shock arrival at planes A and B [11]. Shock propagation time through the Mo cover plate must be subtracted from sample plus cover plate introducing an error of 0.3% in the measured shock velocity. A ceramic shutter covers the expendable mirror until $\sim$1 sec before host is fired [12].

(b) Double x-ray shadowgraph of projectile during flight towards target.

Figure 2: Density of basic silicate melt compared with that of the Earth's mantle and likely liquidus minerals, olivine, pyroxene, and garnet. The hachured band represents the range of melt densities expected in compression of basaltic compositions from an average mid-ocean ridge basalt (2.7 g/cm^3) to komatiite (2.8 g/cm^3) [21,22] using the values of K_s and K_s' derived from our work. Adiabatic compression curves are shown for the possible liquidus minerals, olivine, orthopyroxene, and garnet [23]. The stippled band represents the range of density-depth relations in the Earth derived from two recent seismological whole-Earth models PEM, PREM, and a density model based on free oscillation data [24]. Depth scales are shown for the major terrestrial planets and the Earth's moon [25]; the tick marks on earth scale are at 100

km intervals. Inset shows dynamic compression data for $An_{0.36}Di_{0.64}$ (molar) at an initial temperature of 1400 ° C. The dashed line passing through the data points is a Hugoniot fit to the experimental points. The solid line adjacent to the Hugoniot is calculated from the Birch-Murnaghan equation with $K_s^\circ = 226$ kbar and $K_s' = 4.15$. This curve deviates from the Hugoniot only above ~100 kbar where shock heating becomes important. Adiabatic compression curves of the expected solid of this bulk composition are also shown for an initial temperature of 1400 °. Above 80 kbar the phase assemblage is uncertain but is probably well approximated by the left-hand curve to ~150 kbar. The rightmost curve is a maximum possible density estimate based on an assemblage of high-pressure phase, mixed oxides. Key: an - anorthite; di - diopside; qtz - quartz; cs - coesite; ky - kyanite; gr - grossular; py - pyrope; st - stishovite; ☽ moon; ⊕ Earth; ♂ Mars; ♀ Venus.

Figure 1

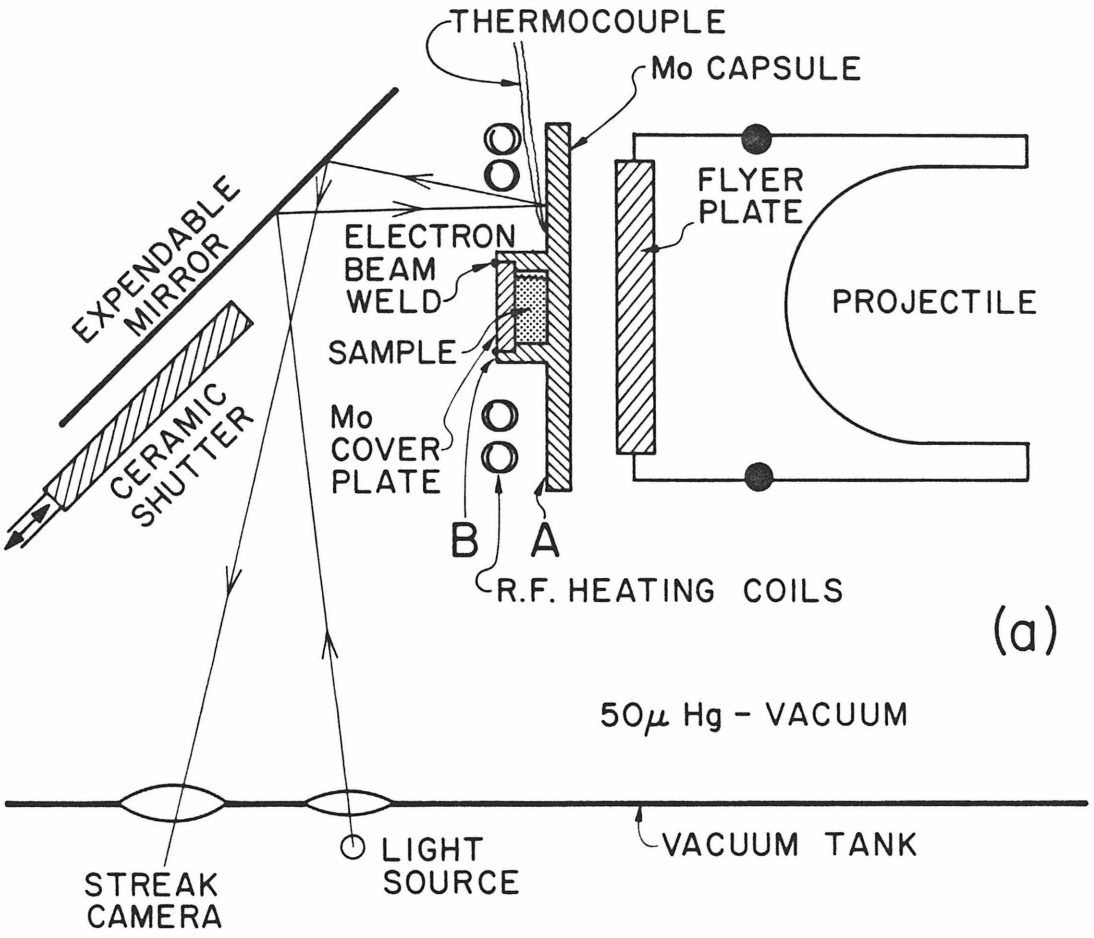
THERMOCOUPLE
Mo CAPSULE
FLYER PLATE
PROJECTILE
EXPENDABLE MIRROR
ELECTRON BEAM WELD
SAMPLE
CERAMIC SHUTTER
Mo COVER PLATE
B
A
R.F. HEATING COILS
(a)
50μ Hg - VACUUM
VACUUM TANK
LIGHT SOURCE
STREAK CAMERA

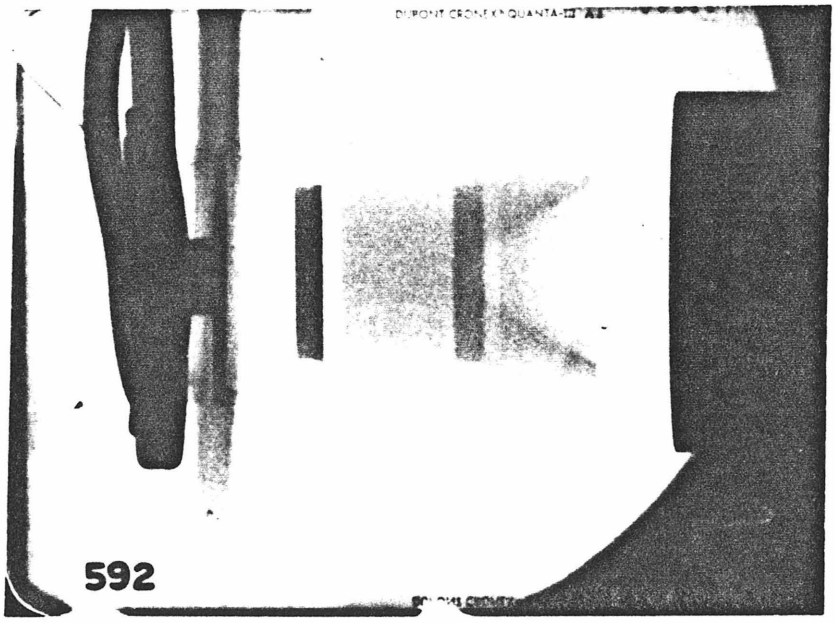
592

(b)

Figure 2

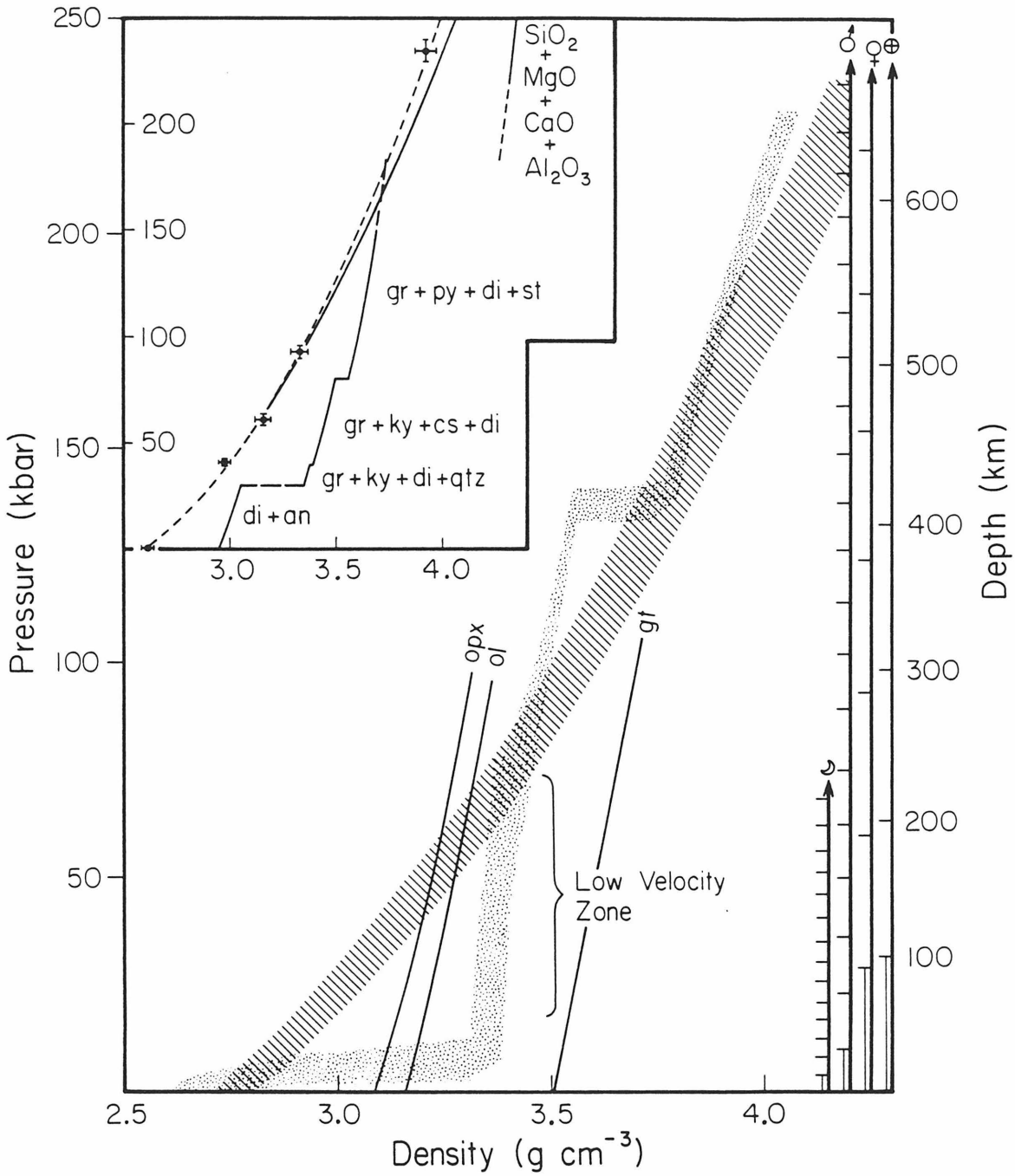
250
200
150
100
50
200
150
100
50
SiO_2 + MgO + CaO + Al_2O_3
gr + py + di + st
gr + ky + cs + di
gr + ky + di + qtz
di + an
3.0
3.5
4.0
Pressure (kbar)
opx
ol
gt
Low Velocity Zone
2.5
3.0
3.5
4.0
Density (g cm^{-3})
600
500
400
300
200
100
Depth (km)

Chapter 2

The Density of Molten Silicates at High Pressures: Technique and Results on a Haplobasaltic Composition

ABSTRACT

A technique has been developed which permits measurements of the shock-wave, pressure-density equation of state of initially molten silicates initially at temperatures of up to 1973 K. A 40 mm propellant gun apparatus is used to accelerate metal flyer plates to speeds of 2.5 km sec^{-1}; at these speeds tungsten flyer plates drive shock waves with amplitudes of 35 to 40 GPa (350-400 kbar) into sample assemblies. Modifications to the standard equation of state experiments that are described here include: design of a molybdenum sample container to contain the molten silicate; use of a 10 kW radio frequency induction heater to heat the sample to temperatures in excess of its melting point immediately prior to impact; and implementation of shuttering systems that protect the optical system from impurities emitted from the hot sample and prevent pre-exposure of the film in the rotating-mirror, continuously-writing, streak camera. The reduction of Hugoniot data taking into account the effect of the sample capsule is described. Data for a haplobasaltic composition (36 mole % anorthite, 64 mole % diopside: $An_{0.36}Di_{0.64}$) at an initial temperature of 1673 K

and density, ρ_0 of 2.607 Mg m^{-3}, yield a shock velocity-particle velocity (U_S–U_P) relation given by $U_S = 3.06+1.36\ U_P$ km sec^{-1} up to values of $U_P = 1.7$ km sec^{-1}. The zero-pressure, bulk sound speed of 3.06 km sec^{-1} is in good agreement with the ultrasonically measured value of Rivers and Carmichael (1981) on a similar composition. At higher pressures (above $\sim$ 25 GPa) the Hugoniot data suggest that the gradual coordination increase of Al^{3+} and Si^{4+} from 4 to 6-fold coordination is essentially complete. These high-pressure Hugoniot data are fit by $U_S = 0.85+2.63\ U_P$ km sec^{-1}. The high-pressure regime appears similar to that obtained in initially solid silicates upon shock compression. Shock temperature calculations yield values of 2400-2600 K at 25 GPa and the states achieved are believed to lie metastably in the liquid field.

INTRODUCTION

The density of a silicate melt (or indeed, of any substance) is one of its most fundamental physical properties. Its reciprocal, the specific volume, is a first derivative of energy with respect to pressure, and if we know its value as a function of pressure and temperature, we have essentially a complete description of its thermodynamic properties (i.e., the equation of state). Knowing the equation of state of a melt, petrologists can gain insights into solid-liquid phase equilibria critical to understanding igneous petrogenesis. The density is also an expression of the liquid's integrated microscopic structure; thus, systematic study of density can yield insights into melt structure. This provides a framework for thinking about the

thermodynamic properties and physical properties (e.g., viscosity, diffusivities) that play critical roles in petrogenesis. Finally, and perhaps more directly relevant to igneous processes, the density contrast between magmas and crystalline solids plays a crucial role in determining the directions and velocities of magma transport within the earth and other planets, and thus knowledge of the densities of melts at conditions relevant to planetary interiors is fundamental to understanding igneous activity and planetary differentiation.

The systematics of the densities of silicate melts at atmospheric pressure are well understood (see, for example, Bottinga and Weill, 1970; Nelson and Carmichael, 1979; Mo *et al.,* 1982; Bottinga *et al.,* 1982), but until recently little was known about melt densities at elevated pressures. Although there have been calculations and inferences of melt density based on measured elastic properties of melts at low pressure (Stolper *et al.,* 1981; Nisbet and Walker, 1982), on molecular dynamics simulations (Angell and Kanno, 1976; Angell *et al.,* 1982, 1983; Matsui and Kawamura, 1980; Matsui et al., 1982), and on analysis of the solidi of congruently melting minerals (Ohtani, 1984; Bottinga, 1985; Rivers, 1985), there have been few actual *measurements* of melt densities at elevated pressure. Until recently, the only available measurements were made with the "falling sphere" technique (Kushiro, 1978, 1980; Fujii and Kushiro, 1977; Scarfe *et al.,* 1979; Sharpe *et al.,* 1983). However, measurements using this technique have been restricted to less than 3 GPa and the accuracy of densities based on it has been questioned (Rivers, 1985).

Shock wave techniques are routinely used to provide accurate measurements of density as a function of pressure along the Hugoniot for solids (see, for example, McQueen *et al.,* 1967, 1970). Pressures in excess of 400 GPa have been achieved using

these techniques (Al'tshuler, 1965). In this paper, we describe a set of experiments in which we have used shock wave techniques to study the density of a haplobasaltic silicate liquid at pressures between 4 and 35 GPa. Preliminary results and a discussion of their implications have been presented elsewhere (Rigden *et al.*, 1984). The focus of this paper will be on the experimental techniques that we have utilized and, in particular, on the modifications to the "standard" shock wave techniques developed for use on cool solids that were necessary in order for us to carry out similar experiments on molten samples.

In a typical shock wave experiment, a high-pressure pulse is generated in a cool, solid sample by high velocity impact of a metal plate. Measurement of the velocity of the high-pressure shock wave and the particle velocity in the sample enables the pressure and density to be calculated via the Rankine-Hugoniot equations. The extraordinary problem that we faced in our experiments was basically this: How do you get the target hot enough so that it is molten prior to impact by the projectile and so that the material whose equation of state is being studied is liquid rather than solid? The solution that we chose was to encapsulate the material in a metallic container, which we then heated by induction. This solution created its own set of problems; for example, how do you hold the capsule? how do you measure the initial temperature? how do you correct the shock velocity for the presence of the metal capsule? In this paper, we describe how we dealt with these and other problems unique to high-temperature shock wave experiments and their data reduction and we present the data set on the haplobasaltic composition studied.

SAMPLE PREPARATION

Sample Container

In contrast to a standard equation of state experiment where a target sample is mounted on a metal driver plate, the sample in this experiment, molten at the time of impact, is totally enclosed in a metal container. If the sample is not completely enclosed, it leaks out of the container upon melting because of surface tension effects. The sample capsule is constructed of molybdenum (ABL low-carbon, vacuum arc-cast molybdenum supplied by AMAX Specialty Metals). The melting point of molybdenum (2890 K) is higher than that of any likely silicate sample, a primary consideration in its choice.

The capsule is sealed by electron beam welding a thin (0.75 mm) molybdenum cap onto the base, which contains a glass sample (Figure 1). During the welding process, the molybdenum capsule must be treated carefully to prevent cracking because the metal is extremely brittle. Initially, the assembly is preheated to red heat for several minutes. This degasses the join where the weld is made and releases volatiles from pore space in the molybdenum. After welding, the capsule is cooled slowly under a broad electron beam to anneal the weld. During cooling, an observation of the weld at 800 to 900 K is made to ensure that it is free from cracks. The welded target is finally heated to 1673 K in a muffle furnace for about 1 hour under 1 bar of nitrogen. This step premelts the sample so that it wets the sides of the container and ensures that the capsule is completely sealed; at this stage the sample will leak out if any cracks are present in the weld. In addition, it is important that the molten sample be free of bubbles because the path of the shock wave should be uninterrupted to

give an accurate estimate of its travel time through the sample. Targets cross-sectioned after this heating procedure showed a clear, bubble-free glass in the sample chamber.

Silicate Sample

Several criteria were used to choose the sample material. (1) The sample should be geologically relevant. (2) Because the presence of bubbles would interfere with travel of the shock wave through the sample, the viscosity must be low enough that bubbles will rise buoyantly to the top of the container during the premelting procedure. If the sample viscosity is <100 Poise, all bubbles >50 micron in diameter should be unable to remain suspended for longer than $\sim$ 5 minutes. (3) The molybdenum sample container undergoes oxidation at a rate strongly dependent on its temperature under the vacuum conditions in the impact tank ($\sim$ 100 microns), so the melting temperature of the silicate sample must be relatively low. Otherwise, oxides are ejected from the hot molybdenum and deposited on nearby unheated or cooler surfaces. These deposits can interfere with the optical path to the recording camera. In addition, the higher the temperature of the sample container, the more strain is placed on ceramic pieces that hold it in place.

The composition chosen for the experiments described in this paper is that of the 1 atm eutectic in the system anorthite-diopside. This composition satisfies the criteria of low melting point (1547 K, Bowen, 1915) and low viscosity ($\sim$ 30 poises at 1673 K, calculated using the method of Bottinga and Weill, 1972). The ideal chemical composition of the sample (64 mole % $CaMgSi_2O_6$; 36mole % $CaAl_2Si_2O_8$) is given in Table 1. This is a good compositional analog for natural basalt from which it

differs mainly in an absence of iron and alkalis and an excess of calcium. The composition of average mid-Atlantic ridge basalt (Melson and Thompson, 1971) is also shown in Table 1 for comparison.

Samples are prepared from spectroscopically pure oxides and $CaCO_3$. The powdered oxides (SiO_2, MgO, Al_2O_3) and $CaCO_3$ are weighed out in the appropriate proportions to make 5 g of sample. Grinding the oxides together for 5 hours in an agate mortar under alcohol produces a homogeneous powder. The starting material is heated in a platinum crucible in a muffle furnace at 1673 K for several hours to melt the sample and drive the CO_2 from the carbonate. Upon removal from the furnace a clear glass that may have many bubbles is produced. To remove bubbles and any volatiles contained in the glass, a second melting is undertaken in a vacuum furnace under air pressure of less than 100 μm Hg at 1673 K. This second melting stage is of about 12 hours' duration and yields a clear, bubble-free glass. The average composition from several such runs, measured with the electron microprobe, is shown in Table 1 and agrees well with the ideal composition. The glass sample is removed from the platinum crucible by using a diamond core drill. It is then ground to fit into the molybdenum container and welded as described above.

EXPERIMENTAL METHOD

The pressure and density in the high-pressure shocked state is determined by application of the Rankine-Hugoniot conservation equations (e.g., Duvall and Fowles, 1963). The initial density ρ_o of the initially molten sample is calculated using partial molar volumes of the constituent oxides given by Stebbins *et al.* (1984). U_S and U_P are the shock and particle velocities (km sec^{-1}) in the molten silicate; these are

determined from shock-transit time through the sample and the measured projectile velocity. Measured quantities for this experiment are sample shock transit time from which U_S is calculated, projectile velocity from which U_P is derived, and the sample temperature from which ρ_0 is determined.

A shock wave is generated in the sample by impact of a metal flyer plate embedded in a lexan projectile. The projectile is launched from a 40 mm bore propellant gun described by Ahrens *et al.* (1971). The front portion of the sample capsule serves as the shock driver plate (Figure 1). This target is mounted in a Zircar fibrous alumina ceramic plate (type ZAL-45) and suspended in the impact tank (Figure 2).

Heating and Sample Geometry

Heating is accomplished by a water-cooled copper induction coil powered by a 10 kW Lepel Radio Frequency generator (model T-10-3-KC-N-W). The 10 kW maximum output of the generator is ample to heat the molybdenum sample assembly. For example, the energy required to heat a typical sample assembly (33g) to 1800 K is about 15 kJ, or, 1.5 seconds of operation at the peak output of the RF generator. Radiant losses (by black body radiation) in the vacuum conditions of the experiment at this temperature amount to approximately 2 kW. Thus, the present apparatus has ample power to attain and maintain the high temperature necessary for this experiment. To minimize electromagnetic radiative losses of high-frequency (250 to 450 kHz) energy, a coaxial line is utilized from the generator to within 12 cm of the load coil. A 12:1 stepdown transformer (Model LCT-4) is inserted in the coaxial line immediately before the line enters the vacuum tank. Without this transformer, the high voltage leads to arcing across the load coil under the poor vacuum ($\sim$ 100

microns) conditions in the tank. It was necessary to extend the coaxial line to within 12 cm of the coil; approximately 80% of the available RF energy was lost between the transformer and load coil (a distance of 50 cm) in the absence of the coaxial line.

Within the tank the coaxial line doubles as a support system for the target assembly and water-cooling system (40 liters/minute flow rate). The target assembly is attached to the brass termination block of the coaxial line. A hollow-centered pie-shaped coil is used because of space constraints and to preserve an optical path from the sample to the recording streak camera. This coil is positioned behind the target assembly with its center on line with the center of the sample. A Pt-Pt10%Rh thermocouple (0.25 mm thick), pressed into a 1.6 mm diameter, 1.0 mm deep well in the driver plate just above the sample (Figure 2), monitors the temperature until the gun is fired. Behind the coil sample assembly, a turning mirror reflects the image of the sample through a window in the impact tank via a system of lenses and mirrors to a continuously writing Beckman-Whitley streak camera (model 339). This turning mirror is mounted on a Zircar fibrous alumina ceramic cylinder (type ALC) which is attached to a leveling table. Under the vacuum conditions in the impact tank ($\sim$ 100 microns), molybdenum undergoes rapid oxidation at high temperatures. An alumina ceramic shutter (Zircar type ZAL-45) covers the mirror until the shot is fired. This protects the mirror from the radiative heat emitted from the sample and also shields it from the stream of molybdenum oxides that are deposited on cool surfaces around the heated sample assembly. The shutter is retracted with a double-acting Bimba (model SSRD-173-DNR-B) air cylinder operating under a pressure of 1.5 bar approximately 1 sec before impact of the flyer plate on the driver plate; this allows a clear optical path to the streak camera. Air lines external to the tank control the air

cylinder.

Measurement of Shock Transit Time

The shock transit time through the sample plus molybdenum cover plate is measured by observing the sample assembly rear surfaces via the streak camera. Both the driver plate rear surface and that of the molybdenum cover plate (Figure 1) are ground and polished with alumina abrasives and polishing powders to a final mirror finish with 0.3 μm diamond paste. A xenon flash lamp (Goto *et al.,* 1979), triggered by passage of the projectile past laser I (Figure 3), illuminates the sample. As the shock wave traverses the polished surfaces, a change in reflectivity is detected by the streak camera (Fig. 4a). An experimental streak record is shown in Figure 4b.

In a standard equation of state experiment, the streak camera shutter is opened before the firing circuit of the gun is completed. Completion of the firing circuit requires that both the camera shutter be held open and the firing key be turned simultaneously. In this experiment the camera shutter is opened after the firing key is turned. This is necessary because light from the hot, radiating sample would otherwise fog the film and obscure the streak record. Although the light intensity from the radiating sample is far lower than from the single 100 μsec duration xenon flash, the film can be overwritten several thousand times in the 1-2 seconds' delay between opening the shutter and turning the firing key. A single sweep of the film in the streak camera occurs in $\sim$ 250 μsec.

Measurement of the Projectile Velocity

The projectile velocity is measured via two techniques. The first involves measuring the time taken for the projectile to travel between three lasers that cross the flight path and are a known distance apart (Figure 3). This measurement is made in the last 0.70 m of the 20 m projectile travel. As the projectile crosses the first 2 mW He-Ne laser, a voltage increase is detected by a PIN photodiode (Hewlett-Packard, 5082-4220) in line with the laser. This triggers an electronic counting system. Passage of the projectile across the second and third lasers gives time intervals to within 0.01 μsec, which allow the projectile velocity to be calculated within 0.2% precision at the highest velocities.

The second method of measuring projectile velocity utilizes dual flash x-ray sources. Two Hewlett-Packard, Field Emission Type 526 Flash x-ray tubes illuminate a 12 x 24 mm cassette containing Kodak type X-OMAT AR, x-ray film with a Dupont Quanta 3 x-ray intensifier screen. This occurs within the last 5 cm of projectile travel. A 30 ns duration 30 KV x-ray pulse is triggered when the projectile crosses the third laser and the second flash x-ray is activated after a time interval dependent on the expected projectile velocity. Measurement of the separation of the two images of the projectile on the x-ray film enables determination of the projectile velocity. The x-ray shadowgraph is also used to check the integrity and orientation of the projectile/flyer assembly. Figure 5 shows a typical x-ray shadowgraph for the molten silicate equation of state experiment.

The calculated velocity (V_{imp} in mm μsec^{-1}) of the projectile from the x-ray shadowgraph is given by:

$$V_{imp} = \frac{1+\delta}{M(\Delta t)}, \qquad (1)$$

where l is the measured distance between images on the film (mm), δ is the parallax (separation for a stationary target in mm), M is the film magnification and Δt is the delay time (μsec) between firing the two x-ray tubes. For the range of possible projectile velocities ($\sim$ 1 km/sec to 2.5 km/sec) l ranges from about 27 mm to 16 mm. The error in projectile velocity is limited by the accuracy with which this distance can be measured and results in an uncertainty of about 2% in the projectile velocity. This second method of measuring projectile velocity is preferred because it gives a velocity closest to the target. The first method provides a back-up measure of projectile velocity.

Capsule Equation of State

The shock equation of state of the molybdenum capsule must be known before the shock and particle velocities for the sample can be calculated. Although the shock equation of state of molybdenum has been measured starting at room temperature (Marsh, 1980), there are no experimental data on the high temperature Hugoniot. We have made a single determination of the shock equation of state of molybdenum at an initial temperature of 1273 K, with a pure molybdenum target heated using the induction coil assembly previously described. The result of this experiment is shown in the P-U_P plane in Figure 6. Also shown is a calculation of the Hugoniot of molybdenum initially at 1273 K.

In calculating this Hugoniot, a Mie-Gruneisen equation of state was assumed. For two Hugoniot states at constant volume (V) but different initial densities, the difference in pressure (ΔP) is given by:

$$\Delta P = \Delta E \gamma / V, \tag{2}$$

where γ is Gruneisen's parameter and ΔE is the energy difference. Using the expressions for the energy of the two Hugoniot states from the Rankine-Hugoniot equation for conservation of energy and taking into account the energy difference between an initial state at room temperature and high temperature, the following expression is derived.

$$P_T = \frac{P_C(V_{0C}-V)/2 - P_C(V/\gamma) - \int_{T_C}^{T} C_P dT}{(V_{0T}-V)/2 - V/\gamma} \qquad (3)$$

Here, the subscripts C and T refer to states initially at room temperature and high temperature, respectively, and C_P is the specific heat at constant pressure from Robie *et al.* (1978). It was first assumed that the Gruneisen parameter is dependent only on volume such that $\gamma = V\gamma_0/V_0$, where $\gamma_0 = 1.52$ is the 1 atm Gruneisen parameter (McQueen *et al.,* 1970), and V and V_0 are the final and initial volumes. This assumption has been found to hold well for porous aluminum, copper and iron (McQueen *et al.,* 1970). A second calculation was made holding γ constant; i.e., $\gamma =$ 1.52 for all pressures. Values assumed in the calculation of the high-temperature Hugoniot are given together with the experimental results in Table 2. The experimentally measured point lies close to the calculated curves at high temperatures. Further experiments are planned to better constrain the high temperature shock equation of state of molybdenum. For this work we used the calculated equation of state with $\gamma/V =$ constant described above.

In a standard equation of state experiment the shock velocity is calculated directly from the transit time through the sample. Using the measured projectile velocity, the shock pressure and particle velocity can then be derived by impedance

match (e.g. Rice *et al.,* 1958). In the present experiment the shock velocity is not directly calculable from the observed shock transit time because the measured transit time on the streak record gives the travel time of the shock through the 4mm thick sample and the 0.75 mm thick molybdenum cover plate. Calculation of the sample transit time, and, hence, the shock velocity requires knowledge of both the high-temperature equation of state of the molybdenum driver plate and also the release isentrope of the sample centered at the Hugoniot state. Both the shock velocity and particle velocity are derived simultaneously in an iterative procedure and the propagation of errors was calculated following the method of Jackson and Ahrens (1979).

The procedure is as follows. The streak records give a measure of the shock transit time through the molten silicate sample and molybdenum cover plate. In order to calculate the Hugoniot state in the sample, the sample shock velocity must be known. Thus, the total transit time must be corrected for the shock travel time through the molybdenum cover plate. Because the shock state in the cover plate is dependent on the state in the sample, it is necessary to make an initial assumption about the state in the cover plate. It is also necessary to make an assumption about the release state in the sample.

The first assumption made is that the shock state in the molybdenum cover plate is the same as that in the molybdenum driver plate. Then the sample velocity shock U_{SS} is given by:

$$U_{SS} = \frac{d_S}{t_T - d_C/U_{SD}}, \tag{4}$$

where d_S and d_C are sample and cap thicknesses, respectively, t_T is the total transit time, and U_{SD} is the shock velocity in the driver plate. Thus, in Figure 7 we estimate

that the initial shock state in the driver and cap is at point D.

Using U_S, an estimate of the shock state in the sample is given by impedance match (Figure 7). For driver and flyer plates of the same material the sample particle velocity is given by:

$$U_{PS} = V_{imp} + \{x-(x^2+4s^2y)^{1/2}\}/2\ s \tag{5}$$

$$x = c + \rho_{0S}\ U_{SS}/\rho_{0D}$$

$$y = \rho_{0S}\ U_{SS}V_{imp}/\rho_{0D}s.$$

Here V_{imp} is projectile velocity, ρ_{0S} and ρ_{0D} are the initial sample, and driver densities and c and s are the coefficients in the equation

$$U_S = c + U_Ps, \tag{6}$$

describing the equation of state of the molybdenum driver plate. This is shown graphically in Figure 7 for a Mo flyer and driver giving state S_1.

A second assumption is now made to better constrain the shock state in the molybdenum cover plate. The sample equation of state is approximated by the straight line of slope $\rho_{0S}\ U_{SS}$ and a state in the molybdenum cover calculated from impedance match (state C_1 of Figure 7).

$$U_{PC} = \frac{-(\rho_{0D}c + \rho_{0S}U_{SS}) + ((\rho_{0D}c + \rho_{0S}U_{SS})^2 + 8\rho_{0D}s\rho_{0S}U_{SS}U_{PS})^{1/2}}{2\rho_{0D}s} \tag{8}$$

Using the known molybdenum equation of state, it is now possible to recalculate the sample shock velocity,

$$U_{SS} = \frac{d_S}{t_T - d_C/(c + sU_{PC})}, \tag{9}$$

and hence make a second estimate of the sample shock state (S_2, Figure 7).

After three iterations using this procedure, U_{SS} and U_{PS} do not change within the experimental uncertainties.

RESULTS

The results of shock wave experiments on molten $An_{0.36}Di_{0.64}$ are given in Table 3 and shown in the particle velocity-shock velocity plane in Figure 8 and in pressure-density space in Figure 9. Above 25 GPa the trend of gradual compression ceases and the material apparently becomes considerably stiffer, leading to little increase in density with increasing pressure. The U_S–U_P data in the low-pressure regime can be fit by a line given by $U_S = 3.06+1.36\ U_P$ km sec^{-1} with $r^2 = 0.99$. In the high-pressure regime, the fit is given by $U_S = 0.85+2.63\ U_P$ km sec^{-1}, $r^2 = 1.00$. A sudden structural rearrangement over a narrow pressure interval would lead to a change in the slope of the $U_S - U_P$ curve. From the goodness of fit to the $U_S - U_P$ data in the low-pressure segment of the data set, we estimate that a structural rearrangement under shock conditions could not be detected from these data unless it resulted in a density jump of $\gtrsim$0.15Mg m^{-3} at the high-pressure end of the data. At the lowest pressure datum a density jump of $\gtrsim$0.06Mg m^{-3} could be detected.

At a particular density a Hugoniot or shock state lies at a higher pressure than an isothermal or isentropic state because of the irreversible energy generated during the shock process. It is useful in discussing processes occurring in planetary interiors to refer to isothermal or isentropic states. For metals and crystalline silicates a Mie-Gruneisen equation of state has been used successfully in reducing Hugoniot data to isothermal or isentropic states (McQueen *et al.*, 1967; Jeanloz and Ahrens, 1980), and

we have used it in analyzing our data.

The difference in energy at constant volume between a Hugoniot state and the state on an isotherm or isentrope is given in the Mie-Gruneisen formulation by:

$$E_H - E_{T,S} = \frac{V}{\gamma}(P_H - P_{T,S}), \tag{10}$$

where the H subscript refers to energy and pressure states along the Hugoniot and T and S subscripts refer to energy and pressure along an isotherm or isentrope.

Energy along the Hugoniot is given by the Rankine-Hugoniot equation for conservation of energy, namely:

$$E_H - E_0 = (P_H + P_0)(V_0 - V_H)/2. \tag{11}$$

Here the zero subscripts refer to the initially (usually 1 atmosphere) state which can be approximated as zero pressure. Energy along an isentrope for a third-order Birch-Murnaghan equation of state is

$$E_S - E_0 = \frac{9}{2} K_S V_0 \left\{ (\xi+1) \left(\frac{X^4}{4} - \frac{X^2}{2} + \frac{1}{4} \right) - \xi \left(\frac{X^6}{6} - \frac{X^4}{4} + \frac{1}{12} \right) \right\} \tag{12}$$

$$X = (V_0/V)^{1/3}$$

and

$$\xi = 3(4 - K')/4.$$

Using the experimental data along the Hugoniot and assuming a Mie-Gruneisen equation of state we have fit the Birch-Murnaghan parameters, K_S and K' by the method of least squares. A value of K' is assumed and K_S is calculated. The calculation is repeated over a range of K' values until the deviation between the observed

and calculated Hugoniot pressures is minimized. The 1 atm Gruneisen parameter is calculated from thermodynamic quantities and we make, as described earlier, the assumption that is commonly made for geophysical materials, i.e., $\gamma = V\gamma_0/V_0$.

It is required to minimize the sum of squares of the function f_i, where

$$f_i = P_{calc} - P_{obs} \tag{13}$$

$$= \frac{E_{Si} - P_{Si}V_i/\gamma}{\frac{V_0 - V_i}{2} - V_i/\gamma} - P_{i.} \tag{14}$$

Here, P_i and V_i are the observed pressure and volume for each experiment. We define $P_{Si}' = P_{Si}/A$ and $E_{Si}' = E_{Si}/A$, where $A = 3K_S/2$. This simplifies the minimization of the sum of the squares with respect to A. For $\frac{\partial \Sigma f_i^2}{\partial A} = 0$,

$$A = \sum_i \left\{ \frac{P_i(E_{Si}' - P_i' V_i/\gamma)}{\left(\frac{V_0 - V_i}{2} - \frac{V_i}{\gamma_i}\right)} \right\} \Big/ \sum_i \left\{ \frac{(E_{Si}' - P_{Si}' V_i/\gamma_i)^2}{\frac{V_0 - V_i}{2} - \frac{V_i}{\gamma_i}} \right\}. \tag{15}$$

The values of the 1 atm thermodynamic quantities α, K_s and C_p for calculation of γ_o were derived from Bottinga and Weill (1970), Rivers and Carmichael (1982) and Weill *et al.* (1980). For γ_0=0.3, a minimum value of $\sum_i f_i^2$ is attained for $K_S = 24.2$ GPa and $K' = 4.85$. Rivers (1985) calculates a value of $K_S = 21.6$ GPa using measured ultrasonic velocities for the composition $An_{0.5}Di_{0.5}$ in good agreement with our results.

SHOCK TEMPERATURES

Temperatures along the Hugoniot can be estimated once again utilizing the Mie-Gruneisen equation of state. In this case:

$$T_H - T_S = \frac{V}{\gamma C_V} (P_H - P_S), \tag{16}$$

where T_H and T_S are temperatures along the Hugoniot and isentrope, respectively, and C_v is the specific heat at constant volume. The temperature along the isentrope is given by

$$T_S = T_0 \exp \left(-\int_{V_0}^{V} \frac{\gamma(V)}{V} \, dV \right), \tag{17}$$

where T_0 is the initial temperature. For the assumed volume dependence of γ this reduces to

$$T_S = T_0 \exp \left\{ -\gamma_0 \left(\frac{V}{V_0} - 1 \right) \right\}. \tag{18}$$

Shock temperatures have been calculated using this method for pressure range where the data is fit by a smooth compression curve. At $\sim$ 25 GPa, the temperature rise is expected to be $\sim$ 900 K. Calculated shock temperatures for $An_{0.36}Di_{0.64}$ initially at 1673 K are shown in Figure 10. Also shown is the liquidus temperature for this composition determined experimentally at low pressures by Presnall *et al.* (1978). Over the pressure range of these experiments, the Hugoniot curve is expected to lie below the melting curve for this composition. Thus, the Hugoniot states would lie in the stable solid field.

DISCUSSION

Crystals or metastable liquids?

Given that the T-P coordinates of our shocked states lies beneath the solidus (Figure 9), it is important to establish that crystallization did not occur during the experiment and that the measured Hugoniot is appropriate for the (metastable) liquid state. There are three lines of evidence that, taken together, argue strongly against crystallization along the liquid Hugoniot.

(1) The agreement of the 1 atm bulk modulus calculated from our data with that measured by ultrasonic techniques on a similar composition by Rivers and Carmichael (1982) is persuasive evidence that crystallization did not occur and that we are measuring a relaxed bulk modulus appropriate for $An_{0.36}Di_{0.64}$.

The frequencies at which the ultrasonic measurements were made were 5-12 MHz. For molten silicates with viscosities below $\sim$ 100 Poise these workers found no frequency dependence to the ultrasonic velocities, which is expected when the frequency is much less than $1/\tau$, the characteristic relaxation time in the melt. Rai *et al.* (1981) inferred that $\tau < 2$ nsec for an alkali olivine basalt at 1573 K with $\eta \sim 55$ Poise (calculated from Bottinga and Weill, 1972). At 1673 K, $\eta \sim 30$ Poise for the composition used in our experiments. In view of this we would also expect that $\tau < 2$ ns.

In a shock wave experiment the characteristic time is the rise time τ_r of the shock wave. It is strongly suggested that $\tau < \tau_r$ because of the close agreement between the ultrasonic and shock bulk modulus. The rise time can be estimated from the following equation:

$$\tau_r = \frac{\eta\, U_P}{U_S\, \Delta P_{V(max)}} \quad \text{(Jeanloz and Ahrens, 1979),} \tag{19}$$

where $\Delta P_{V(max)}$ is the maximum pressure offset between the equilibrium Hugoniot and the Raleigh line at $P_H(U_P, U_S)$. The values of U_P, U_S, and ΔP_V at a given P_H can be calculated from the fit to the experimental shock data. The precise value of η at a given shock state is unknown, but effective viscosity is expected to decrease with increasing pressure (e.g., Jeanloz and Ahrens, 1979; Chhabildas and Asay, 1979). As an upper bound we have assumed that $\eta = 30$ poises at all pressures; this is the value at 1 atmosphere and 1673 K calculated from Bottinga and Weill (1972). Shock rise times are expected to be $\lesssim 10^{-9}$ seconds for the present experiments. Hence, it is expected that $\tau < 10^{-9}$ sec.

(2) If it can be shown that the density of molten $An_{0.36}Di_{0.64}$ at a given pressure along the Hugoniot exceeds that of the crystalline equivalents, it is strong evidence that crystallization did not occur during the shock process unless reaction between solids leads to a greater density than a simple mixture.

Ahrens *et al.* (1977) report considerable success in modeling the Hugoniots of two terrestrial rocks, Westerley Granite and Centerville Diabase, as a mixture of their known constituent mineralogies. In order to place constraints on the likely Hugoniot of crystalline $An_{0.36}Di_{0.64}$, we have examined the results of shock compression of end-member mineralogies. A theoretical Hugoniot for a mixture of anorthite and diopside in the appropriate proportions was constructed using the results of Svendsen and Ahrens (1983) and Boslough *et al.* (1986). The theoretical Hugoniot is constructed by summing specific volumes of the Hugoniots of anorthite and diopside at a given pressure:

$$1/\rho(P) = m_{Di}/\rho_{Di}(P) + m_{An}/\rho_{An}(P), \quad (20)$$

where m_{Di} and m_{An} are the mass fractions of diopside and anorthite, respectively (0.58 and 0.42), and ρ_{Di} and ρ_{An} are the densities at P. The results of this calculation are shown in Figure 9 compared with the experimental results for molten $An_{0.36}Di_{0.64}$. The calculated solid Hugoniot is centered at 300 K, whereas the experimental Hugoniot is centered at 1673 K. Hence, the solid densities at high pressure would be expected to be even lower than those calculated. Assuming a thermal expansion of $2x10^{-5}K^{-1}$ for the crystalline assemblage, the density at 1673 K would be 2.94 Mg m^{-1} compared with 3.02 Mg m^{-1} at 300 K. Over most of the pressure range of these experiments, the measured Hugoniot density of molten $An_{0.36}Di_{0.64}$ exceeds that of the calculated crystalline Hugoniot density. Thus, the high densities observed for the molten silicate are not likely to be the result of crystallization.

(3) The characteristic time in a shock wave experiment is very short; based on equation (19), shock rise times can be estimated to be on the order of $<$ 1 ns for this material (Figure 11). From the theory of transformation kinetics we shall attempt to constrain the likelihood of crystallization under the conditions of our experiments, i.e., on a timescale of $\lesssim$ 1 ns.

Time-temperature-transformation (TTT) curves for a variety of silicate materials have been measured experimentally by Uhlmann and his co-workers (for example, Uhlmann and Klein, 1976; Uhlmann *et al.,* 1981; Cranmer *et al.,* 1981). These curves express the time required at a given temperature to produce particular volume fraction crystallized. The range of measured curves for lunar glasses is shown in Figure 11. Also shown is the curve for anorthite glass. All curves have a characteristic shape with a minimum time (the nose, T_{NOSE}) at a temperature that is $\sim 0.77T_E$,

where T_E is the melting temperature. Using a simplified model developed by Uhlmann *et al.*, (1979, 1981) we have also calculated the location of the nose of the TTT curve for molten $An_{0.36}Di_{0.64}$ at 1 atm. At times less than this the material cannot crystallize at any temperature. This time for the composition we have studied falls within the range of lunar glass curves taken from the literature.

In order to ascertain whether crystallization will occur under shock conditions we have estimated the direction in which τ_{NOSE} is expected to move with increasing pressure. If τ_r, the characteristic time in a shock wave experiment, is much less than τ_{NOSE}, then there is insufficient time for crystallization to occur on this timescale. The position of τ_{NOSE} is a function of T_E, the viscosity at T_E and the crystal nucleation and growth rate. In the absence of experimental data on nucleation and growth rates at high pressures, we have assumed that these terms do not change from their 1 atm values. The 1 atm values depend primarily on the heat and entropy of fusion. The liquidus temperature is expected to increase steeply at high pressures. As a maximum estimate we have taken $T_E = 2773$ K at 20 GPa, the expected melting temperature for forsterite at this pressure from the experimental results of Ohtani and Kumazawsa (1981). Molecular dynamics simulations for silicates at high pressures indicate an increase in ion diffusivities and consequent decrease in viscosities of up to half an order of magnitude at pressures of 10 - 50 GPa in alkali-aluminosilicate melts (Angell *et al.*, 1982, 1983). At one atmosphere the decrease in viscosity from $0.77T_E$ to 2135 K ($0.77T_E$ at 20 GPa) is expected to be six orders of magnitude. Assuming a reduction of seven orders of magnitude in viscosity and $T_E = 2773$ K leads to a likely minimum estimate of $\tau_{NOSE} \sim 2 \times 10^{-5}$ sec. This is four to five orders of magnitude greater than the calculated shock rise times and strongly suggests that there is

insufficient time for crystallization to occur under shock conditions.

In summary, we note that there are three lines of evidence that the measured Hugoniot states for molten $An_{0.36}Di_{0.64}$ represent liquid compression states. Firstly, the calculated 1 atm value of bulk modulus agrees well with the value measured for a similar composition by Rivers and Carmichael (1982), using ultrasonic methods. Secondly, comparison of the calculated crystalline Hugoniot for this composition and the experimental results on the molten silicate show that the molten silicate density at a given pressure is higher than that of the calculated crystal density arguing against crystallization. Lastly, comparison of the time available during the shock wave experiment with the time calculated for crystallization to occur indicates that the crystallization time is too long by many orders of magnitude.

Microscopic significance of the "smooth" compression of haplobasaltic liquid

The apparent smooth compression of $An_{0.36}Di_{0.64}$ to 25 GPa contrasts with the behavior of the crystalline equivalent under both dynamic and static high pressure. Compression of a mixture of crystalline anorthite and diopside would show discontinuous increases in density as phase transformations occur. Under shock conditions diopside is known to transform to a high pressure phase above 60 GPa (Svendsen and Ahrens, 1983), i.e., beyond the range of our experiments. Static high pressure experiments in a diamond cell by Liu (1979) show that diopside is stable to at least 20 GPa at 1300 K. Above that pressure, transformation to a high pressure phase probably occurred, but this phase was unquenchable and reverted to glass upon pressure release. Anorthite breaks down to a mixture of garnet, kyanite and silica at 3 GPa

and 1673 K (Goldsmith, 1980). Under dynamic conditions anorthite exhibits a mixed phase region between about 10 and 40 GPa (Boslough *et al.,* 1986; Jeanloz and Ahrens, 1980); above 40 GPa it is present as a high pressure phase assemblage. The mixed phase region is accompanied by a dramatic change in the slope of the $U_S - U_P$ curve over a substantial range in U_P (Boslough *et al.,* 1986).

The absence of such discontinuous jumps in density for the molten silicate suggests that compression is occurring by continuous changes in ion coordinations and/or continual distortion of the tetrahedral alumino-silicate network. Continual changes in coordination from 4→5→6 have been demonstrated by molecular dynamics simulations on molten alkali-aluminosilicates (Angell *et al.,* 1982,1983). The distortion of the tetrahedral network probably occurs mostly at relatively low pressures. Ohtani *et al.* (1985) see no evidence for the presence of octahedrally coordinated Al^{3+} in albite glasses quenched from different pressures up to 3 GPa but detect its presence at 6 GPa and above. These workers attribute compression below 3 GPa to distortion of the tetrahedral network. Above 25 GPa the compressibility of the molten silicate decreases suddenly, suggesting that a high pressure liquid structure has been attained. It is expected that, once the oxygen atoms in the liquid approach a densely packed state, a substantial stiffening of the melt will be attained and this may be contribute to the change above 25 GPa.

CONCLUSIONS

We have carried out shock wave experiments on a molten silicate to determine its density at elevated pressure. The basalt analog, $An_{0.36}Di_{0.64}$, undergoes relatively smooth compression to 25 GPa; above this pressure a marked lowering of the

compressibility occurs. A Birch-Murnaghan isentrope calculated from the Hugoniot data up to 25 GPa has a 1 atm bulk modulus, $K_S = 24.2$ GPa and its pressure derivative, $K' = 4.85$. This 1 atm bulk modulus is consistent with the value calculated by Rivers and Carmichael (1982) using their ultrasonic measurements on a slightly different composition.

Although calculated shock temperatures lie below those expected for the fusion curve of this composition over the pressure range of these experiments, crystallization is not expected to occur. Rather, it is believed that continuous compression of the melt structure occurs, involving rearrangement of the tetrahedral framework at low pressures and gradual changes in coordination, with continued increases in pressure until an arrangement is reached in which Al and Si are nearly entirely in octahedral coordination.

ACKNOWLEDGEMENTS

We appreciate the excellent technical assistance of E. Gelle, W. Ginn, C. Manning and M. Long in building and carrying out these experiments. E. Bus and W. Kershaw prepared many of the samples. This work was supported under NSF Grants EAR80-18819 and EAR84-07784. S.M. Rigden gratefully acknowledges the support of an IBM Pre Doctoral Fellowship during 1984/1985. This manuscript is to be submitted to *J. Geophys. Res.* with co-authors T.J. Ahrens and E.M. Stolper.

REFERENCES

Ahrens, T.J., J.H. Lower and P.L. Lagus, 1971. Equation of state of forsterite. *J. Geophys. Res., 76,* 514-528.

Ahrens, T.J., I. Jackson and R. Jeanloz, 1977. Shock compression and adiabatic release of a titaniferous mare basalt. *Proc. Lunar Sci. Conf. 8th,* 3437-3455.

Al'tshuler, L.V., 1965. Use of shock waves in high-pressure physics. *Sov. Phys. Usp., 85,* 52-91.

Angell, C.A. and H. Kanno, 1976. Density maxima in high-pressure supercooled water and liquid silicon dioxide. *Science, 193,* 1121-1122.

Angell, C.A., P.A. Cheeseman, and S. Tamaddon, 1982. Pressure enhancement of ion mobilities in liquid silicates from computer simulation studies to 800 kilobars. *Science, 218,* 885-887.

Angell, C.A., P. Cheeseman, and S. Tamaddon, 1983. Water-like transport property anomalies in liquid silicates investigated at high T and P by computer simulation techniques. *Bull. Mineral., 106,* 87-97.

Boslough, M.B., S.M. Rigden and T.J. Ahrens, 1986. Hugoniot equations of state of anorthite glass and lunar anorthosite. *Geophys. J. Roy. Astr. Soc.,* in press.

Bottinga, Y. and D.F. Weill, 1970. Densities of silicate liquid systems calculated from partial molar volumes of oxide components. *Am. J. Sci., 269,* 169-182.

Bottinga, Y. and D.F. Weill, 1972. The viscosity of magmatic silicate liquids: a model for calculation. *Am. J. Sci., 272,* 438-475.

Bottinga, Y., D. Weill and P. Richet, 1982. Density calculations for silicate liquids. I Revised method for aluminosilicate compositions. *Geochim. Cosmochim. Acta, 46,* 909-919.

Bottinga, Y., 1985. On the isothermal compressibility of silicate liquids at high pressure. *Earth Planet. Sci. Lett., 74,* 350-360.

Bowen, N.L., 1915. The crystallization of haplobasaltic, haplodioritic and related magmas. *Am. J. Sci., 40,* 161-185.

Chhabildas, L.C. and J.R. Asay, 1979. Rise time measurements of shock transitions in aluminum, copper and steel. *J. Appl. Phys., 50,* 2749-2756.

Cranmer, D., R. Salomaa, H. Yinnon and D.R. Uhlmann, 1981. Barrier to crystal nucleation in anorthite. *J. Non Cryst. Solids, 45,* 127-136.

Duvall, G.F. and G.R. Fowles, 1963. Shock waves in *High Pressure Physics and Chemistry,* R.S. Bradley, ed., Vol. 2, pp 209-291. Academic Press, N.Y.

Fujii, T. and I. Kushiro, 1977. Density, viscosity and compressibility of basaltic liquid at high pressures. *Carnegie Inst. Wash. Y'book, 76,* 419-424.

Goldsmith, J.R., 1980. The melting and breakdown reactions of anorthite at high pressures and temperatures. *Am. Mineral., 65,* 272-284.

Goto, T., G.R. Rossman and T.J. Ahrens, 1979. Absorption spectroscopy of solids under shock compression. *Proc. 6th AIRAPT International High Pressure Conference, High Pressure Science and Technology, Vol II,* K.D. Timmerhaus and M.S. Barker, eds., pp 895-904. Plenum Press.

Jackson, I. and T.J. Ahrens, 1979. Shock wave compression of single-crystal forsterite. *J. Geophys. Res., 84,* 3039-3048.

Jeanloz, R. and T.J. Ahrens, 1979. Release adiabat measurements on minerals: the effect of viscosity. *J. Geophys. Res., 84,* 7545-7547.

Jeanloz, R., and T.J. Ahrens, 1980. Anorthite: Thermal equation of state to high pressures. *Geophys. J. Roy. Astr. Soc., 62,* 529-549.

Kushiro, I., 1978. Viscosity and structural changes of albite ($NaAlSi_3O_8$) melt at high pressures. *Earth Planet. Sci. Lett., 41,* 87-90.

Kushiro, I., 1980. Viscosity, density and structure of silicate melts at high pressures, and their petrological applications in *Physics of Magmatic Processes,* R.B. Hargraves, ed., pp 93-120. Princeton University Press, Princeton, N.J.

Liu, L.-G., 1979. The System enstatite-wollastonite at high pressures and temperatures with emphasis on diopside. *Phys. Earth and Planet. Int., 19,* P15-P18.

Marsh, S.P., 1980. LASL Shock Hugoniot Data. University of California Press, Berkeley, 658 pp.

Matsui. Y. and K. Kawamura, 1980. Instantaneous structure of an $MgSiO_3$ melt by molecular dynamics. *Nature, 285,* 648-649.

Matsui, Y., K. Kawamura and Y. Syono, 1982. Molecular dynamics calculations applied to silicate systems: molten and vitreous $MgSiO_3$ and Mg_2SiO_4 under low and high pressures in *High Pressure Research in Geophysics.* S. Akimoto and M.H. Manghnani, eds., pp 511-524. Center for Academic Publications, Tokyo, Japan.

McQueen, R.J., S.P Marsh and J.N. Fritz, 1967. Hugoniot equation of state of twelve rocks. *J. Geophys. Res., 72,* 4999-5036.

McQueen, S.P., S.P. Marsh, J.W. Taylor, J.N. Fritz and W.J. Carter, 1970. The equation of state of solids from shock wave studies. in *High Pressure Impact Phenomena,* R. Kinslow, ed., pp 293-417, Academic Press, N.Y.

Melson, W.G. and G. Thompson, 1971. Petrology of a transform fault zone and adjacent ridge segments. *Phil. Trans. Roy. Soc. Lond., A268,* 423-441.

Mo, X., I.S.E. Carmichael, M. Rivers and J. Stebbins, 1982. The partial molar

volume of Fe_2O_3 in multicomponent silicate liquids and the pressure dependence of oxygen fugacity in magmas. *Min. Mag.,* 237-245.

Nelson, S.A. and I.S.E. Carmichael, 1979. Partial molar volumes of oxide components in silicate liquids. *Contrib. Mineral. Petrol., 71,* 117-124.

Nisbet, E.G. and D. Walker, 1982. Komatiites and the structure of the Archaean mantle. *Earth Planet. Sci. Lett., 60,* 105-113.

Ohtani, E. and M. Kumazawa, 1981. Melting of forsterite Mg_2SiO_4 up to 15 GPa. *Phys. Earth Planet. Int., 27,* 32-38.

Ohtani, E., 1984. Generation of komatiite magma and gravitational differentiation in the deep upper mantle. *Earth Planet. Sci. Lett., 67,* 261-272.

Ohtani, E., F. Taulelle and C.A. Angell, 1985. Al^{3+} coordination changes in liquid aluminosilicates under pressure. *Nature, 314,* 78-81.

Presnall, D.C., S.A. Dixon, J.R. Dixon, T.H. O'Donnell, N.L. Brenner, R.L. Schrock and D.W. Dycus, 1978. Liquidus phase relations on the join diopside-forsterite-anorthite from 1 atm to 20 kbar: their bearing on the generation and crystallization of basaltic magma. *Contr. Mineral. Petrol., 66,* 203-220.

Rai, C.S., M.H. Manghnani and K.W. Katahara, 1981. Ultrasonic studies on a basalt melt. *Geophys. Res. Lett., 8,* 1215-1218.

Rice, M.H., R.G. McQueen and J.M. Walsh, 1958. Compression of solids using strong shock waves, in *Solid State Physics,* vol. 6. F. Seitz and D. Turnbull, eds., pp 1-63, Academic Press, N.Y.

Rigden, S.M., T.J. Ahrens and E.M. Stolper, 1984. Densities of liquid silicates at high pressures. *Science, 226,* 1071-1074.

Rivers, M., 1985. Ultrasonic studies of silicate liquids. PhD Dissertation, University of

California, Berkeley.

Rivers, M., and I.S.E. Carmichael, 1982. Ultrasonic velocity and attenuation of liquids in the system $NaAlSi_3O_8$–$CaAl_2Si_2O_8$–$CaMgSi_2O_6$. *EOS (Transactions of the AGU), 63,* 1136.

Robie, R.A., B.S. Hemingway and J.R. Fisher, 1978. Thermodynamic Properties of Minerals and Related Substances at 298.15 K and 1 Bar (10^5 Pascals) Pressure and Higher Temperatures. *Geol. Soc. Amer. Bull., 1452.*

Scarfe, C.M., B.O. Mysen, and D. Virgo, 1979. Changes in viscosity and density of melts of sodium disilicate, sodium metasilicate and diopside composition with pressure. *Carnegie Inst. Wash. Y'book, 78,* 547-551.

Sharpe, R., T.N. Irvine, B.O. Mysen and R.M. Hazen, 1983. Density and viscosity of melts of Bushveld Chilled Margin rocks. *Carnegie Inst. Wash. Y'book, 82,* 300-305.

Stebbins, J.R., I.S.E. Carmichael and L.K. Moret, 1984. Heat capacities and entropies of silicate liquids and glasses. *Contrib. Mineral. Petrol., 86,* 131-148.

Stolper, E.M., D. Walker, B.H. Hager and J.F. Hays, 1981. Melt segregation from partially molten source regions: The importance of melt density and source region size. *J. Geophys. Res., 86,* 6261-6271.

Svendsen, B., and T.J. Ahrens, 1983. Dynamic compression of diopside and salite to 200 GPa. *Geophys. Res. Lett., 10,* 501-504.

Touloukian, Y.S., R.K. Kirby, R.E. Taylor, and P.D. Desai, 1970. *Thermal Expansion of Metallic Elements and Alloys.* Plenum, New York.

Uhlmann, D.R. and L.C. Klein, 1976. Crystallization kinetics, viscous flow and thermal histories of lunar breccias 15286 and 15498. *Proc. Lunar Sci. Conf. 7th,*

2529-2541.

Uhlmann, D.R., P.I.K. Onoroto and G.W. Sheer, 1979. A simplified model for glass formation. *Proc. Lunar and Planet. Sci. Conf. 10th,* 375-381.

Uhlmann, D.R., H. Yinnon and C.Y. Fang, 1981. Simplified model evaluation of cooling rates for glass-containing lunar compositions. *Proc. Lunar and Planet. Sci. Conf. 12B,* 281-288.

Weill, D.F., R. Hon and A. Navrotsky, 1980. The igneous system $CaMgSi_2O_6$ – $CaAl_2Si_2O_8$ – $NaAlSi_3O_8$: variations on a classic them by Bowen, in *Physics of Magmatic Processes,* R.B. Hargraves, ed., pp 49-92, Princeton University Press, Princeton, N.J.

Table 1: Sample and Natural Basalt Compositions

	Average of 8 Analyses[1] Wt%	Ideal Composition Wt%	Average MAR Basalt[2] Wt%
SiO_2	50.5±0.5	50.34	49.21
TiO_2			1.39
Al_2O_3	15.4±0.8	15.38	15.81
FeO			9.18
MnO			0.16
MgO	10.5±1.0	10.80	8.53
CaO	23.9±0.3	23.48	11.14
Na_2O			2.71
K_2O			0.26
P_2O_5			0.15
Total	100.3	100.00	100.54

[1] Analyzed by electron microprobe

[2] Average Mid-Atlantic Ridge basalt, Melson and Thompson (1971)

Table 2: Molybdenum Equation of State Parameters

Parameters used to calculate high temperature Hugoniot

$\rho_o = 10.182$ g cm^{-3} [1]
$\alpha = 2.07 \times 10^{-5}$ K^{-1} [2]
$\gamma_o = 1.52$ [3]
c $= 5.14$ km sec^{-1} [4a]
s $= 1.22$ [4a]
$C_P = 34.139 - 4.4926 \times 10^{-3}\,T + 3.7012 \times 10^{-6}T^2 - 1.5722 \times 10^{2}T^{-0.5}$ [5]

Calculated Hugoniot at 1300 K [6]

$\rho_o = 9.973$ gcm^{-3}
c $= 5.06$ km sec^{-1}
s $= 1.24$

Measured Hugoniot at 1300 K

$U_S = 5.33 \pm 0.10$ km sec^{-1} [1]
$U_P = 0.219 \pm 0.003$ km sec^{-1} [1]
$P_H = 11.63 \pm 0.25$ GPa [7]
$\rho_H = 10.400 \pm 0.014$ g cm^{-1} [7]

[1] measured
[2] Touloukian *et al.* (1970)
[3] McQueen *et al.* (1970)
[4] Robie *et al.* (1978)
[5] Marsh (1980)
[6] Calculated as described in text.
[7] Calculated from Rankine-Hugoniot equations
[a] coefficients in the equation $U_S = c + U_P s$

Table 3: Molten $An_{0.36}Di_{0.64}$ Hugoniot Data (T_o=1673 K, ρ_0=2.607 Mg m^{-3} [1])

Shot#	Flyer Plate	Impact[2] Velocity (km sec^{-1})	Shock[3] Velocity (km sec^{-1})	Particle[3] Velocity (km sec^{-1})	Hugoniot[3] Pressure (GPa)	Hugoniot[3] Density (Mg m^{-3})
592	Al	1.05 ±0.03	3.75 ±0.06	0.44 ±0.02	4.3 ±0.2	2.951 ±0.027
593	Al	1.50 ±0.02	3.79 ±0.06	0.65 ±0.01	6.4 ±0.2	3.141 ±0.029
605	Al	2.00 ±0.05	4.26 ±0.15	0.87 ±0.03	9.7 ±0.4	3.275 ±0.041
627	Cu	1.69 ±0.03	4.79 ±0.06	1.22 ±0.03	15.3 ±0.4	3.495 ±0.030
607	W	1.80 ±0.04	5.38 ±0.06	1.72 ±0.05	24.2 ±0.7	3.832 ±0.033
654	W	2.04 ±0.05	5.85 ±0.08	1.92 ±0.06	29.4 ±0.9	3.882 ±0.038
628	W	2.22 ±0.05	6.28 ±0.08	2.06 ±0.06	33.9 ±1.0	3.883 ±0.036

[1]Stebbins *et al.* (1984)
[2] measured
[3] calculated

FIGURE CAPTIONS

Figure 1: Schematic cross section through the molybdenum/silicate sample assembly. The base constructed in one piece and a thin (0.75 mm) cap is welded onto the base using an electron beam welding technique. Surfaces A and B are polished to a mirror finish. Light reflected from these polished surfaces during the course of the experiment is detected by a streak camera. A Pt-Pt10%Rh thermocouple is pressed into the driver plate (surface A) close to the top of the sample.

Figure 2: Photograph of a sample assembly in the impact tank. The brass termination block of the copper coaxial cable is used to hold the ceramic target plate. The sample assembly is aligned with the barrel of the gun (visible at far right). The copper heating coil, sheathed thermocouple and turning mirror mounted on a ceramic pedestal are visible behind the sample. A ceramic shutter activated by a compressed air cylinder protects the mirror until just before the shot is fired.

Figure 3: Schematic downward-looking cross-sectional view of some important features of the molten silicate equation of state experiment. Three lasers (I, II, and III) across the barrel are used to initiate trigger signals to x-ray source and xenon flash lamp. The double flash x-ray sources form a dual image of the projectile enroute to the target on x-ray film; this is used to calculate the projectile velocity and also shows whether target movement has occurred during heating. A second estimate

of projectile velocity is made by recording travel times between lasers I, II and III. A turning mirror mounted on a ceramic pedestal behind the target is protected during sample heating by a ceramic shutter; this is withdrawn immediately prior to firing the gun. The xenon flash lamp illuminates the target; light is focussed onto the target and reflected from the polished rear surfaces of the sample assembly via the turning mirror, a 305 mm - f 2.5 Kodak Aero-Ektar objective lens and field mirror to the streak camera.

Figure 4: Streak record from molten silicate shock wave experiment.

(a) Cutaway view of the sample. Before passage of the shock wave through the reflective surfaces, light is reflected continuously from the rear of the sample. A change of reflectivity as the shock wave exits the metal driver plate (at the same time entering the sample) is detected by the streak camera. A similar change occurs as the shock wave exits the sample assembly. An idealized streak record is superimposed on the sample cutaway view.

(b) An actual streak record from a typical experiment (Shot # 607). The time (t_1-t_o) represents the transit time of the shock wave through the silicate sample and molybdenum cover plate.

Figure 5: X-ray shadowgraph of typical molten silicate equation of state experiment used to measure projectile velocity (Shot # 592). The shadowgraph shows a double exposure of the projectile carrying a metal flyer plate during its flight towards

the sample. The target assembly can also be seen. Shadow images of the sample, coil, mirror, and thermocouple are visible to the left of the projectile.

Figure 6: Result of shock wave equation of state experiment on molybdenum initially at 1273K. Two calculated Hugoniot curves (see text) centered at 1273 K are also shown assuming $\gamma = 1.52$ and $\gamma/V = \text{const}$, $\gamma_0 = 1.52$. The experimental point can be fit by the calculated curve barely within experimental error. The effect of the differing assumptions about γ is minor. The Hugoniot for molybdenum centered at room temperature is also shown (equation of state parameters are from Marsh, 1980).

Figure 7: Method for data reduction of molten silicate equation of state experiments. The solid curves represent the direct and reflection Hugoniots of molybdenum at high temperature. Pressures at a given volume are calculated via equation (3) in the text and particle and shock velocities derived via the Rankine-Hugoniot equation. In this figure a molybdenum flyer plate is assumed. The initial estimate of shock velocity in the molten silicate (equation 4) allows an impedance match solution of the sample shock state (dashed line intersection with Mo reflection Hugoniot, state S_1). Assuming the release state in the sample lies along this straight line "sample reflection Hugoniot," an estimate of the shock state in the Mo cap is made by impedance match (Equation 8). Subsequent estimates of sample shock velocity yielding states $S_{2,3,...n}$ and shock states in the Mo cap ($C_{2,3...n-1}$) are indicated by the dash-dot lines and do not change within the experimental uncertainties.

Figure 8: Results of equation of state experiments on molten silicate shown in the shock velocity - particle velocity plane with linear fits to the low- and high- pressure data. Below $\sim$ 25 GPa: $U_S = 3.06 + 1.36\ U_P$ km sec^{-1}, $r^2 = 0.99$. At pressures higher than $\sim$ 25 GPa: $U_S = 0.85 + 2.63\ U_P$ $kmsec^{-1}$, $r^2 = 1.00$.

Figure 9: Results of equation of state experiments on molten silicate shown in the pressure density plane. Best fit Hugoniot and Birch-Murnaghan isentrope are shown for the data up to 25 GPa. The isentrope is centered at 1673 K with $K_S = 24.2$ GPa and $K' = 4.85$. The dashed curve is a calculated solid (T_0=300 K) Hugoniot based on the experimentally determined Hugoniots for diopside and anorthite.

Figure 10: Calculated shock temperatures for $An_{0.36}Di_{0.64}$ with $T_0 = 1673$ K. The liquidus temperature for this composition is also shown up to 2 GPa (after Presnall *et al.*, 1978). The two shock temperature curves are calculated assuming $\gamma = 0.3$ constant and γ/V = constant, $\gamma_0 = 0.3$.

Figure 11: Comparison of estimated shock rise times with critical cooling time for glass formation from the theory of transformation kinetics. Stippled field encompasses time-temperature-transformation (TTT) curves for formation of lunar glasses taken from the literature (Uhlmann and Klein, 1976; Uhlmann *et al.*, 1981). Also shown is a TTT curve for anorthite glass (Cranmer *et al.*, 1981). The value of τ_{NOSE}

(1 atm) for $An_{0.36}Di_{0.64}$ was calculated using the simplified model of Uhlmann *et al.*, 1979. The value of τ_{NOSE} (20 GPa) represents a likely minimum estimate as described in the text. Shock rise times are calculated as described in the text for 3 P $< \eta <$ 30 P. Shock temperatures at different pressures are derived from Fig. 9. Shock rise times are more than 5 orders of magnitude less than the critical cooling time for glass formation at 20 GPa, suggesting that crystallization is not expected to occur under shock conditions.

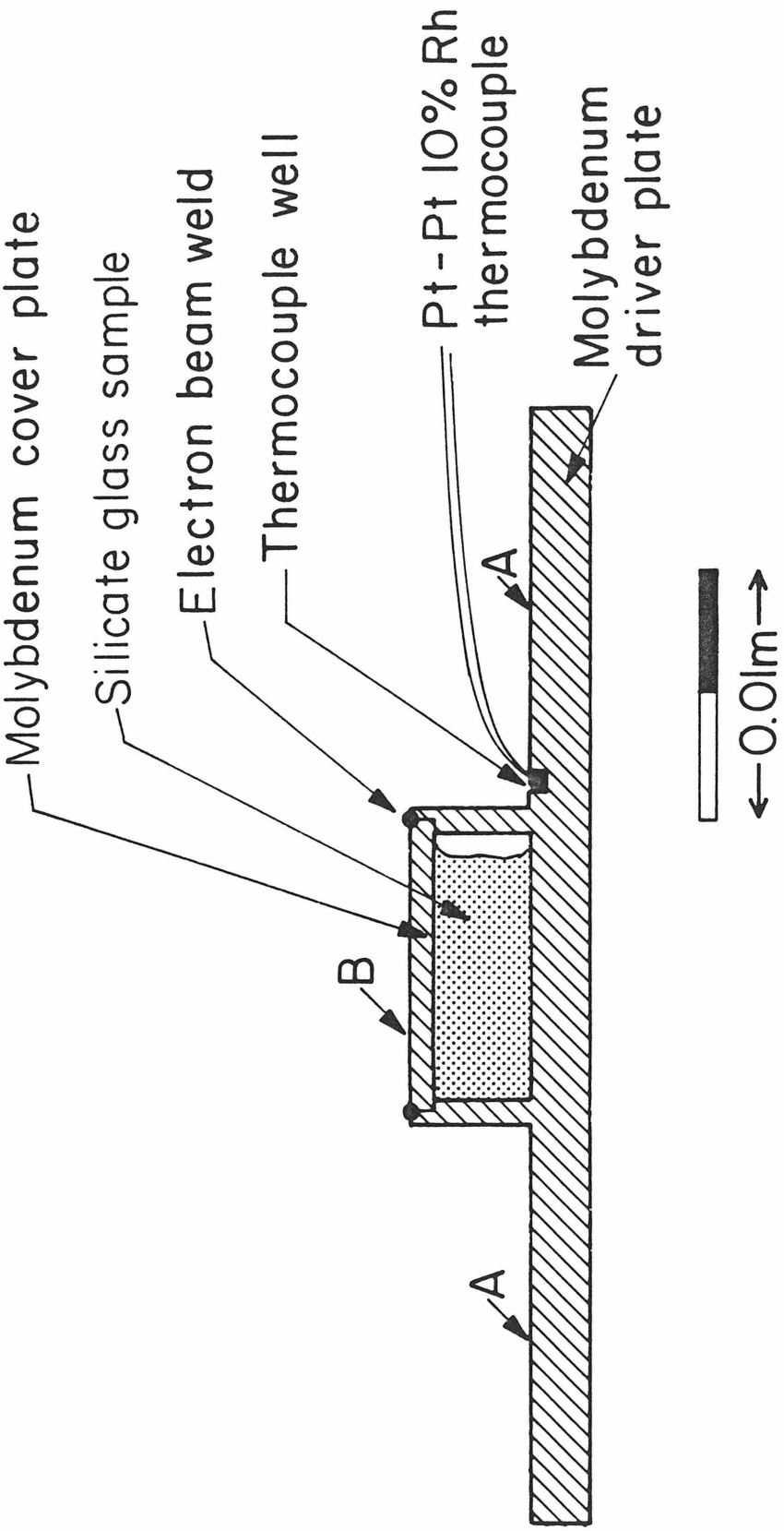
Molybdenum cover plate
Silicate glass sample
Electron beam weld
Thermocouple well
Pt-Pt 10% Rh thermocouple
Molybdenum driver plate
A
B
A
0.01m

Figure 1

Figure 2

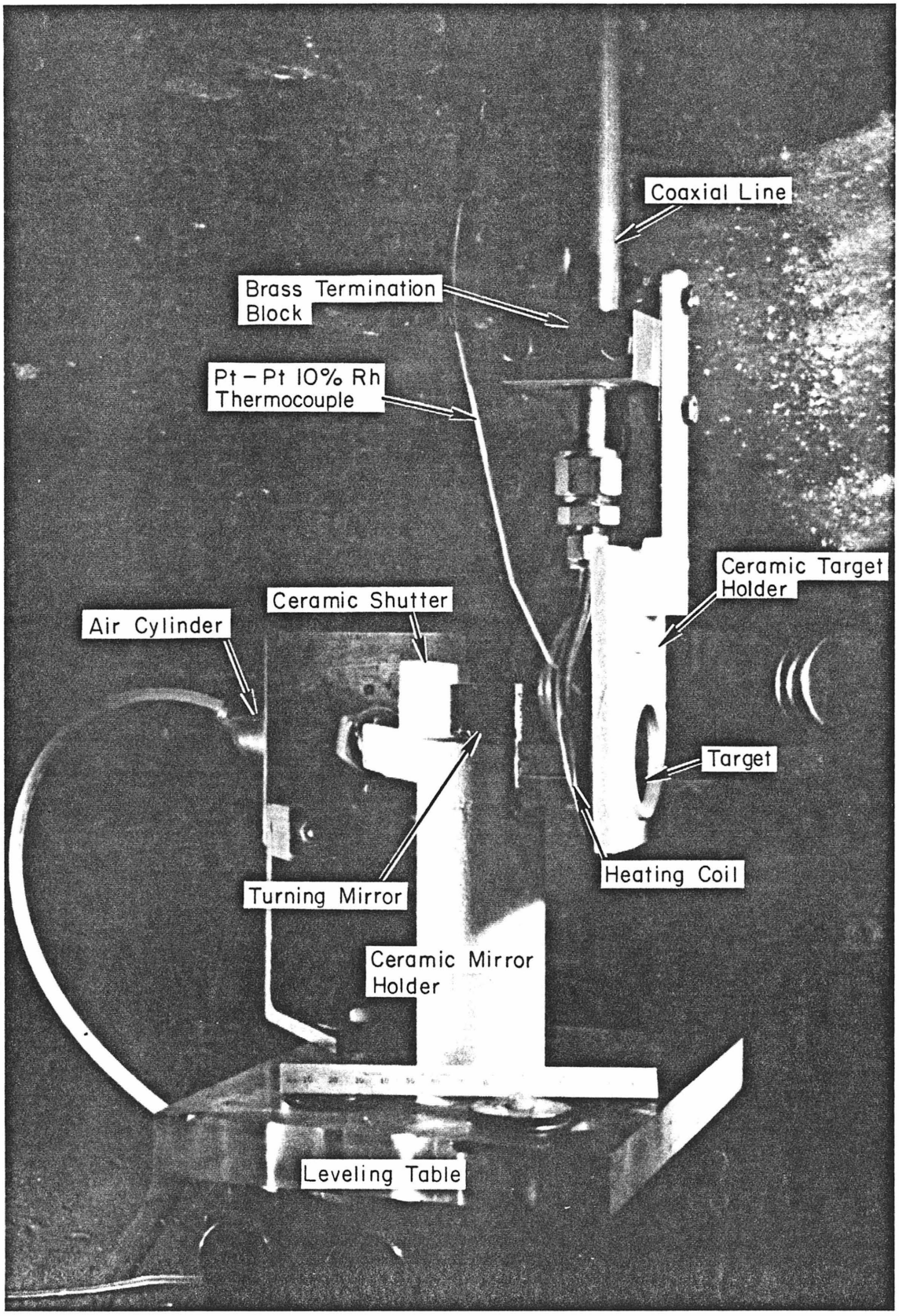
Coaxial Line
Brass Termination Block
Pt – Pt 10% Rh Thermocouple
Ceramic Target Holder
Ceramic Shutter
Air Cylinder
Target
Heating Coil
Turning Mirror
Ceramic Mirror Holder
Leveling Table

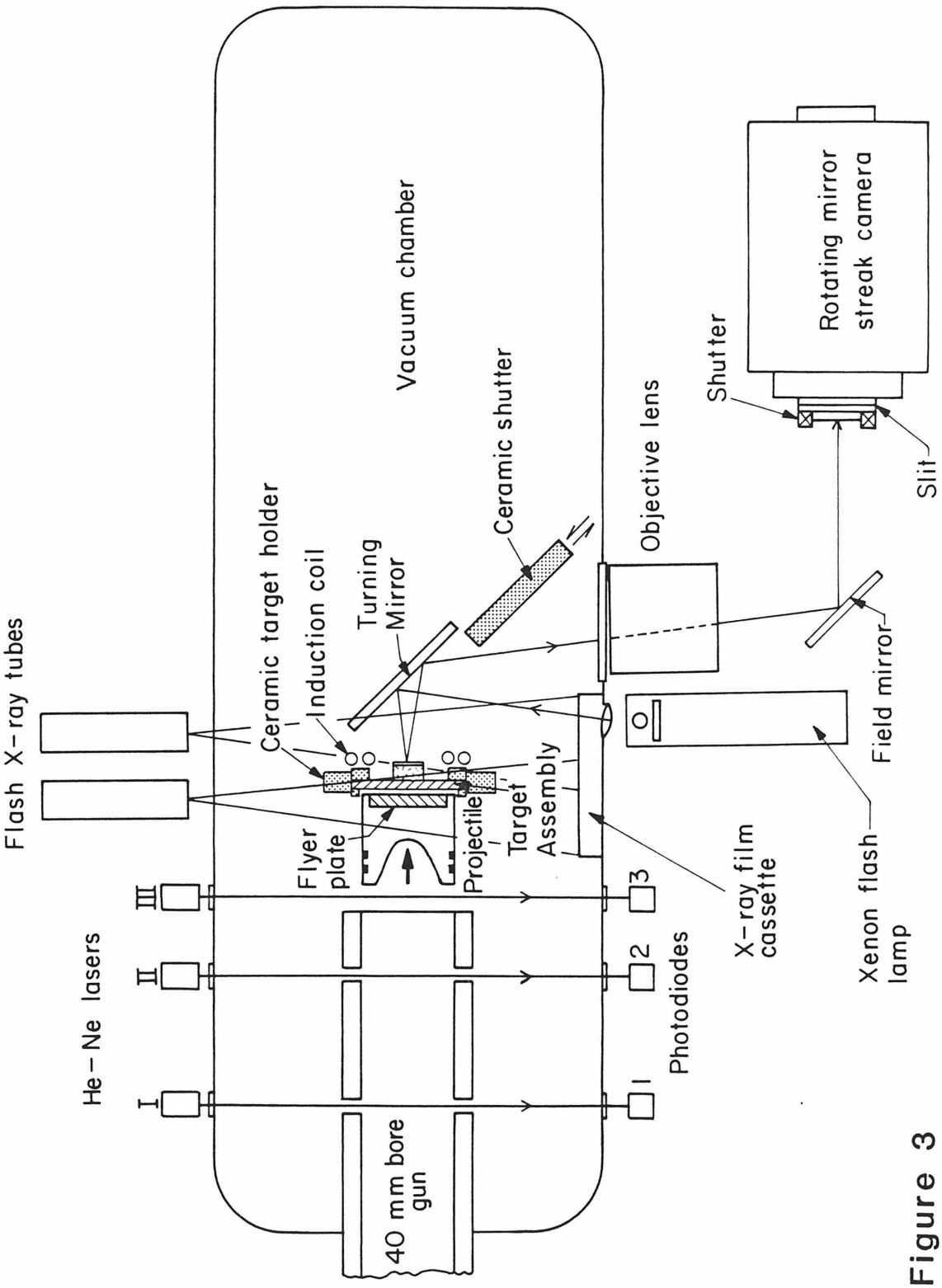
Flash X-ray tubes
He-Ne lasers
I
II
III
1
2
3
Photodiodes
40 mm bore gun
Vacuum chamber
Ceramic target holder
Induction coil
Turning Mirror
Ceramic shutter
Flyer plate
Projectile
Target Assembly
X-ray film cassette
Objective lens
Shutter
Rotating mirror streak camera
Slit
Field mirror
Xenon flash lamp

Figure 3

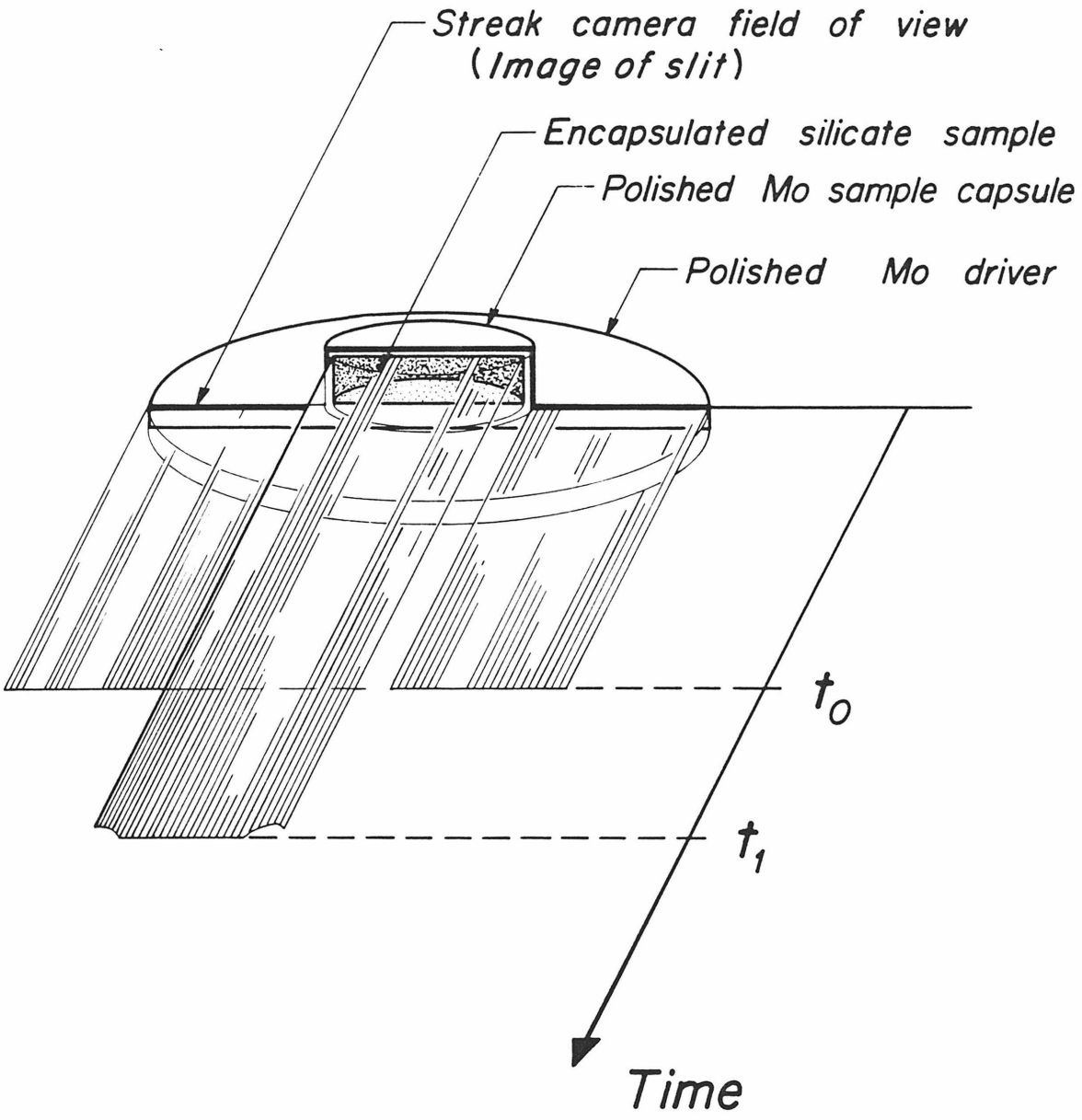
Streak camera field of view
(Image of slit)
Encapsulated silicate sample
Polished Mo sample capsule
Polished Mo driver
t_0
t_1
Time

Figure 4a

Figure 4b

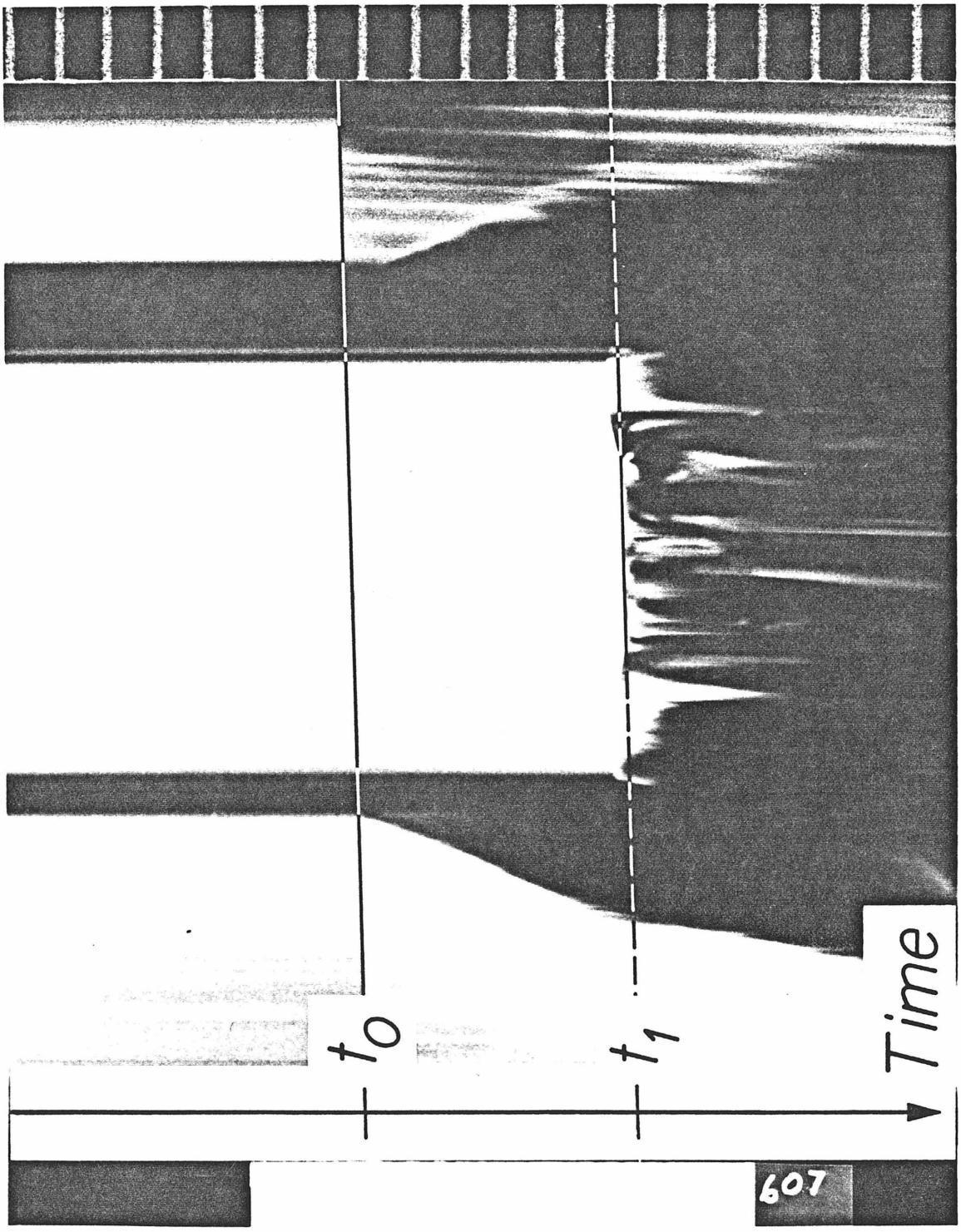

Figure 5

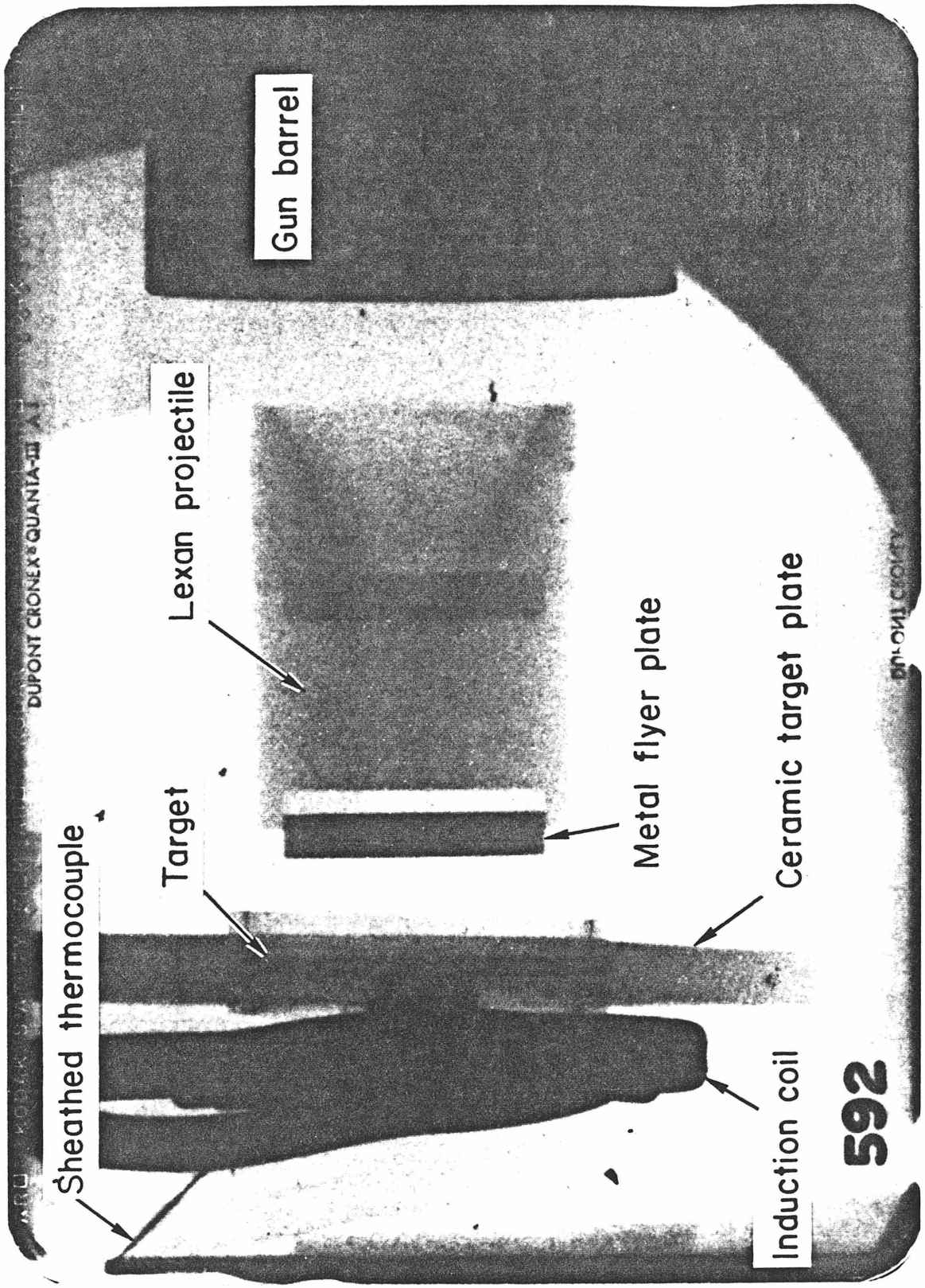
Gun barrel
Lexan projectile
Target
Sheathed thermocouple
Metal flyer plate
Ceramic target plate
Induction coil
592

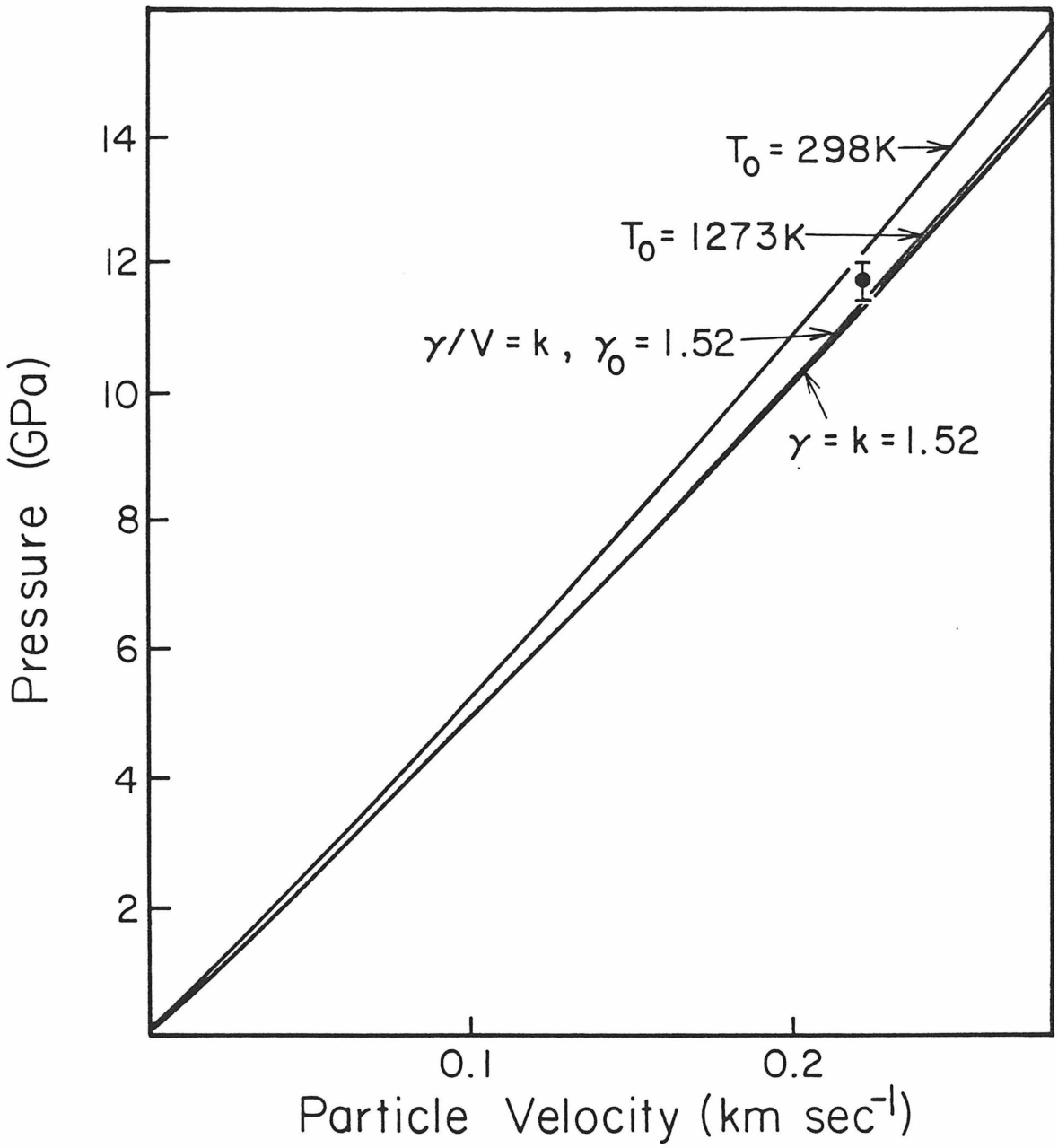
Pressure (GPa)
14
12
10
8
6
4
2
0.1
0.2
Particle Velocity (km sec^{-1})
T_0 = 298K
T_0 = 1273K
$\gamma/V = k$, $\gamma_0 = 1.52$
$\gamma = k = 1.52$

Figure 6

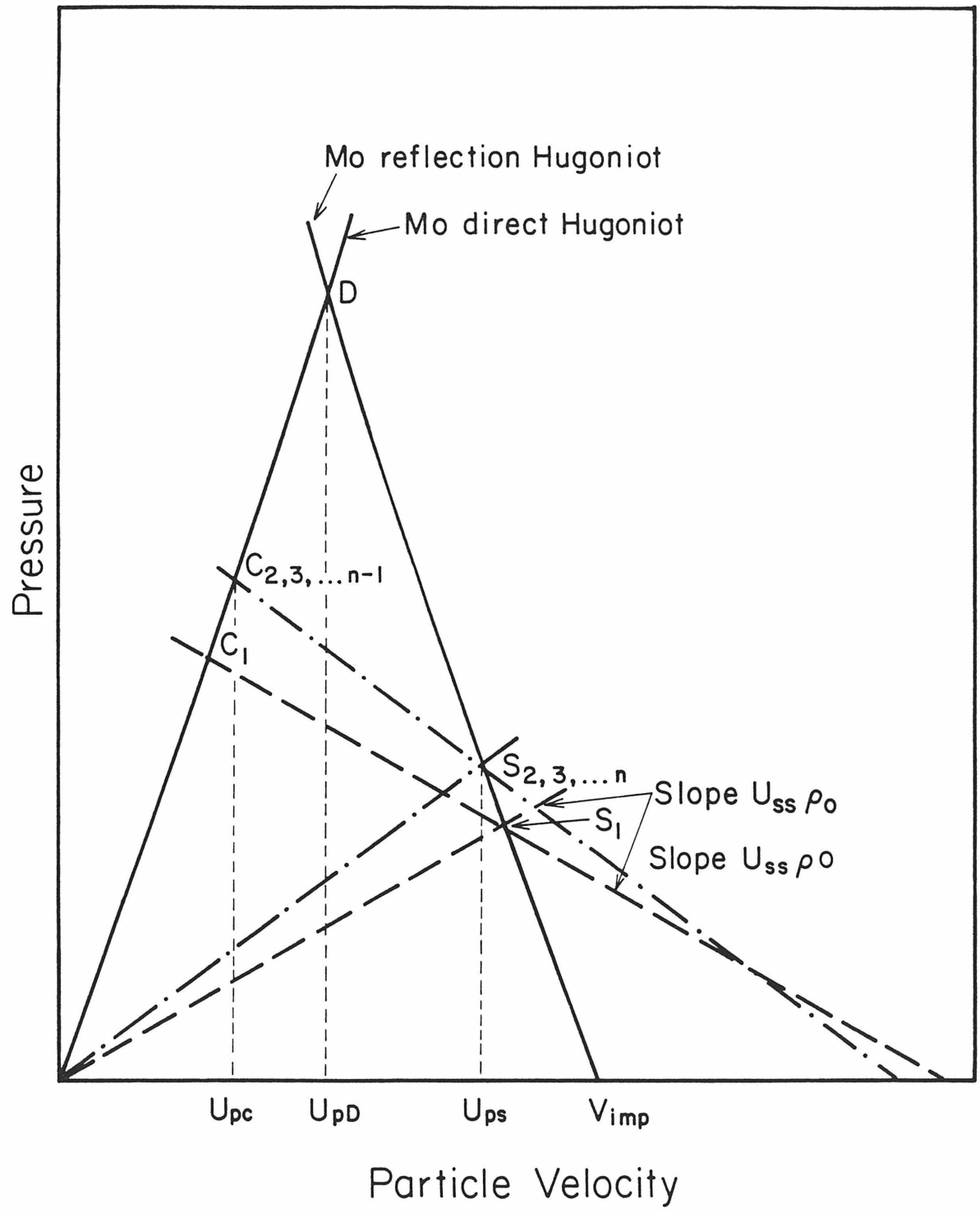
Mo reflection Hugoniot
Mo direct Hugoniot
D
Pressure
$C_{2,3,\ldots n-1}$
C_1
$S_{2,3,\ldots n}$
Slope $U_{ss}\rho_o$
S_1
Slope $U_{ss}\rho o$
U_{pc}
U_{pD}
U_{ps}
V_{imp}
Particle Velocity

Figure 7

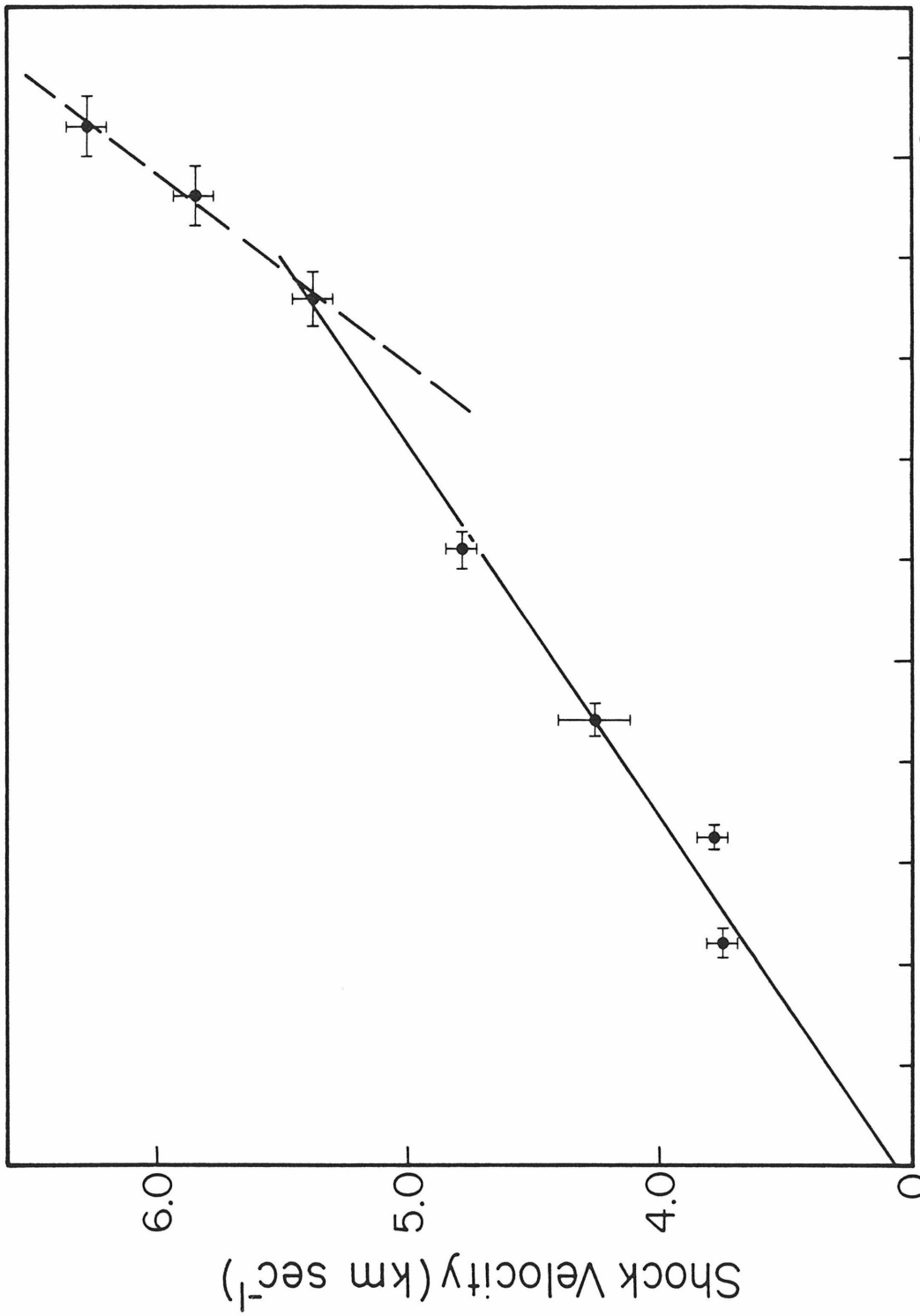
Shock Velocity (km sec^{-1})
6.0
5.0
4.0
0
1.0
2.0
Particle Velocity (km sec^{-1})

Figure 8

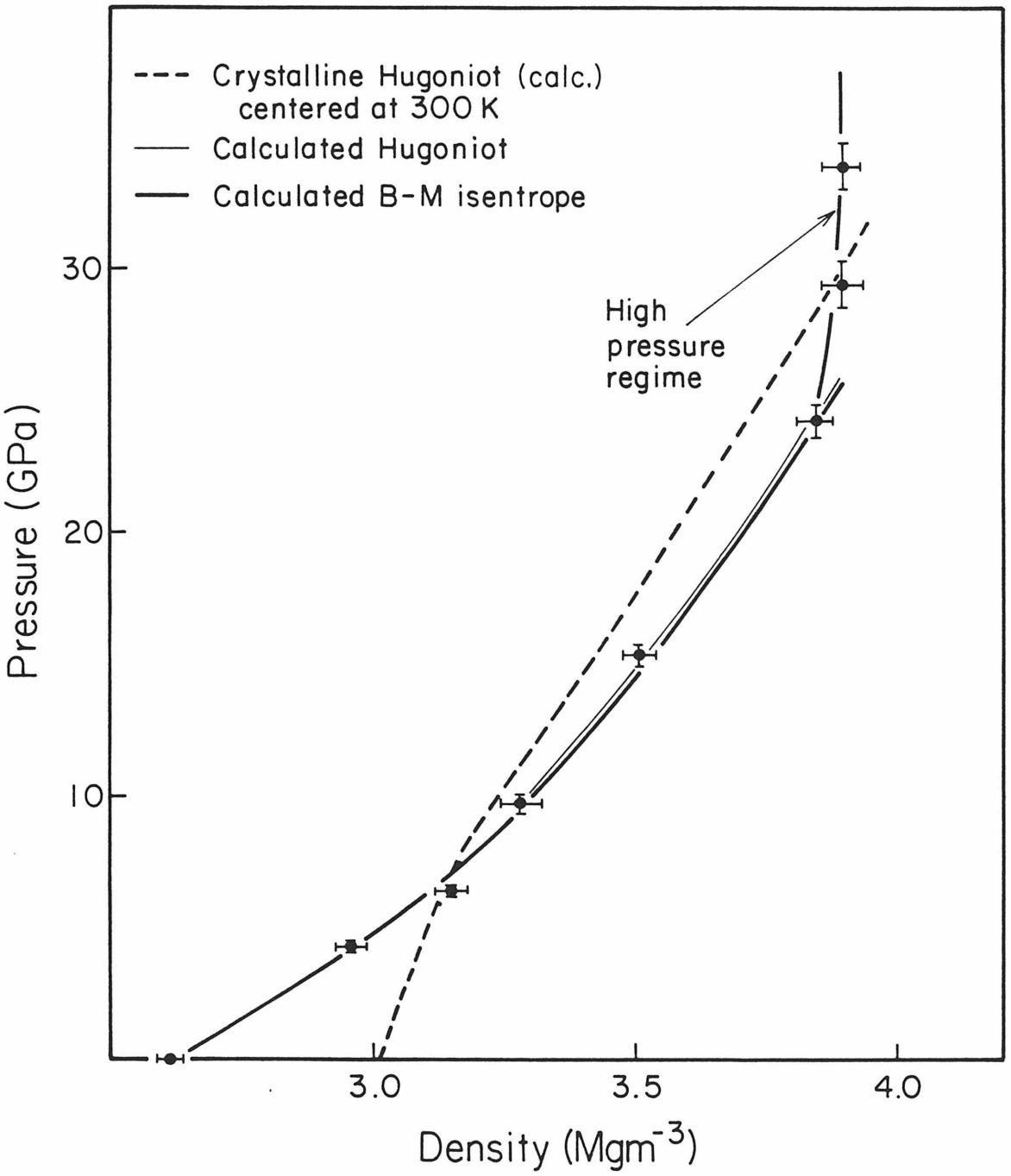
Crystalline Hugoniot (calc.)
centered at 300 K
Calculated Hugoniot
Calculated B-M isentrope
High
pressure
regime
Pressure (GPa)
10
20
30
3.0
3.5
4.0
Density (Mgm^{-3})

Figure 9

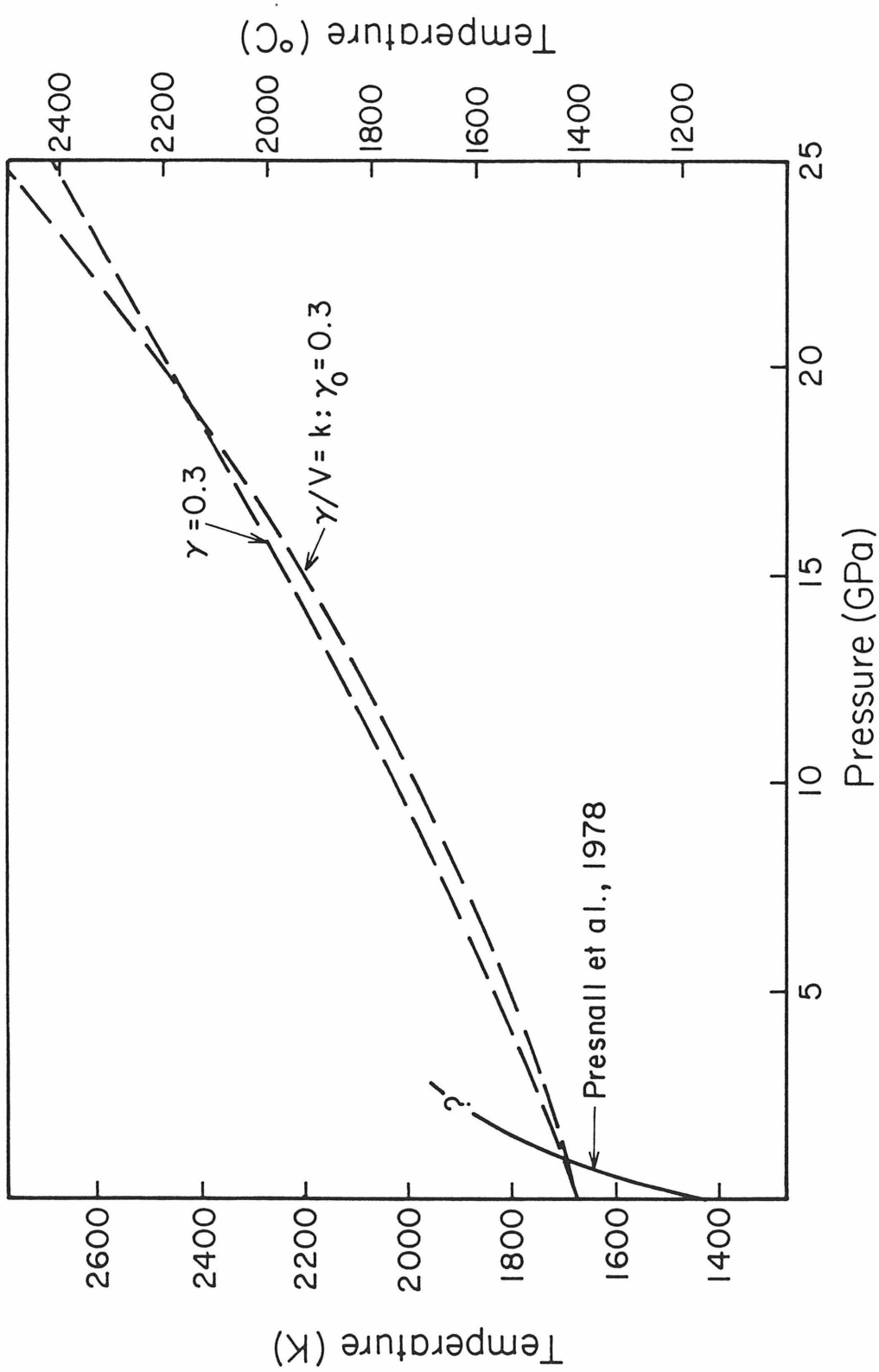
Temperature (°C)
2400
2200
2000
1800
1600
1400
1200
25
20
15
10
5
Pressure (GPa)
Temperature (K)
2600
2400
2200
2000
1800
1600
1400
γ=0.3
γ/V= k: γ₀=0.3
?
Presnall et al., 1978

Figure 10

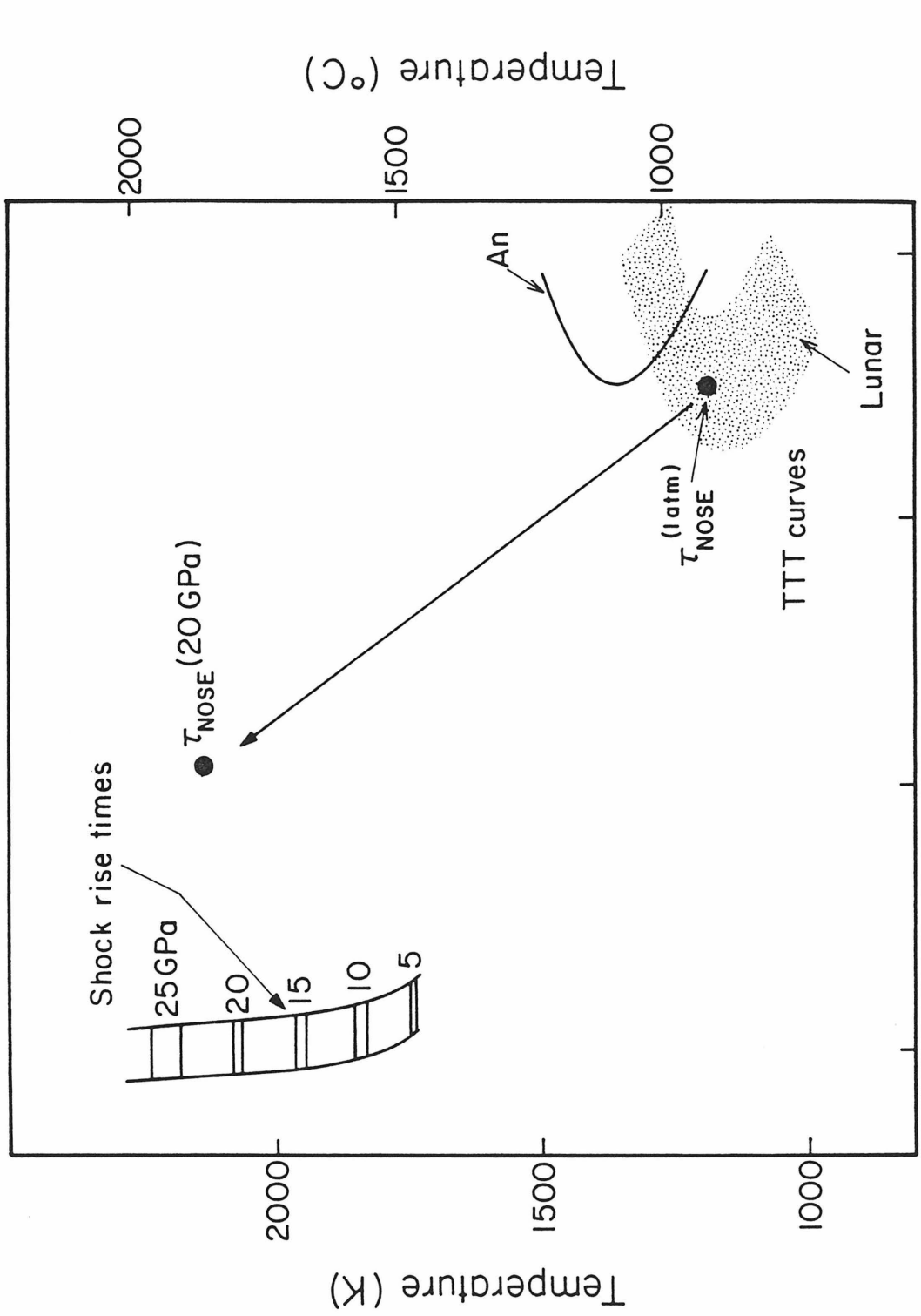
Temperature (°C)
2000
1500
1000
An
Lunar
TTT curves
$\tau_{NOSE}^{(1atm)}$
τ_{NOSE}(20 GPa)
Shock rise times
25 GPa
20
15
10
5
Temperature (K)
2000
1500
1000
-10
-5
0
5
Time (log sec)

Figure 11

Chapter 3

High Pressure Equation of State of Molten Anorthite ($CaAl_2Si_2O_8$) and Diopside ($CaMgSi_2O_6$)

ABSTRACT

We have measured the Hugoniot equation of state of molten diopside and molten anorthite. The diopside data are described by a straight line fit to the shock velocity-particle velocity results of $U_S = 3.30 + 1.44\ U_P$ km sec^{-1}, and our preferred fit to the anorthite data is given by $U_S = 2.86 + 1.42\ U_P$ km sec^{-1}. Reduction of our shock wave data to a third-order Birch-Murnaghan isentrope using a Mie-Gruneisen equation of state gives $K_S = 22.4$ GPa and $K' = 6.9$ for diopside. For anorthite we calculate $K_S = 17.9$ GPa and $K' = 5.3$. Our equation of state data for molten diopside can be used to constrain the diopside solidus at high pressures. We expect a marked shallowing of the solidus above $\sim$ 10 GPa but in the absence of data on the variation of heat capacity and thermal expansion at elevated pressures are unable to specify solidus temperatures. Comparison of these data with those of Rigden *et al.* (1986) for a composition intermediate between anorthite and diopside suggests that these liquids mix

ideally with respect to volume up to $\sim$ 40 GPa. Changes in coordination of Al and Si from tetrahedral at low pressures to octahedral at high pressures are believed to occur gradually within the resolution of our data. Although 1 atm bulk moduli for a wide compositional range of silicate melts are similar, the variation in integrated compression to high pressures as reflected in both K and K′ is primarily related to the proportion of tetrahedrally (Al^{3+}, Si^{4+}, Fe^{3+}) coordinated cations in the melt at 1 atm.

INTRODUCTION

Clinopyroxene and plagioclase are important constituents of igneous rocks found at the earth's surface. In normative terms they comprise about 50% of common basaltic rocks. Thus, the properties of these endmember components and their mixing behaviors can be expected to provide useful insights into those factors influencing the petrogenesis of basic to ultrabasic magmas deep within the earth and other planets. The density of magma at depth may have an especially strong influence on petrogenesis because this controls not only the rate of magma migration, and hence the opportunity for fractionation and for interaction with country rocks, but also the direction in which magmas will move (Walker *et al.,* 1978; Stolper *et al.,* 1981).

The comparison between the behavior of diopsidic liquid, which contains no alumina, and anorthitic liquid, which is rich in alumina, may provide insight into the structural role played by aluminum in silicate melts. In particular, the expected change from tetrahedral to octahedral coordination of Al^{3+} by oxygen (e.g., Waff, 1975) at significantly lower pressures than the equivalent change for Si^{4+} (Angell *et*

al., 1982, 1983; Matsui *et al.*, 1982) might manifest itself in higher low-pressure compressibilities of Al-rich melts and different density systematics with increasing pressure.

The density of a substance is a direct reflection of its molecular structure, integrated over macroscopic dimensions. By studying the variations in density of individual liquid compositions at constant pressure, it may be possible to infer aspects of melt structure. At pressures of several tens of GPa, the volumes of crystalline materials of geological interest can be modelled as if they were ideal mixtures of dense oxides (e.g. McQueen *et al.*, 1967; Boslough *et al.*, 1986), implying that their molecular-level structures are simply related to such oxides. A key question addressable with knowledge of liquid silicate equations of state is whether melts display an analogous correlation with closely packed volumes and structures.

In this paper we report the results of shock wave equation of state experiments for molten diopside between 8.5 and 39 GPa and for molten anorthite between 9 and 35 GPa. These data are compared with previous results on a composition intermediate between these two end-members, the 1 atm anorthite-diopside eutectic (36 mole % $CaAl_2Si_2O_8$, 64 mole % $CaMgSi_2O_6$: Rigden *et al.*, 1984; 1986). Using the experimental results on the equation of state of molten anorthite and diopside we are able to: (1) place constraints on the solidus of diopside to high pressures; (2) investigate the degree of ideal mixing in molten silicates at high pressures; and (3) consider how changes in ion coordination affect the integrated compressibility for molten silicates.

EXPERIMENTAL TECHNIQUE

Samples of diopsidic glass were prepared from MgO, $CaCO_3$ and SiO_2. These components were weighed out in appropriate proportions to make 5 g of sample and ground together in an agate mortar under alcohol for 5 hours. This mixture was placed in a Pt crucible and heated from 1173 K to 1723 K over two hours in a muffle furnace to decarbonate and melt the sample. The resultant glass was heated again to 1773 K under a vacuum of $\sim$100 μm for 24 hours. The glass was quenched by removing from the furnace and was immediately placed in a box furnace to anneal for several days at 923 K. Homogeneous, bubble-free anorthite glass (Boslough *et al.*, 1986) was obtained from Corning Glass Co. (Corning, N.Y.). The composition, $An_{99.5}Ab_{0.4}Or_{0.1}$, is close to that of pure anorthite. Average microprobe analyses of both compositions are given in Table 1 for comparison with the theoretical compositions.

Discs of both samples were cored from the prepared glasses and electron-beam welded into molybdenum capsules as described by Rigden *et al.* (1986). The diopside-bearing capsules were heated to 1723 K in a muffle furnace under a nitrogen atmosphere to check the integrity of the weld. Because of the high melting point of anorthite (1826 K), this procedure was not possible with the anorthite-bearing capsules. Anorthite-bearing capsules were preheated to 1926 K in the vacuum tank of the 40 mm gun prior to firing the gun, cooled to $<$673 K and observed on a screen mounted outside the impact tank. In this step we were able to check whether the sample had leaked, indicating a faulty weld, and whether the sample had moved in its ceramic holder, a concern because of the high temperatures required for this experiment. Test samples that were removed from the vacuum chamber after this step and

cross-sectioned contained clear, bubble-free glass.

Shock wave experiments to measure the density of molten diopside and anorthite at high pressures were carried out in a 40 mm propellant gun using the techniques of Rigden *et al.* (1986). Silicate samples contained in molybdenum capsules were suspended in the impact tank of the 40 mm gun and heated by induction under a vacuum of $\sim$100 μm to temperatures $\sim$100 K above their melting points. High pressures are generated in the sample by impact of a metallic flyer plate travelling at velocities of up to 2.5 km/sec. Measurement of the projectile velocity and the velocity of the shock wave that is generated in the sample allows determination of the pressure-density state in the sample by application of the Rankine-Hugoniot conservation equations (Rigden *et al.*, 1986).

RESULTS

The results of shock wave equation of state experiments on 5 samples of molten diopside and 6 samples of molten anorthite are given in Tables 2 and 3 and shown in Figures 1-4. Also shown in Figures 3 and 4 are data from crystalline anorthosite (McQueen *et al.*, 1967), anorthite glass (Boslough *et al.*, 1986) and crystalline diopside (Ahrens *et al.*, 1966; Svendson and Ahrens, 1983). Both sets of data are plotted in the shock velocity - particle velocity (U_S–U_P) plane in Figures 1 and 2. The diopside data are fit by a straight line given by $U_S = 3.30 + 1.44\ U_P$ km sec^{-1} with $r^2 = 0.99$. Two fits of the anorthite data are shown. The first, $U_S = 2.86 + 1.42\ U_P$ km sec^{-1}, $r^2 = 0.99$, does not include the highest pressure point. When all the data are fit, the resultant line is given by $U_S = 2.85 + 1.27\ U_P$ km sec^{-1}, $r^2 = 0.98$.

The Hugoniot density-pressure (ρ – P) curves (Figures 3 and 4) calculated from the straight line U_S – U_P fits to the experimental data (Figures 1 and 2) appear compatible with gradual compression without large jumps in density. By comparison, the crystalline anorthite Hugoniot shows a mixed phase region above ~10 GPa. Crystalline diopside does not show any phase changes along the Hugoniot in the pressure range of our experiments and is considerably less compressible than molten diopside as shown by the steepness of its compression curve.

Using the experimental data along the Hugoniot and assuming a Mie-Gruneisen equation of state we have fit the isentropic bulk modulus, K_S, and its pressure derivative, K' , to a third-order Birch-Murnaghan equation of state by the method of least squares previously described by Rigden *et al.* (1986). Input parameters in calculating K_S and K' are the Hugoniot pressures and densities (Tables 2 and 3), the initial density, ρ_0, and the Gruneisen parameter, γ. The Gruneisen parameter is calculated from the 1 atm thermodynamic quantities: α_P, the isobaric coefficient of thermal expansion; V, the molar volume; K_S, the adiabatic bulk modulus; and C_P, the isobaric heat capacity. It is assumed, in common with Rigden *et al.* (1986) that γV is constant. The values of input parameters and best-fit values of K_S and K' are given in Table 4. The calculated fit to the data is slightly better for anorthite when the five lowest pressure data are used alone (R.M.S. = 0.4 GPa compared with R.M.S. = 0.5 GPa for the complete data set). Both fits to the data are shown in Figure 4. For both diopside and anorthite, the values of bulk modulus calculated from our experimental data are in good agreement with the values calculated from measured ultrasonic velocities at 1 atm (Table 4). The values of K_S and K' for diopside are similar to those derived by Bottinga (1985) by analysis of the fusion curve of diopside

(K_S = 24.2 GPa, K' = 5.3).

DISCUSSION

Calculation of the solidus of diopside

One simple application of the equation of state of a melt with the same composition as an end member mineral is to the calculation of the solidus of that mineral at high pressures, providing that the mineral melts congruently. Such a calculation would not be very informative in the case of anorthite because it melts congruently only at low pressures and is not stable at all above a few GPa (e.g., Goldsmith, 1980). Diopside, although not precisely congruent in its melting behavior, is an ideal candidate for such a calculation because it is stable to high temperatures and to pressures of $\sim$ 20 GPa or more (Liu, 1979) and its solidus has been measured up to 5 GPa in several independent studies (Boyd and England, 1963; Williams and Kennedy, 1969; Boettcher *et al.*, 1982).

Because molten diopside is more compressible than crystalline diopside (Figure 3), the difference in volume between liquid and solid, ΔV, at high pressure is expected to decrease. In Figure 3 we show the molten diopside results compared with shock wave results on crystalline diopside. In this pressure range (up to 40 GPa) these crystalline data are consistent with the static compression results of Levien *et al.* (1979). Crystalline diopside will be more compressible at high temperatures but will also have a lower initial density. Using the data tabulated in Table 5 we estimate that $\Delta V \rightarrow 0$ at $\sim$ 20 GPa for the 1673 K isotherms. If $\Delta V \rightarrow 0$ along the solidus, then the slope of the solidus, dT/dP, will become flat and the melting temperature will

level off.

The calculation of the solidus of diopside is, in principle, very simple to carry out. At any point on the fusion curve:

$$\frac{dT_M}{dP} = \frac{\Delta V_{fusion}}{\Delta S_{fusion}} = \frac{\Delta V_f^0 + \int_{0,T_0}^{P,T_0} \Delta\left(\frac{\partial V}{\partial P}\right)_T dP + \int_{T_0,P}^{T_M,P} \Delta\left(\frac{\partial V}{\partial T}\right)_P dT}{\Delta S_f^0 + \int_{T_0,0}^{T_M,0} \Delta\left(\frac{\partial S}{\partial T}\right)_P dT + \int_{0,T_M}^{P,T_M} \Delta\left(\frac{\partial S}{\partial P}\right)_T dP}, \quad (1)$$

where ΔV_f^0 and ΔS_f^0 are the volume and entropy of fusion at 1 atm. and T_0 (1665K), and the integrands $\Delta(\partial V/\partial P)_T$, $\Delta(\partial V/\partial T)_P$, $\Delta(\partial S/\partial T)_P$ and $\Delta(\partial S/\partial P)_T$ represent the additional terms required to describe the volume and entropy of fusion at higher temperatures and pressures. In estimating these terms we employ the following thermodynamic relations,

$$\left(\frac{\partial V}{\partial P}\right)_T = -\beta_T V, \quad (1a)$$

$$\left(\frac{\partial S}{\partial P}\right)_T = -\left(\frac{\partial V}{\partial T}\right)_P = -\alpha_P V, \text{ and} \quad (1b)$$

$$\left(\frac{\partial S}{\partial T}\right)_P = \frac{C_P}{T}, \quad (1c)$$

where α_P is the isobaric coefficient of thermal expansion, β_T is the isothermal compressibility and C_P is the isobaric heat capacity. The values of all parameters used in calculating the fusion curve of diopside are given in Table 5. Recent compilations of heat capacity, entropy of fusion, and volume of molten silicates have been made by two separate groups (Richet and Bottinga, 1984; Bottinga *et al.*, 1982; Bottinga *et al.*, 1983, and Stebbins *et al.*, 1984). These results were used in conjunction

with our equation of state for molten diopside to estimate the position of the solidus of diopside.

We emphasize that although the calculation of the solidus is in principle very simple, in practice it is highly dependent on the input parameters. Although a large and growing data base on the thermodynamic properties of molten and crystalline silicates, including diopside, has become available in recent years, the uncertainties in their values, particularly as functions of temperature and pressure, translate into substantial uncertainties in the calculated position of the diopside solidus. This is demonstrated in Figure 5 in which we compare several calculations of the diopside solidus with experimental determinations to 5 GPa. All of the calculated curves emanate from the same 1 atm "melting point", taken as the solidus of diopside, 1664 K (Kushiro, 1972), and all employ the same equation of state for the melt.

In Figure 5a the input parameters that result in the wide range of calculated solidi differ only in the choice of the 1 atm volume of diopside liquid. As pointed out by Rivers (1985), the small differences between the measured values of Dane (1941) and Licko and Danek (1982) and the calculated values from the compilations of Bottinga *et al.* (1983) and Stebbins *et al.* (1984) translate into dramatic differences in the calculated fusion curves at pressures greater than 5 GPa. The fact that the liquid produced at the solidus at 1 atm differs in composition from pure diopside and the unknown degree to which this persists at high pressures contributes to the uncertainties in the uncompressed liquid volume.

In Figure 5b, we demonstrate the importance of precise values for the C_P function of the liquid phase in this type of calculation. The 1 atm values of Stebbins *et al.* (1983) and Bottinga (1985) are not very different, but the effects of this small

difference add up when the solidus is extrapolated over a large range as we have done in Figure 5.

An equally important uncertainty in these calculations arises from the unknown effect of pressure on α_P for the liquid and solid. In particular, we must know the variation of $\Delta(\alpha_P V)$ with pressure in order to carry out this calculation as this parameter enters into both the numerator and denominator of (1) through (1b). This parameter varies with pressure according to:

$$\frac{\delta}{\delta P}(\alpha_P V) = \alpha_P \frac{\delta V}{\delta P} + V \frac{\delta \alpha}{\delta P}. \qquad (2)$$

From the 1 atm compressibilities we can estimate $\delta V/\delta P$ and, using the relation $\delta\alpha/\delta P = -\delta\beta/\delta T$, we can estimate $\delta\alpha/\delta P$. For both molten and crystalline diopside $\frac{\delta}{\delta P}(\alpha_P V)$ is small compared with $\alpha_P V$, but the initial slope calculated at 1 atm and 1673 K is about three times as great for the liquid as for the crystal suggesting that $\Delta\alpha_P V$ decreases with increasing pressure. Maximum and minimum estimates of the slope of the solidus at any pressure can be made by assuming that $\Delta\alpha_P V$ is either equal to its 1 atm value or equal to zero. These two extremes are compared in Figure 5c for several different estimates of $\Delta\alpha_P V$.

It is expected that the real value lies between the two extremes illustrated in Figure 5c. The first assumption ($\Delta\alpha_P V$ = 1 atm value) will be more valid at low pressures, whereas the second ($\Delta\alpha_P V = 0$) would be more valid at high pressures. We have attempted to take this into account in the calculation illustrated in Figure 5d. Using the relation for $\frac{\delta}{\delta P}(\alpha_P V)$ given above, we have calculated this value for both molten and solid diopside at 1 atm, reducing $\Delta\alpha_P V$ as a function of pressure

until $\Delta\alpha_P V = 0$. For the calculated values of $\frac{\delta}{\delta P}(\alpha_P V)$ this occurs at $\sim$ 9 GPa. At higher pressures we assume $\Delta\alpha_P V = 0$. This calculation gives excellent agreement with the experimental data on the diopside solidus up to 5 GPa and the curve becomes quite shallow at pressures above 10 GPa.

Despite the sensitivity of the calculated solidus to the thermodynamic properties of the melt and solid phases, Figure 5 demonstrates that over the range of pressures at which the solidus has been determined experimentally, essentially all choices of these properties predict solidus positions compatible with experimental determinations. We thus conclude that our shock wave equation of state for diopside liquid is consistent with available phase equilibrium data. It is equally clear, however, that above 5 GPa, although the solidus most certainly flattens out (i.e., $\Delta V \rightarrow 0$) as predicted by Herzberg (1984) and Rigden *et al.* (1984), and recently observed for natural peridotite at about 10 GPa (Takahashi and Scarfe, 1985), the existence or precise position of a maximum on the diopside solidus cannot be predicted with confidence from our data in the absence of more reliable information on liquid compositions along the solidus, on the 1 atm volume of the melt, and on the α_P function of diopsidic melt and solid. Perhaps the best way to proceed would be to use our data in conjunction with an experimental determination of the diopside solidus to constrain values of these uncertain parameters.

Mixing properties of anorthite-diopside liquids

One of the most striking and important features of silicate liquids in the composition range of interest to geologists is that they mix essentially ideally; that is, the molar volume of a liquid intermediate in composition between two other liquids is

equal to the average of their molar volumes, weighted according to the proportions in which they are mixed. This simple behavior of molar volume has great practical significance because it permits the accurate calculation of melt densities as a function of composition (Bottinga and Weill, 1970; Nelson and Carmichael, 1979; Bottinga *et al.*, 1982, 1983; Stebbins *et al.*, 1984); indeed, it is on this basis that the 1 atm densities used in reducing our shock wave data were obtained. This feature also provides a basic structural insight: the local environments occupied by a particular cation in silicate melts are not greatly influenced by melt composition. In those cases where deviations from ideal behaviour are detected (e.g., Bottinga *et al.*, 1983), inferences about variations in molecular level structures with composition may be drawn.

In Figure 6 we show the change in normalized volume, V/V_0, with pressure for anorthite, $An_{0.36}Di_{0.64}$ and diopside along 1673 K isotherms calculated from our shock wave data (using the 5 point fit to the anorthite data) and that of Rigden *et al.* (1986). The intermediate composition has a compressibility intermediate between its end members. In order to test how closely we can match the volumes of $An_{0.36}Di_{0.64}$ by ideal mixing of anorthite and diopside, we have calculated this volume at pressures up to 40 GPa from the volumes of the end members and compared this with the volumes calculated from the data of Rigden *et al.* (1984, 1986). The deviation from ideal mixing (Figure 7) is shown to be $< 2\%$ up to 40 GPa and $< 1\%$ up to 20 GPa. We consider this to be an impressive result, given that the deviations from ideal mixing for a wide range of aluminosilicate melt compositions at 1 atm are also on the order of 1% (Bottinga and Weill, 1970; Nelson and Carmichael, 1979; Bottinga *et al.*, 1983) and the compressions involved between 1 atm and 40 GPa are between 35 and 42%. If this can be shown to hold for a wider range of compositions at high

pressures, it will permit the precise calculation of melt densities at elevated pressures in a simple fashion. Such a scheme for calculation of melt densities would contribute significantly to efforts to model the evolution of melts evolving at pressures on the order of tens of GPa. Although not likely to be important in the evolution of common, modern igneous rocks, petrogenesis at these pressures may have been important early in the history of the earth (e.g., Stolper *et al.*, 1981; Herzberg, 1984; Rigden *et al.*, 1984) and in the development of komatiites (Nisbet and Walker, 1982; Herzberg, 1983; Ohtani, 1984).

The approximately linear mixing behavior of volumes in the system anorthite-diopside suggests that at a particular pressure, local environments for each cation are, over this composition range, essentially unchanged on mixing. This is particularly significant with regard to aluminum because it implies that at a particular pressure the proportions of Al^{3+} and Si^{4+} in tetrahedral and octahedral coordination with oxygen are similar in anorthite and in the anorthite-diopside mixture we studied. The rate of conversion of tetrahedrally to octahedrally coordinated Al^{3+} with increasing pressure thus appears, based on our limited data, to be independent of composition in this system.

Al^{3+} and Si^{4+} coordination changes

There appears to be little disagreement that aluminum changes from dominantly tetrahedral coordination in melts at 1 atm to octahedral coordination at "high" pressures. Just what is meant by "high" pressures and the pressure range over which this transformation takes place are, however, controversial. Boettcher and his co-workers (Boettcher *et al.*, 1982, 1984) have maintained that aspects of the phase equilibria of

aluminosilicate systems, especially the compositional changes in feldspar-silica eutectics with increasing pressure, the slopes of univariant reactions involving liquid and aluminosilicates in P-T space, and the appearance near the liquidus of crystalline phases with octahedrally coordinated aluminum, indicate that substantial conversion of Al^{3+} from tetrahedral to octahedral coordination occurs in the vicinity of 1-2 GPa. Spectroscopic studies of glasses quenched from melts in this pressure range, including melts saturated with crystalline phases containing octahedrally coordinated Al^{3+} have failed to detect octahedral Al^{3+} in the glasses (Sharma *et al.,* 1979; Taylor and Brown, 1979a, Hamilton *et al,* 1986). Glasses quenched from 6-8 GPa do appear to contain octahedral aluminum (Ohtani *et al.,* 1985) and molecular dynamics calculations support the suggestion that the coordination change in Al^{3+} occurs gradually and predominantly at lower pressures than for Si^{4+} (Angell *et al.,* 1982, 1983).

Our results, although not definitive, support the hypothesis that Al coordination changes are gradual, unless they are completed at pressures lower than the lowest we have studied in our experiments. The smooth compression curves obtained for all of the compositions we have studied and the similarity in shape of the $\rho - P$ curves for all of our compositions independent of their Al content suggest this. Although we cannot rule out abrupt density changes in pressure intervals between our data points, conversion of all of the Al from tetrahedral to octahedral coordination would result in density jumps of $\sim$ 0.2 M gm^{-3} and $\sim$ 0.1 M gm^{-3} in the anorthite and anorthite-diopside compositions. These changes should be ultimately detectable via our experiments if they occur over narrow pressure intervals.

The smooth compression curves that we have observed for the three compositions that we have studied are also consistent with a gradual transformation of Si

from tetrahedral to octahedral coordination over a pressure interval of several tens of GPa. Density increases of $\sim$0.6 - 0.9 M gm^{-3} would be expected to accompany this structural change in the compositions we have studied; these would be difficult to miss in our data if they occurred over narrow pressure intervals.

Structures of silicate melts at high pressures and the compositional dependence of the elastic properties of silicate melts

Based on the results presented in this paper and in Rigden *et al.* (1986), the 1 atm bulk moduli of liquids in the system anorthite-diopside are only weakly dependent on composition, varying from 18-22 GPa for anorthite, to 24 GPa for the 1 atm eutectic composition, to 22-23 GPa for pure diopside at 1673 K. Similar values (21, 22, and 24 GPa) were obtained by Rivers (1985) by ultrasonic measurements. This lack of variation in compressibility with composition is rather surprising. It is widely believed, based on analogy with their crystalline equivalents and on a variety of spectroscopic investigations (Taylor and Brown, 1979b; Sharma and Yoder, 1978; Sharma *et al.*, 1983; Binsted *et al.*, 1985), that the structures of molten anorthite and diopside are very different. Anorthite liquid is thought to be an essentially fully polymerized network of silicate and aluminate tetrahedra, probably with four-membered rather than six-membered rings, and diopside melt is thought to be less polymerized, with network-breaking components in roughly close-packed arrangements between silicate polymers (e.g., Gaskell, 1982). We would therefore have expected that molten anorthite would be significantly more compressible than molten diopside, since its tetrahedral framework would be more capable of distortions via bending of the T-O-T (tetrahedral-oxygen-tetrahedral) angles and since the more open tetrahedral

framework would be expected to be more compressible than the more compact diopsidic structure. This line of reasoning appears to be correct in the case of the crystals: the bulk modulus of crystalline anorthite at room temperature is 92 GPa (Liebermann and Ringwood, 1976), whereas that for crystalline diopside is 113 GPa (Levien *et al.*, 1979): a difference of 20 GPa compared to a difference of only $\sim$ 3 GPa in the case of the melts. This line of reasoning also correctly anticipates the very low bulk modulus of silica glass (and presumably melt).

Why is anorthitic melt not significantly more compressible than diopsidic melt? Perhaps substantial Mg^{2+} is tetrahedrally coordinated by oxygens (Angell and Kadiyala, 1986) and the structure of diopside liquid is not that different from that of molten anorthite. Unless significant Fe^{2+} can also be tetrahedrally coordinated by oxygens, this does not help to explain the fact that molten fayalite at 1673 K also has a bulk modulus of 21.5 GPa (Rivers, 1985). We would surely have expected that this presumably substantially depolymerized structure would have been more incompressible than anorthite or diopside melt! This is the case for crystalline fayalite, the bulk modulus of which (138 GPa, Sumino, 1979) is tens of GPa higher than those of crystalline anorthite and diopside.

We do not want to give the incorrect impression that bulk moduli of silicate melts are all the same. Addition of the oxides of the large alkali cations leads to significant decreases in the bulk moduli of silicate melts and silica-rich compositions are more compressible than the intermediate compositions we have mentioned above (Rivers, 1985). Nevertheless, the simple notion, so successful in the case of crystalline

materials, that degree of polymerization correlates in some simple way with compressibility, appears incorrect for molten silicates.

Moreover, although the 1 atm bulk moduli of melts along the join anorthite-diopside and molten fayalite are similar, the pressure derivative of the bulk modulus, K' , shows variations with composition. It varies from 4-5 for anorthite melt to 7 for diopside melt based on our data, to 10 - 14 for molten fayalite based on Rivers's (1985) fit of the data on the solidus of Ohtani (1979) using different measurements of initial volume by Shiraishi *et al.* (1978) and Mo *et al.* (1982).

We are thus faced with the following paradox: For crystalline materials in the composition range of interest, the 1 atm bulk modulus varies with composition by tens of GPa and in a way that is consistent with our intuitive notion that the degree of close-packing of oxygen atoms in the crystal structure ought to lead to high compressibility, and the pressure derivative of the bulk modulus shows little variation away from a value of about 4. For molten materials, the 1 atm bulk modulus shows only minor variation with composition (a few GPa), but the pressure derivative of bulk modulus apparently varies by a factor of 2 or more.

Accepting the existence of the paradox stated above, at least part of the answer lies in the incorrectness of the assumption that molten anorthite, diopside, and olivine differ dramatically in their degree of packing. As shown in Tables 7 and 8, the volumes per mole of oxygen atoms in molten anorthite, diopside and fayalite are essentially identical at 1673 K: 13.5-13.7 $m^3 mole^{-1} \times 10^{-6}$. Perhaps even more surprising than the fact that they are all so similar, is that molten anorthite is actually

more closely packed than the pyroxene liquid.

This observation, when coupled with the similarity in 1 atm bulk moduli of these liquids, leads us to propose the following: Molten anorthite, diopside, and olivine can be viewed as loose packings of oxygen atoms with cations in the interstices. On average, the packing of the oxygen atoms is similar over this range of compositions. An increase in pressure results in a gradual collapse of this loose packing. The precise nature of the increased packing efficiency cannot be specified at this time; it could involve reducing the number of holes or defects in the structure or an actual change in the packing geometry. Of primary importance is that the effect is approximately independent of melt composition over this composition range and is principally a function of the arrangement of oxygen atoms.

This view is certainly oversimplified. In detail, we note that volume per oxygen is a function of melt composition (Table 8); based on the data summarized in Stebbins et al. (1984), the volume per oxygen atom of molten forsterite is about 8% lower than that for molten fayalite. However, we also note that the 1 atm bulk moduli of these two melts are expected to be about 22-25 GPa (Rivers, 1985), again, not too different from those that we have discussed above. Addition of larger cations, particularly the alkalies and the large alkaline earths, leads to higher volumes. However, addition of alkalies, while increasing the volume per oxygen of the melts, also leads to significantly lower 1 atm bulk moduli. As shown in Figure 8, this effect is systematic based on the data of Rivers (1985). The change in the volume per oxygen with pressure is roughly independent of the size of the cation below a certain partial molar

volume per oxygen ($\sim$ 30 $m^3 mole^{-1} \times 10^{-6}$); above this critical value of partial molar volume, the change in the volume per oxygen with pressure increases regularly with cation size. This suggests to us that when the smaller cations are present, although they influence the compressibility, oxygen-oxygen interactions still dominate the compression of the melt. However, the larger alkali cations spring the oxygens apart to such an extent that in the environment of these cations, oxygen packing is not the dominant factor. Cation-oxygen bonds, which are very springy for the large alkali atoms (i.e., they have low field strength), dominate the compression in these cases, and compressibilities increase dramatically as these alkalies are added to the melt.

The view we have proposed here for the compression of silicate melts differs from the standard view for solids that changes in the arrangement of coordination polyhedra, and in the cation-oxygen bond lengths in these polyhedra are the principal controls on compressibility (e.g., Hazen and Finger, 1982). We do not believe, however, that these concepts, applied to the melts we have studied, would readily account for the approximate constancy of the pressure derivative of volume for the wide range of components, including both tetrahedrally and octahedrally coordinated cations, that is illustrated in Figure 8. Our view also implies that the oxygen atoms are "larger" than the cations in the melt, consistent with the approach taken by Pauling (1960), but not with that of Prewitt (1977).

We should clarify what is implied by our statement that the oxygen atoms in the melt are "loosely packed." Fayalite liquid is about 15% less dense than solid fayalite. The olivine structure is based on a hexagonal close-packing of oxygen atoms

(Kamb, 1968a). Bernal (1959, 1964) concluded that random close-packing of identical spheres results in a structure about 15% less dense than crystalline close-packing. Thus, the fact that the oxygen packing for liquid fayalite is approximately 15% more open than that of the close-packed solid suggests that the liquid structure of fayalite is essentially a random close-packing of oxygen atoms with cations filling the interstices. The implication is that the anorthitic and diopsidic melts, with their similar volumes per oxygen atom, are based on similar random packings of oxygens.

Having rationalized, if not explained, the small variations in 1 atm bulk modulus of liquids in the system anorthite-diopside and for molten fayalite, we are left with the puzzling fact that the pressure derivative of bulk modulus shows substantial variations with composition. If the only mechanism operating on the compression of molten silicates was the gradual rearrangement of oxygen atoms in similar dense packings, we would not expect a large change in the pressure derivative from composition to composition.

First, it is useful to clarify what is done in deriving K' from shock wave data. We arbitrarily assumed that the equation of state of the melts we have studied can be fit by a third-order Birch-Murnaghan equation of state. On average, over the pressure range that we have explored, this fits the data adequately (Figures 3 and 4 and Rigden *et al.*, 1984, 1986).

The compression behaviour of the silicate melts studied here is considered as physically representing two responses. The first is simply the pressing of oxygens (and cations) together. This would correspond to measuring compressibility at

infinitely high frequency, so that no structural relaxation can occur. We would expect, based on data for crystalline silicates and oxides (Anderson *et al.*, 1968) in which the pressing together of atoms is the major mode of compression, that a Birch-Murnaghan equation of state, with a roughly constant and low value of K' ($\sim$ 4-5), would adequately describe this unrelaxed component of compression in melts. This component of the compressibility is expected to be similar to that of crystalline silicates at the same temperature; to the extent that the melt contains defects and holes, the unrelaxed compressibility would be greater than that of the solids. This effect might account for up to a factor of two greater compressibility of melts than solids (e.g., Kamb, 1968b).

The second mode of compression in silicate melts, which probably accounts for most of the increase in density that we have observed up to the high pressures that we have explored in our shock wave experiments, is due to relaxation phenomena in the melts. In this we include the unspecified gradual changes in oxygen packing discussed above, warping of the polyhedral framework, and coordination changes in the melts. The most important coordination changes will be conversion of cations that are dominantly in tetrahedral coordination at low pressure (e.g., Fe^{3+}, Al^{3+}, Si^{4+}) to mostly octahedral coordination at high pressures, although substitution of cations into anion positions, as occurs in the perovskite structure and has also been inferred by Ross and Rogers (1985) for molten alkali halides, may also become important at the highest pressures.

It would be surprising if the effects of relaxation phenomena could be as simply described in terms of a general equation of state as could the simple pressing together of the atoms. These changes probably occur over a finite range of pressures rather than continuously over all pressures as does simple interatomic compression. For example, it is likely that a relaxation phenomenon is responsible for the anomalously high compressibility of silica glass at low pressure. It is well known that the compression of silica glass cannot be described adequately by a single, simple equation of state. At low pressures, bulk modulus is low and K' is actually negative (Bridgman and Simon, 1953; Peselnick *et al.*, 1967; Schroeder *et al.*, 1981). But once the framework has distorted, and the volume of the glass is fully compressed by changing of Si-O-Si bond angles (Bridgman and Simon, 1953; Gaskell, 1966), K' becomes positive (Schroeder *et al.*, 1981), and compression can be described principally in terms of pressing together of atoms.

As we discussed above, the fact that we do not see evidence of abrupt increases in density suggests to us that coordination changes take place gradually with increasing pressure. Nevertheless, it would be surprising if Al^{3+} and Si^{4+} converted to octahedral coordination at the same rate with increasing pressure. We would expect that as, in the solids, Al^{3+} would convert to octahedral coordination at lower pressures than would Si^{4+}. As in the case of the distortions in the polyhedral framework discussed above, the more abruptly that these changes take place, the more imperfect would be our application of a single Birch-Murnaghan equation to the data. The important point to emphasize is that the K and K' values that we have derived from our data are averaged over the entire pressure interval that we have studied

experimentally.

Suppose that we have two melt compositions that, at 1 atm, have essentially identical bulk moduli. Can we anticipate which melt, averaged over several hundred kilobars, will have the higher value of K' ? Presuming that most of the difference in compression between the two melts over this pressure range will reflect differences in the concentration of cations that will convert from tetrahedral to octahedral coordination, the more aluminous and silica-rich composition would experience more compression over this pressure interval, and hence its bulk modulus averaged over this pressure interval would be lower (i.e., it would be more compressible). Hence, the rate of increase in K with pressure for the more Al-Si-rich melt will be lower over the pressure interval in which these coordination changes occur, and its value of K' averaged over this pressure interval will be lower. We would thus expect, as is indeed observed, that K' increases for melts in the order anorthite, $An_{0.36}Di_{0.64}$, diopside, olivine. This effect is illustrated schematically in Figure 9.

Thus, given the approximate constancy of 1 atm bulk moduli for these molten silicates, it is not surprising that K' averaged over the pressure interval in which coordination changes take place would vary systematically with melt composition in precisely the fashion that we have observed. It is possible, given our data and this concept, to estimate the magnitude of K' , providing that K at 1 atm is known. In order to do so, however, we must first examine an interesting regularity in our data.

If we compare the 1 atm partial molar volumes of oxide components in silicate melts to the molar volumes of the solid, dense oxides (Figure 10), we see that for

essentially all of the oxides other than those dominantly in tetrahedral coordination (Si^{4+}, Al^{3+}, Fe^{3+}), they are similar, plus or minus about 10 percent. In other words, these "network-breaking" components are already in a roughly close-packed arrangement at 1 atm and no great increases in their packing efficiency with increasing pressure, other than those due to simple compression, are expected. This regularity suggests to us that at sufficiently high pressures, where essentially all of the Si and Al are octahedrally coordinated, the partial molar volumes of SiO_2 and Al_2O_3 in melt will be similar to the molar volumes of stishovite and corundum. Under these conditions, the molar volume of the melt should approach that of a mixture of dense oxides of the same composition, just as has been observed for multicomponent crystalline silicates at high pressures (e.g., McQueen *et al.,* 1967; Al'tschuler and Sharipdzhanov, 1971; Svendson and Ahrens, 1983; Boslough *et al.,* 1986). Table 7 (Column 6) shows that, at 40 GPa, this expectation is realized in our experiments: the volumes of the three melt compositions that we have studied are, based on a best-fit Birch-Murnaghan equation of state, within 10 percent of those of the equivalent mixture of dense oxides. In addition, the parameters derived from the full anorthite data set yield a volume essentially equal to the calculated dense oxide mixture at 40 GPa. A possible explanation is that crystallization along the Hugoniot occurred at the highest pressure point facilitated by a close approach in structure between liquid and solid at this high pressure.

There is other evidence for the approach of melt densities to those of dense oxides at pressures of several hundred kilobars. Lyzenga *et al.* (1982) concluded, based

on shock wave experiments in which they melted stishovite, that the molar volume of molten SiO_2 at 70 GPa is about 3 percent greater than that of SiO_2 in crystalline stishovite. The recent experiments of Jeanloz and Heinz (1984), in which they have determined the solidus of a magnesian silicate perovskite between 30 and 60 GPa, suggest that the liquid and solid volumes are essentially identical over this pressure range.

We are now in a position to estimate the value of K' for silicate melts averaged over the 0-40 GPa pressure range for a wide range of compositions. Given (a) the 1 atm molar volume, obtainable precisely from either the compilation of Bottinga *et al.* (1983) or Stebbins *et al.* (1984); (b) the 1 atm bulk modulus of the melt, which can be calculated using the algorithm given in Rivers (1985); and (c) the assumption that the volume of the melt at $\sim$ 40 GPa is 5-10 percent greater than than of the equivalent mixture of dense high pressure phases, then the value of K' consistent with a third-order Birch-Murnaghan equation of state and these values of K_0, V(1 atm), and V(40 GPa) can be readily derived. The results of such a calculation for several melt compositions are listed in Table 8.

The values of K' calculated in this way for molten anorthite, the anorthite-diopside eutectic melt, and molten diopside are similar to those we have determined experimentally. The values for forsterite and fayalite are significantly higher; the value for fayalite is consistent with the value needed to account for its solidus (Rivers, 1985). The calculated values of K' for the pyroxene liquids, enstatite and ferrosilite, are similar to our experimentally determined value for diopsidic melt.

We have generalized our limited data a long way in concluding that *all* melts will bear the same relation – approximately 5-10 percent less dense – to dense high-pressure phases at 40 GPa. Nevertheless, this simple approach does appear to explain, to a remarkably precise degree, the high values of K' implied for fayalite melt by the completely independent calculation from the solidus (Rivers, 1985). It also suggests a simple rule of thumb that, if substantiated by further experiments, would be extremely valuable in thinking about the densities of melts at high pressures. The volumes per oxygen at 40 GPa of stishovite and corundum are significantly lower than the other common oxides (e.g., at 1673 K, these volumes are about 6.5 and 7.8 $m^3mole^{-1} \times 10^{-6}$, respectively, compared with values of 9.5-13 $m^3mole^{-1} \times 10^{-6}$ for MgO, CaO, and FeO and 28-43 $m^3mole^{-1} \times 10^{-6}$ for Na_2O and K_2O *). Therefore, the ultimate high pressure volumes of melts rich in silica and alumina will be lower than those of melts poor in these constituents. Given that 1 atm volumes and bulk moduli of common silicate compositions are similar, this suggests that silica- and alumina-rich melts will have low values of K' relative to more basic melts. This effect is in essence the reason for the high K' values shown in Table 8 for the olivines and the explanation for the lower K' values of anorthite and the pyroxenes, and is illustrated schematically in Figure 9.

* Note the trend with decreasing cationic charge.

CONCLUSIONS

(1) Shock wave equation of state measurements on molten diopside and anorthite complement the existing data on a composition intermediate these two end-members and enable inferences to be made about the differences in compressibility between these compositions. For molten diopside we calculate a best-fit K_S = 22.4 GPa and K' = 6.9 at 1773 K compared with the ultrasonically determined value of K_S = 24.4 GPa at 1758 K (Rivers, 1985). Two different fits to the anorthite results at 1923 K were calculated. For the entire data set K_S = 22.0 GPa and K' = 4.1. When the highest pressure point was omitted from the fit, the RMS was reduced slightly, giving K_S = 17.9 GPa, K' = 5.3. Rivers (1985) gives K_S = 20.6 GPa at 1833 K based on ultrasonic measurements.

(2) From the equation of state of molten diopside we can place constraints on the dT/dP slope of the fusion curve at high pressures. We expect that the slope will be quite shallow at pressures above 10 GPa, but in the absence of data on the change of α_P with pressure, no precise determination of temperatures can be made. Our best fit to the experimental solidus data uses a model for $\Delta(\alpha_P V)$ that decreases linearly with pressure.

(3) The volume of the intermediate $An_{0.36}Di_{0.64}$ melt composition can be calculated to within $\pm 2\%$ based on ideal mixing of the molten anorthite and diopside components at pressures up to 40 GPa (the limit of our experimental data) despite the fact that volumes increase 35-42% over this pressure range. If this can be shown to hold over a range of compositions, it will be extremely useful in calculations of the densities of

melts at elevated pressures.

(4) Our results support the hypothesis that changes in coordination of Al^{3+} and Si^{4+} from tetrahedral at low pressures to octahedral at high pressures occur gradually within the resolution of the shock wave experiments. The expected density changes of coordination changes over a small pressure interval would be expected to show up in our Hugoniot density measurements. This would be particularly dramatic for Si.

(5) Bulk moduli for molten silicates are remarkably similar for a wide range of compositions of petrological interest, based on both our experimental data and from ultrasonic measurements of Rivers (1985). We propose that this results from the similar packing of oxygen atoms in silicate liquids at atmospheric pressure and that the degree of compression at higher pressures is primarily related to the ability of the structure to collapse by coordination changes of Al^{3+} and Si^{4+} from tetrahedral to octahedral. For identical values of bulk modulus this would be reflected in the higher values of K' for less compressible (Al^{3+}, Si^{4+}, Fe^{3+} - poor) melts. At $\sim$ 40 GPa melts are proposed to achieve $\sim$ 1.0-1.1 times the volume of dense high-pressure phases at this pressure.

(6) Estimates of K' for molten silicates, assuming that their volumes are 5-10% greater than crystalline dense phases at 40 GPa, have been made using 1 atm bulk moduli calculated from Rivers (1985). The olivine liquids, fayalite and forsterite, have $K' \sim 10$, and pyroxene liquids, enstatite, and ferrosilite have $K' \sim 7$ - 8, similar to diopside. Our estimate of K' for fayalite is consistent with the value calculated by Rivers (1985) from an analysis of its fusion curve up to the 7 GPa triple point of

Ohtani (1979).

ACKNOWLEDGEMENTS

We wish to thank E. Bus, E. Gelle, C. Manning, M. Long and L. Young for their invaluable technical help. R. Heuser carried out microprobe analyses. We have benefited from discussions with C.A. Angell, J. Bass, P.H. Gaskell and B. Kamb. Support was provided by NSG Grant EAR84-07784. This manuscript is to be submitted to *J. Geophys. Res.* with co-authors E.M. Stolper and T.J. Ahrens.

REFERENCES

Ahrens, T.J., J.T. Rosenberg and M.H. Rudeman, 1966. Dynamic properties of rocks. Stanford Research Institute, Final Report, DA-45-146-X2-277, SRI Project FGU-4816.

Al'tschuler, L.V. and I.I. Sharipdzhanov, 1971. Additive equations of state of silicates at high pressures. *Izv. Earth Physics, 3,* 11-28.

Anderson, O.L., E. Schreiber, R.C. Leibermann and N. Soga, 1968. Some elastic constant data on minerals relevant to geophysics. *Rev. Geophys., 6,* 491-524.

Angell, C.A., P.A. Cheeseman and S. Tamaddon, 1982. Pressure enhancement of ion mobilities in liquid silicates from computer simulation studies to 800 kilobars. *Science, 218,* 885-887.

Angell, C.A., P.A. Cheeseman and S. Tamaddon, 1983. Water-like transport property anomalies in liquid silicates investigated at high T and P by computer simulation techniques. *Bull. Mineral., 106,* 87-97.

Angell, C.A. and P.P Kadiyala, 1986. Compressibility and ion mobility in (+3, +1) and (+2, +2) cation substituted silicate melts (jadeite versus dioxide) from 50 GPa to the negative pressure instability limit - a computer simulation study. Abstract in *Physique et Chemie de Liquides Silicates.* Association Europeene de Geochimie.

Bass, J.D., R.C. Liebermann, D.J. Weidner and S.J. Finch, 1982. Elastic Properties from acoustic and volume compression experiments. *Phys. Earth Planet. Int., 25,* 140-158.

Beattie, A.G. and G.A. Samara, 1971. Pressure dependence of the elastic constants of $SrTiO_3$. *J. Appl. Phys., 42,* 2376-2381.

Bernal, J.D., 1959. A geometrical approach to the structure of liquids. *Nature, 183,* 141-147.

Bernal, J.D., 1964. The structure of glasses. *Proc. Roy. Soc. A, 280,* 299-322.

Binsted, N., G.N. Greaves and C.M.B. Henderson, 1985. An EXAFS study of glassy and crystalline phases of compositions $CaAl_2Si_2O_8$ (anorthite) and $CaMgSi_2O_6$ (diopside). *Contrib. Mineral. Petrol., 89,* 103-109.

Boettcher, A.L., C. Wayne Burnham, K.E. Windom and S.R Bohlen, 1982. Liquids, glasses and the melting of silicates to high pressures. *J. Geol., 90,* 127-138.

Boettcher, A., Q. Guo, S. Bohlen and B. Hanson, 1984. Melting in feldspar-bearing systems to high pressures and the structure of aluminosilicate liquids. *Geology, 12,* 202-204.

Boslough, M.B., S.M. Rigden and T.J. Ahrens, 1986. Hugoniot equations of state of anorthite glass and lunar anorthosite. *Geophys. J. Roy. Astr. Soc.,* in press.

Bottinga, Y., 1985. On the isothermal compressibility of silicate liquids at high pressure. *Earth Planet. Sci. Lett., 74,* 350-360.

Bottinga, Y. and D.F. Weill, 1970. Densities of silicate liquid systems calculated from partial molar volumes of oxide components. *Am. J. Sci., 269,* 169-182.

Bottinga, Y., D. Weill and P. Richet, 1982. Density calculations for silicate liquids. I: Revised method for aluminosilicate compositions. *Geochim. Cosmochim. Acta, 46,* 909-919.

Bottinga, Y., P. Richet and D.F. Weill, 1983. Calculation of the density and thermal expansion coefficient of silicate liquids. *Bull. Mineral., 106,* 129-138.

Boyd, F.R. and J.L. England, 1963. Effect of pressure on the melting of diopside, $CaMgSi_2O_6$, and albite, $NaAlSi_3O_8$, in the range up to 50 kilobars. *J. Geophys. Res., 68,* 311-323.

Bridgman, P.W. and I. Simon, 1953. Effect of very high pressure on glass. *J. Appl. Phys., 25,* 405-413.

Chang, E. and E.K. Graham, 1975. The elastic constants of cassiterite SnO_2 and their pressure and temperature dependence. *J. Geophys. Res., 80,* 2595-2599.

Dane, E.B., Jr, 1941. Densities of molten rocks and minerals. *Am. J. Sci., 239,* 809-818.

Finger, L.W. and Y. Ohashi, 1976. The thermal expansion of diopside to 800 ° C and a refinement of the crystal structure at 700 ° C. *Am. Mineral., 61,* 303-310.

Gaskell, P.H., 1966. Thermal properties of silica. *Trans. Faraday Soc., 62* 1493-1504.

Gaskell, P.H., 1982. A structural interpretation of the density of alkali silicate glasses. *Journal de Physique, 43,* C9:101-C9:105.

Gieske, J.H. and G.R. Barsch, 1968. Pressure dependence of the elastic constants of single crystal aluminum oxide. *Phys. Stat. Sol., 29,* 121-131.

Goldsmith, J.R., 1980. The melting and breakdown relationships of anorthite at high pressures and temperatures. *Am. Mineral., 65,* 272-283.

Hamilton, D.L., W. Chesworth, G. Kennedy and C. Fyfe, 1986. The absence of 6-fold coordinated Al in jadeite melt near the jadeite liquidus. *Geochim. Cosmochim. Acta, 50,* 123-124.

Hankey, R.E. and D.E. Schuele, 1970. Third order elastic constants of Al_2O_3. *J. Acous. Soc. Am., 48,* 190-202.

Hazen, R.M. and L.W. Finger, 1982. *Comparative Crystal Chemistry.* John Wiley & Sons, N.Y. 231 pp.

Herzberg, C.T., 1983. Solidus and liquidus temperatures and mineralogies for anhydrous garnet-lherzolite to 15 GPa. *Phys. Earth Planet. Int., 32,* 193-202.

Herzberg, C.T., 1984. Chemical stratification in the silicate earth. *Earth Planet. Sci. Lett., 67,* 249-260.

Ito, H., K. Kawada and S. Akimoto, 1974. Thermal expansion of stishovite. *Phys. Earth Planet. Int., 8,* 277-281.

Jeanloz, R. and A.B. Thompson, 1983. Phase transitions and mantle discontinuities. *Rev. Geophys. Space Phys., 21,* 51-74.

Jeanloz, R. and D. Heinz, 1984. Experiments at high temperature and pressure: laser heating through the diamond cell. *Journal de Physique, 45,* C8:83- C8:92.

Jones, L.E.A., 1979. Pressure and temperature dependence of the single crystal elastic moduli of the cubic perovskite $KMgF_3$. *Phys. Chem. Minerals, 4,* 23-42.

Kamb, B., 1968a. Structural basis of the olivine-spinel stability relation. *Am. Mineral., 53,* 1439-1455.

Kamb, B., 1968b. Ice polymorphism and the structure of water in *Structural Chemistry and Molecular Biology.* A. Rich and N. Davidson, eds., pp 507-542. W.H. Freeman, San Francisco.

Knittle, E., R. Jeanloz and G.L. Smith, 1986. Thermal expansion of silicate perovskite and stratification of the earth's mantle. *Nature, 319,* 214-216.

Kushiro, I., 1972. Determination of liquidus relations in synthetic silicate systems with electron probe analyses: the system forsterite- diopside-silica at 1 atm. *Am. Mineral., 57,* 1260-1271.

Levien, L., D.J. Weidner and C.T. Prewitt, 1979. Elasticity of diopside. *Phys. Chem. Minerals, 4,* 105-113.

Levien, L. and C.T. Prewitt, 1981. High-pressure study of diopside. *Am. Mineral., 66,* 315-323.

Licko, T. and V. Danek, 1982. Densities of melts in the system $CaSiO_3$–$CaMgSi_2O_6$–$Ca_2MgSi_2O_7$. *Phys. Chem. Glasses, 23,* 67-71.

Liebermann, R.C. and A.E. Ringwood, 1976. Elastic properties of anorthite and the nature of the lunar crust. *Earth Planet. Sci. Lett., 31,* 69-74.

Liebermann, R.C., L.E.A. Jones and A.E. Ringwood, 1977. Elasticity of aluminate, titanate, stannate and germanate compounds with the perovskite structure. *Phys. Earth Planet. Int., 14,* 165-178.

Liu, L.-G., 1979. The system enstatite-wollastonite at high pressures and temperatures with emphasis on diopside. *Phys. Earth Planet. Int., 19,* P15-P18.

Lyzenga, G.A., T.J. Ahrens and A.C. Mitchell, 1982. Shock temperatures of SiO_2 and their geophysical implications. *J. Geophys. Res., 88,* 2431-2444.

Manghnani, M.H., 1969. Elastic constants of single-crystal rutile under pressures to 7.5 kilobars. *J. Geophys. Res., 74,* 4317-4328.

Matsui, Y., K. Kawamura and Y. Syono, 1982. Molecular dynamics calculations applied to silicate systems: Molten and vitreous $MgSiO_3$ and Mg_2SiO_4 under low and high pressures in *High Pressure Research in Geophysics,* S. Akimoto and M.H. Manghnani, eds., pp 511-524. Center for Academic Publications, Tokyo, Japan.

McQueen, R.J., S.P. Marsh and J.N. Fritz, 1967. Hugoniot equation of state of twelve rocks. *J. Geophys. Res., 72,* 4299-5036.

Mo, X., I.S.E. Carmichael, M. Rivers and J. Stebbins, 1982. The partial molar volume of Fe_2O_3 in multicomponent silicate liquids and the pressure dependence of the oxygen fugacity in magmas. *Min. Mag.,* 237-245.

Nelson, S.A. and I.S.E. Carmichael, 1979. Partial molar volumes of oxide components in silicate liquids. *Contrib. Mineral. Petrol., 71,* 117-124.

Nisbet, E.G. and D. Walker, 1982. Komatiites and the structure of the Archaean

mantle. *Earth Planet. Sci. Lett., 60,* 105-113.

Ohtani, E., 1979. Melting relations of fayalite up to about 200 kbar. *J. Phys. Earth, 27,* 189-208.

Ohtani, E., 1984. Generation of komatiite magma and gravitational differentiation in the deep upper mantle. *Earth Planet. Sci. Lett., 67,* 261-272.

Ohtani, E., F. Taulelle and C.A. Angell, 1985. Al^{3+} coordination changes in liquid aluminosilicates under pressure. *Nature, 314,* 78-81.

Pauling, L., 1960. *The Nature of the Chemical Bond.* Cornell University Press, Ithaca, N.Y., 3rd Edition, 644pp.

Peselnick, L., R. Meister and W.H. Wilson, 1967. Pressure derivatives of elastic moduli of fused quartz to 10 kb. *J. Phys. Chem. Solids, 28,* 635-639.

Prewitt, C.T., 1977. Effect of pressure on ionic radii. *Geol. Soc. Am. Abstracts with Programs, 9,* 1134.

Reid, A.F. and A.E. Ringwood, 1975. High pressure modification of $ScAlO_3$ and some geophysical implications. *J. Geophys. Res., 80,* 3363-3370.

Richet, P. and Y. Bottinga, 1984. Anorthite, wollastonite, diopside, cordierite and pyrope: thermodynamics of melting, glass transitions, and properties of the amorphous phases. *Earth Planet. Sci. Lett., 67,* 415-432.

Rigden, S.M., T.J. Ahrens and E.M. Stolper, 1984. Densities of liquid silicates at high pressures. *Science, 226,* 1071-1074.

Rigden, S.M., T.J. Ahrens and E.M. Stolper, 1986. Equation of state of molten silicate at high pressures, to be submitted to *J. Geophys. Res.*

Ringwood, A.E. and A. Major, 1971. Synthesis of majorite and other high-pressure garnets and perovskites. *Earth Planet. Sci. Lett., 12,* 411-418.

Rivers, M.L., 1985. Ultrasonic studies of silicate liquids. Ph.D. Dissertation, University of California, Berkeley.

Robie, R.A., B.S. Hemingway and J.R. Fisher, 1978. Thermodynamic Properties of Minerals and Related Substances at 298.15 K and 1 Bar (10^5 Pascals) Pressure and Higher Temperatures. *U.S. Geological Survey Bull., 1452.*

Ross, M. and F.J. Rogers, 1985. Structure of dense shock-melted alkali halides: Evidence for a continuous pressure-induced structural transformation in the melt. *Phys. Rev., 31,* 1463-1468.

Schroeder, J., K.J. Dunn and F.P. Bundy, 1981. Brouillon scattering from amorphous SiO_2 under hydrostatic pressure up to 133 kbar. General Electric Report No 81CRCD216. Schenectady, N.Y.

Sharma, S.K. and H.S. Yoder, 1978. Structural study of glasses of akermannite, diopside and sodium melilite compositions by Raman spectroscopy. *Carnegie Inst. Washington Yearb., 77,* 649-652.

Sharma, S.K., D. Virgo and B. Mysen, 1979. Raman study of the coordination of aluminum in jadeite melts as a function of pressure. *Am. Mineral., 64,* 779-787.

Sharma, S.K., B. Simons and H.S. Yoder, 1983. Raman study of anorthite, calcium Tschermak's pyroxene and gehlenite in crystalline and glassy states. *Am. Mineral., 68,* 1113-1125.

Shiraishi, Y., K. Ikeda, A. Tamura and T. Saito, 1978. On the viscosity and density of the molten FeO-MgO system. *Transactions of the Japanese Institute of Metallurgy, 19,* 264-274.

Sinclair, W. and A.E. Ringwood, 1978. Single crystal analysis of the structure of stishovite. *Nature, 272,* 714-715.

Skinner, B.J., 1966. Thermal Expansion. In: S.P. Clark, Jr., ed., Handbook of Physical Constants. *Geol. Soc. Am. Mem., 97.*

Stebbins, J.F., I.S.E. Carmichael and D.J. Weill, 1983. The high-temperature liquid and glass heat contents and heats of fusion of diopside, albite, sanidine and nepheline. *Am. Mineral., 68,* 717-730.

Stebbins, J.F., I.S.E. Carmichael and L.K. Moret, 1984. Heat capacities and entropies of silicate liquids and glasses. *Contrib. Mineral. Petrol., 86,* 131-148.

Stolper, E., D. Walker, B.H. Hager and J.F. Hays, 1981. Melt segregation from partially molten source regions. The importance of melt density and source region size. *J. Geophys. Res., 86,* 6261-6271.

Sumino, Y., 1979. The elastic constants of Mn_2SiO_4, Fe_2SiO_4 and Co_2SiO_4, and the elastic properties of olivine group minerals at high temperature. *J. Phys. Earth, 27,* 209-238.

Svendsen, B. and T.J. Ahrens, 1983. Dynamic compression of diopside and salite to 200 GPa. *Geophys. Res. Lett., 10,* 501-504.

Takahashi, E. and C.M. Scarfe, 1985. Melting of peridotite to 14 GPa and the genesis of komatiite. *Nature, 315,* 566-568.

Taylor, M. and G.E. Brown, Jr, 1979a. Structure of mineral glasses -II. The SiO_2–$NaAlSiO_4$ join. *Geochim. Cosmochim. Acta, 43,* 1467-1473.

Taylor, M. and G.E. Brown, Jr., 1979b. Structure of mineral glasses -I. The feldspar glasses $NaAlSi_3O_8$, $KAlSi_3O_8$, $CaAl_2Si_2O_8$. *Geochim. Cosmochim. Acta, 43,* 61-75.

Touloukian, Y.S., R.K. Kirby, R.E. Taylor and P.D. Desai, 1970. *Thermal Expansion of Metallic Elements and Alloys.* Plenum, N.Y., 1348 pp.

Waff, H.S., 1975. Pressure-induced coordination changes in magmatic liquids.

Geophys. Res. Lett., 2, 193-196.

Walker, D., E.M. Stolper and J.F. Hays, 1978. A numerical treatment of melt/solid segregation: Size of the eucrite parent body and stability of the terrestrial low-velocity zone. *J. Geophys. Res., 83,* 6005-6013.

Wang, H. and G. Simmons, 1973. Elasticity of some mantle crystal structures 2. Rutile GeO_2. *J. Geophys. Res., 78,* 1262-1273.

Weidner, D.J., J.D. Bass, A.E. Ringwood and W. Sinclair, 1982. The single-crystal elastic moduli of stishovite. *J. Geophys. Res., 87,* 4740-4746.

Williams, D.W. and G.C. Kennedy, 1969. Melting curve of diopside to 50 kilobars. *J. Geophys. Res., 74,* 4359-4366.

Yagi, T., H.-K. Mao and P.M. Bell, 1978. Structure and crystal chemistry of perovskite-type $MgSiO_3$. *Phys. Chem. Minerals, 3,* 97-110.

Yagi, T., H.-K. Mao and P.M. Bell, 1982. Hydrostatic compression of perovskite-type $MgSiO_3$. in S.K. Saxena, ed., *Advances in Physical Geochemistry, vol. 2.* 353pp. Springer-Verlag, N.Y.

Table 1: Sample Analyses and Theoretical Compositions

	Diopside		Anorthite	
	Sample[1]	Ideal	Sample	Ideal
SiO_2	55.71	55.49	43.48	43.20
Al_2O_3	-	-	36.36	36.64
MgO	16.93	18.62	0.0	0.0
CaO	26.07	25.89	20.73	20.16
Total	98.71	100.00	100.57	100.00

[1]Average of 5 electron microprobe analyses: Analyst, R. Heuser

Table 2: Molten Diopside Hugoniot Data
($T_0 = 1773$ K, $\rho_0 = 2.613$ Mg m^{-3})

Shot #	Flyer Plate	Impact Velocity km sec^{-1}	Shock Velocity km sec^{-1}	Particle Velocity km sec^{-1}	Hugoniot Pressure GPa	Hugoniot Density Mg m^{-3}
660	Cu	1.03 ±0.03	4.45 ±0.04	0.73 ±0.02	8.5 ±0.3	3.128 ±0.027
656	Cu	1.50 ±0.03	4.76 ±0.06	1.08 ±0.03	13.3 ±0.3	3.378 ±0.029
630	Cu	2.00 ±0.04	5.28 ±0.07	1.43 ±0.03	19.7 ±0.5	3.589 ±0.031
658	W	2.12 ±0.04	6.19 ±0.08	1.98 ±0.05	31.8 ±0.8	3.840 ±0.035
659	W	2.42 ±0.04	6.54 ±0.11	2.24 ±0.05	38.0 ±1.0	3.976 ±0.048

Table 3: Molten Anorthite Shock Data
(T_0 = 1923 K, ρ_0 = 2.545 Mg m^{-3})

Shot #	Flyer Plate	Impact Velocity km sec^{-1}	Shock Velocity km sec^{-1}	Particle Velocity km sec^{-1}	Hugoniot Pressure GPa	Hugoniot Density Mg m^{-3}
666	Cu	1.24 ±0.03	3.95 ±0.04	0.91 ±0.03	9.2 ±0.3	3.310 ±0.029
673	Cu	1.30 ±0.02	3.93 ±0.04	0.96 ±0.02	9.6 ±0.2	3.368 ±0.034
664	Cu	1.52 ±0.03	4.36 ±0.08	1.11 ±0.03	12.4 ±0.4	3.417 ±0.036
665	Cu	1.80 ±0.03	4.63 ±0.05	1.32 ±0.03	15.5 ±0.3	3.560 ±0.031
663	W	2.03 ±0.04	5.40 ±0.13	1.95 ±0.05	26.8 ±0.8	3.990 ±0.064
672	W	2.49 ±0.03	5.76 ±0.08	2.37 ±0.03	34.9 ±0.7	4.328 ±0.052

Table 4: Input parameters and output for equation of state calculation

	Diopside	Anorthite		
T_0	1773	1923		K
ρ_0	2.613[1]	2.550[1]		Mg m^{-3}
α	6.0×10^{-5} [2]	3.8×10^{-5} [2]		K^{-1}
C_p	360 [1]	418 [1]		J(mole-K)$^{-1}$
# points	5	5	6	
K_S	22.4	17.9	22.0	GPa
RMS	0.4	0.4	0.5	GPa
K'	6.9	5.3	4.1	

[1]Stebbins *et al.* (1984)

[2]Dane (1941), Licko and Danek (1982)

Table 5: Parameters used for calculation of fusion curve of diopside

	Crystalline Diopside	Molten Diopside	
T_0	1664[1]	1664	K
V_0	69.11[2]	a) 81.09[3]	$m^3mole^{-1} \times 10^{-6}$
		b) 82.34[4]	$m^3mole^{-1} \times 10^{-6}$
		c) 82.95[5]	$m^3mole^{-1} \times 10^{-6}$
ΔS_f^0	82.88[6]		$J(mole–K)^{-1}$
K_T	90.7[7]	21.9[8]	GPa
K'	4.5[7]	6.9[8]	
α	3.2×10^{-5} [9]	a) 6.0×10^{-5} [3,5]	K^{-1}
		b) 6.5×10^{-5} [4]	K^{-1}
		c) 7.3×10^{-5} [10]	K^{-1}
C_p	a) $328.19 + 1.888 \times 10^{-3} T$	334.57[11]	$J(mole–K)^{-1}$
	$-2.5192 \times 10^3 T^{1/2} - 1.443 \times 10^6 T^{-2}$ [12]		
	b) $243.9 + 1.069 \times 10^{-2} T$ [13]	353 [13]	$J(mole–K)^{-1}$

[1]Kushiro (1972)
[2]Calculated using room temperature volume of Robie *et al.* (1978)
[3]Dane (1941)
[4]Stebbins *et al.* (1984)
[5]Licko and Danek (1982)
[6]Stebbins *et al.* (1983)
[7]Calculated using bulk modulus of Levien and Prewitt (1981) and dK/dT of Bottinga (1985)
[8]Calculated from shock data on molten diopside and thermodynamic parameters to yield K_T at 1664K.
[9]Finger and Ohashi (1976), Skinner (1966)
[10]Bottinga *et al.* (1983)
[11]Richet and Bottinga (1984)
[12]Bottinga (1985)
[13]Rivers (1985)

Table 6: Data used to calculate high-pressure, high-temperature volumes of high pressure phases

Phase	K_T(300 K) GPa	dK/dP	dK/dT $GPaK^{-1}$	V(300 K) $m^3mole^{-1}x10^{-6}$	α $K^{-1}x10^5$	$d\alpha/dT$ $K^{-2}x10^8$
$MgSiO_3$(pv)[a]	260[1]	4[2]	-0.027[3,4]	24.46[5]	2.5[6,7]	1.7[6,7]
$CaSiO_3$(pv)[a]	227[8]	4[2]	-0.027[3]	28.13[8]	3.2[7]	1.7[7]
Al_2O_3	252.7[9]	4.3[9]	-0.017[9]	25.58[9]	1.62[7]	1.1[7]
SiO_2(st)[b]	316[10]	4[10,11]	-0.035[12]	14.00[13]	1.71[14]	1.0[14]
$FeSiO_3$(pv)[a]	260[15]	4[2]	-0.027[15]	25.49[2]	2.5[15]	1.7[15]

[1] Yagi *et al.* (1982)
[2] Jeanloz and Thompson (1983)
[3] Jones (1979).
[4] Beattie and Samara (1971)
[5] Yagi *et al.* (1978).
[6] Knittle *et al.* (1986).
[7] Touloukian *et al.* (1970)
[8] Ringwood and Major (1971), Reid and Ringwood (1975), Liebermann *et al.* (1977)
[9] Hankey and Schuele (1970), Gieske and Barsch (1968)
[10] Weidner *et al.* (1982)
[11] Bass *et al.* (1981)
[12] Manghnani (1969), Wang and Simmons (1973), Chang and Graham (1975)
[13] Sinclair and Ringwood (1978)
[14] Ito *et al.* (1974)
[15] Assumed to be the same as $MgSiO_3$(pv)
[a] perovskite structure
[b] stishovite

Table 7: Volume/oxygen of molten silicates and high-pressure phases at 1673 K

	1 atm			40 GPa		
Composition	$V_o^{m\ 1}$	$V_o^{dp\ 2}$	V_o^m/V_o^{dp}	V_o^m	V_o^{dp}	V_o^m/V_o^{dp}
	$m^3mole^{-1}x10^{-6}$			$m^3mole^{-1}x10^{-6}$		
$CaMgSi_2O_6$	13.73	9.28	1.48	8.86	8.02	1.10
$Di_{0.64}An_{0.36}$	13.63	9.10	1.50	8.28	7.89	1.05
$CaAl_2Si_2O_8$	13.51	8.86	1.53	7.90[3]	7.71	1.03
	13.51	8.86	1.53	7.67[4]	7.71	0.99

[1] Volume per mole of oxygens in the melt

[2] Volume per mole of oxygens in a densely packed solid

[3] Calculated using K, K′ from 5 point fit to shock data

[4] Calculated using K, K′ from fit to full data set

Table 8: Parameters used to constrain K′ for various molten silicates assuming V_o^{dp}/V_o^m (40 GPa) ~ 1.1

Composition	K[1] GPa	V_o^m (1 atm)[2,3] $m^3mole^{-1}x10^{-6}$	V_o^{dp} (40 GPa)[4] $m^3mole^{-1}x10^{-6}$	V_o^m (40 GPa) $m^3mole^{-1}x10^{-6}$	K′ [5]
Fe_2SiO_4	20.5	13.53	8.48	9.33	11
Mg_2SiO_4	24.9	12.67	8.02	8.82	9.6
$MgSiO_3$	21.8	12.90	7.49	8.24	6.6
$FeSiO_3$	17.6	13.47	7.80	8.58	8
$CaMgSi_2O_6$	23.8	13.73	8.02	8.82	6.2
$An_{0.36}Di_{0.64}$	22.3	13.63	7.89	8.68	6.3
$CaAl_2Si_2O_8$	20.5	13.51	7.70	8.47	6.3

[1] Calculated using coefficients of Rivers (1985) at 1673 K

[2] Stebbins *et al.* (1984)

[3] Volume per mole of oxygens in melt

[4] Volume per mole of oxygens in densely packed solid

[5] value to give V_o^m/V_o^{cp} (40 GPa) ~1.1

FIGURE CAPTIONS:

Figure 1: Shock wave data for molten diopside (T_0 = 1773 K, ρ_0 = 2.613 Mg m^{-3}) in the shock velocity-particle velocity plane. Best straight-line fit to the data are given by $U_S = 3.30 + 1.44\ U_P$ km sec^{-1}, $r^2 = 0.99$. The solid circle at $U_P = 0$ is the measured ultrasonic velocity at 1 atm and 1758 K (Rivers, 1985).

Figure 2: Shock wave data for molten anorthite (T_0 = 1923 K, ρ_0 = 2.545 Mg m^{-3}) shown in the shock velocity-particle velocity plane. The solid line is a straight line fit to the five lowest velocity data and is given by $U_S = 2.68 + 1.42\ U_P$ km^{-1}; $r^2 = 0.99$. The dot-dash straight line fit which includes all six data is given by $U_S = 2.85 + 1.27$ U_P km sec^{-1}, $r^2 = 0.98$. The solid circle at $U_P = 0$ is the measured ultrasonic velocity at 1 atm and 1833 K (Rivers, 1985).

Figure 3: Shock wave data for molten diopside (T_0 = 1773 K) in the pressure-density plane. The heavy solid line is the best fit to the data and the dashed line is the best-fit Birch-Murnaghan isentrope with K_S = 22.4 GPa, K' = 6.9. Also shown are data for crystalline diopside. Solid circles are from Svendsen and Ahrens (1983) and crosses are from Ahrens *et al.* (1966).

Figure 4: Shock wave data for molten anorthite (T_0 = 1923 K) in the pressure-density plane. The heavy solid line is the best-fit to the five lowest pressure data and the dashed line is the best fit a Birch-Murnaghan isentrope with K_S = 17.9 GPa, K' = 5.3. The best fit Hugoniot to the complete data set is given by the dash-dot line; the accompanying isentrope has K_S = 22.0 GPa, K' = 4.1. Also shown are shock wave data for anorthite glass (crosses: Boslough *et al.*, 1986) and anorthsite (open circles: McQueen *et al.*, 1967).

Figure 5: Calculation of the fusion curve of diopside. The heavy curve labelled W-K is from experimental determinations of Williams and Kennedy (1969). Heat capacity and liquid volumes used in the calculations are from Rivers (1985) and Stebbins *et al.* (1984) and the thermal expansion of the melt is from Dane (1941) and Licko and Danek (1982) unless otherwise specified. All input data are listed in Table 5.

a) Effect of different initial liquid volumes ($V_{L\&D}$: Licko and Danek, 1982; V_S: Stebbins *et al.*, 1984; V_D: Dane, 1941).

b) Effect of different heat capacity functions (ΔC_{PB}: Bottinga, 1985; ΔC_{PR}: Rivers, 1985).

c) Result of changing thermal expansion of molten diopside (B–α: Bottinga *et al.*, 1983; S–α: Stebbins *et al.*, 1984; (D,L&D-α: Dane, 1941; Licko and Danek, 1982). The curve labelled $\Delta\alpha = 0$ is calculated assuming that the thermal expansions of molten and crystalline diopside are the same; it is expected that this is a good approximation at high pressures.

d) Calculation assumes a thermal expansion that changes as a function of pressure as described in the text. Experimental data (open symbols are above the liquidus; closed symbols are below the liquidus) are also shown; circles: Boyd and England (1963), squares: Boettcher *et al.* (1982), Williams and Kennedy (1969), W–K_C: data of Williams and Kennedy (1969) corrected for effect of pressure on thermocouple emf.

Figure 6: Variation of normalized volume (V/V_0: ratio of volume at high pressure to that at 1 atm) of molten anorthite, diopside and $An_{0.36}Di_{0.64}$ with pressure along 1673 K isotherms calculated from our shock wave data. The volume, and hence compressibility of $An_{0.36}Di_{0.64}$, is intermediate between anorthite and diopside.

Figure 7: Percent deviation of measured volume of $An_{0.36}Di_{0.64}$ (from shock wave data; Rigden *et al.,* 1986) from volume calculated as an ideal mixture of molten anorthite and diopside (this work) at 1673 K as a function of pressure. At 40 GPa the deviation is $\sim 2\%$ and is $< 1\%$ below 20 GPa.

Figure 8: Variation of the change in partial molar volume/oxygen with pressure $\left\{\frac{\partial V_i^m}{\partial P}, \text{Rivers, 1985}\right\}$ for silicate melts with partial molar volume of oxide components ($\overline{V}_{O,i}^m$). Below $\overline{V}_{O,i}^m \sim 30\ m^3mole^{-1} \times 10^{-6}$, $\left\{\frac{\partial V_i^m}{\partial P}\right\}$ is essentially independent of $\overline{V}_{O,i}^m$. Above this value it increases in a regular fashion. This suggests that

oxygen-oxygen interactions dominate the compressibility of the melt for small cations and it is only when the cations increase beyond a certain size that they begin to play a part in the compressibility. This is strikingly illustrated for the alkali oxides.

Figure 9: Illustration of effect of different K' for melts with identical K and V. A higher value of K' leads to less compression. Melt A has a lower proportion of Al and Si than melt B. Both melts attain a volume approximately 10% greater than that of a high-pressure phase mixture at $\sim$ 40 GPa. The magnitude of K' for materials with similar K is believed to be related to the potential for compression as reflected in the relative proportions of tetrahedral Al^{3+} and Si^{4+} in the melt structure at low pressures.

Figure 10: Variation of the ratio of partial molar volume in silicate melt and volume of densely packed oxide ($\overline{V}_i^m/V_i^{oxide}$) with V_i^{oxide} at 1673 K and 1 atm. Except for those cations believed to be dominantly in tetrahedral coordination in melts at low pressures (Fe^{3+}, Al^{3+} and Si^{4+}), $\overline{V}_i^m/V_i^{oxide}$ is similar over a wide range of volume, suggesting a roughly close-packed arrangement. The stippled region shows a $\pm 10\%$ variation about $\overline{V}_i^m/V_I^{oxide} = 1.0$.

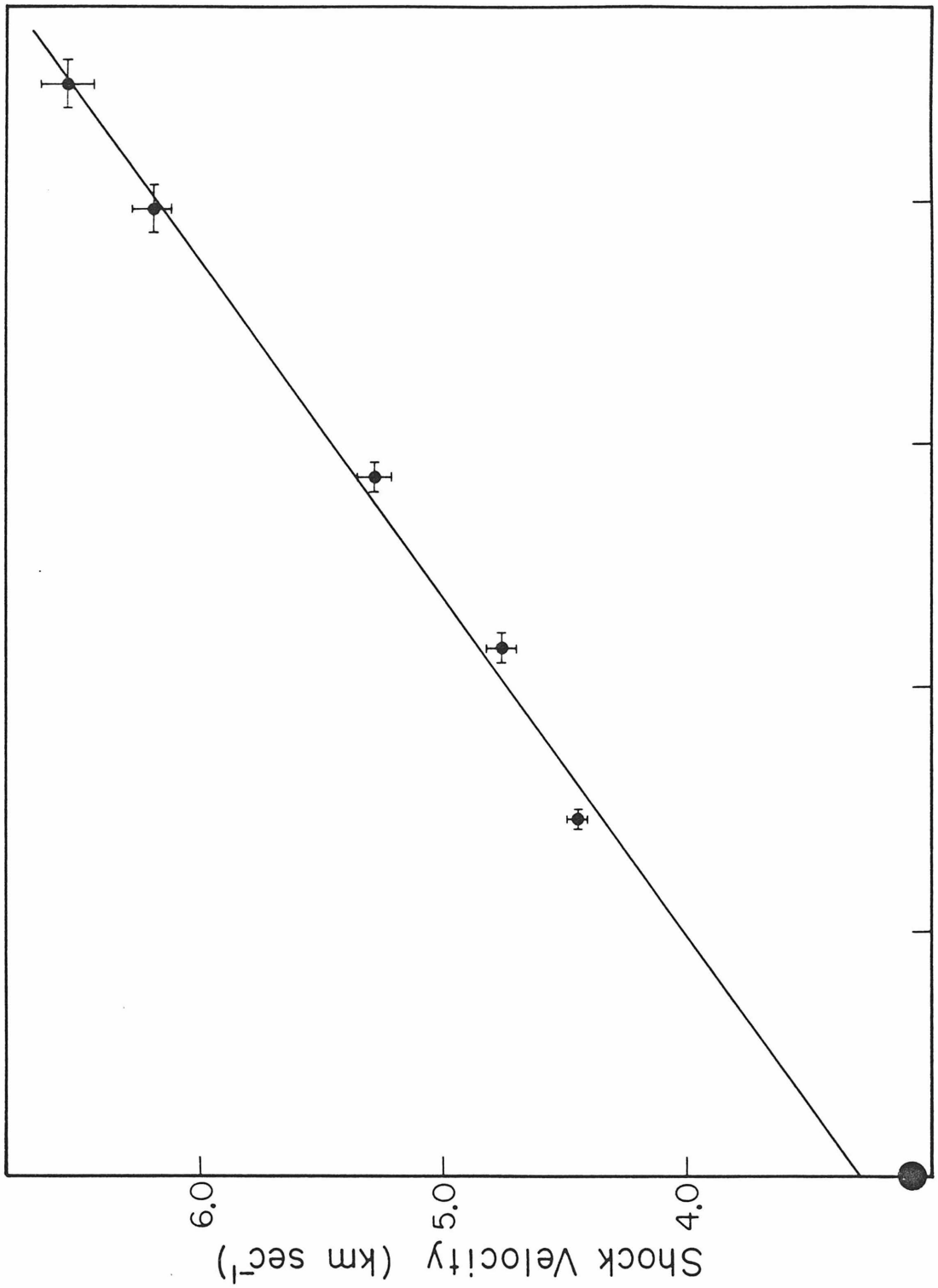
Shock Velocity (km sec⁻¹)
6.0
5.0
4.0
0.5
1.0
1.5
2.0
Particle Velocity (km sec⁻¹)

Figure 1

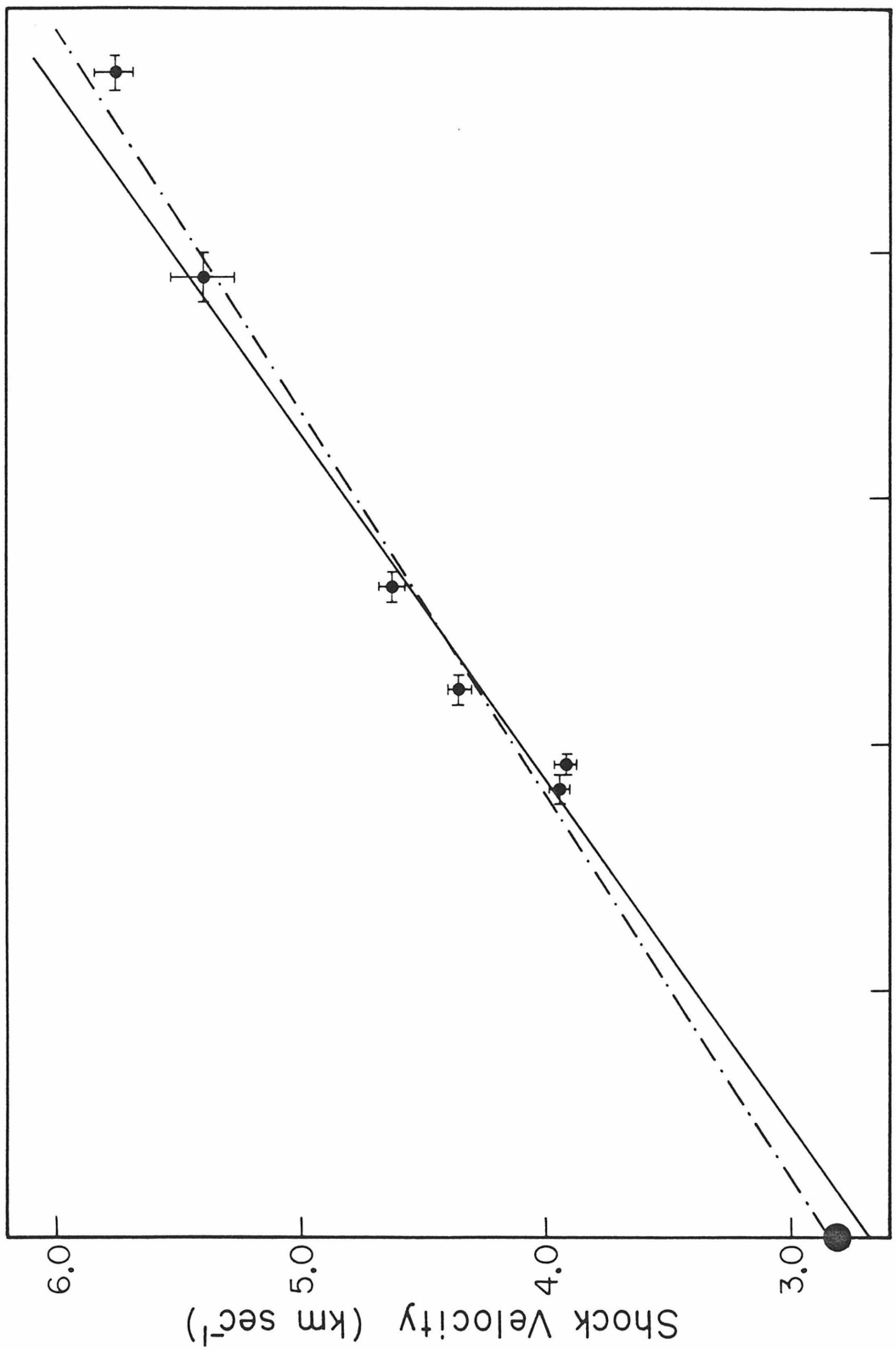
Shock Velocity (km sec^{-1})
6.0
5.0
4.0
3.0
0.5
1.0
1.5
2.0
2.5
Particle Velocity (km sec^{-1})

Figure 2

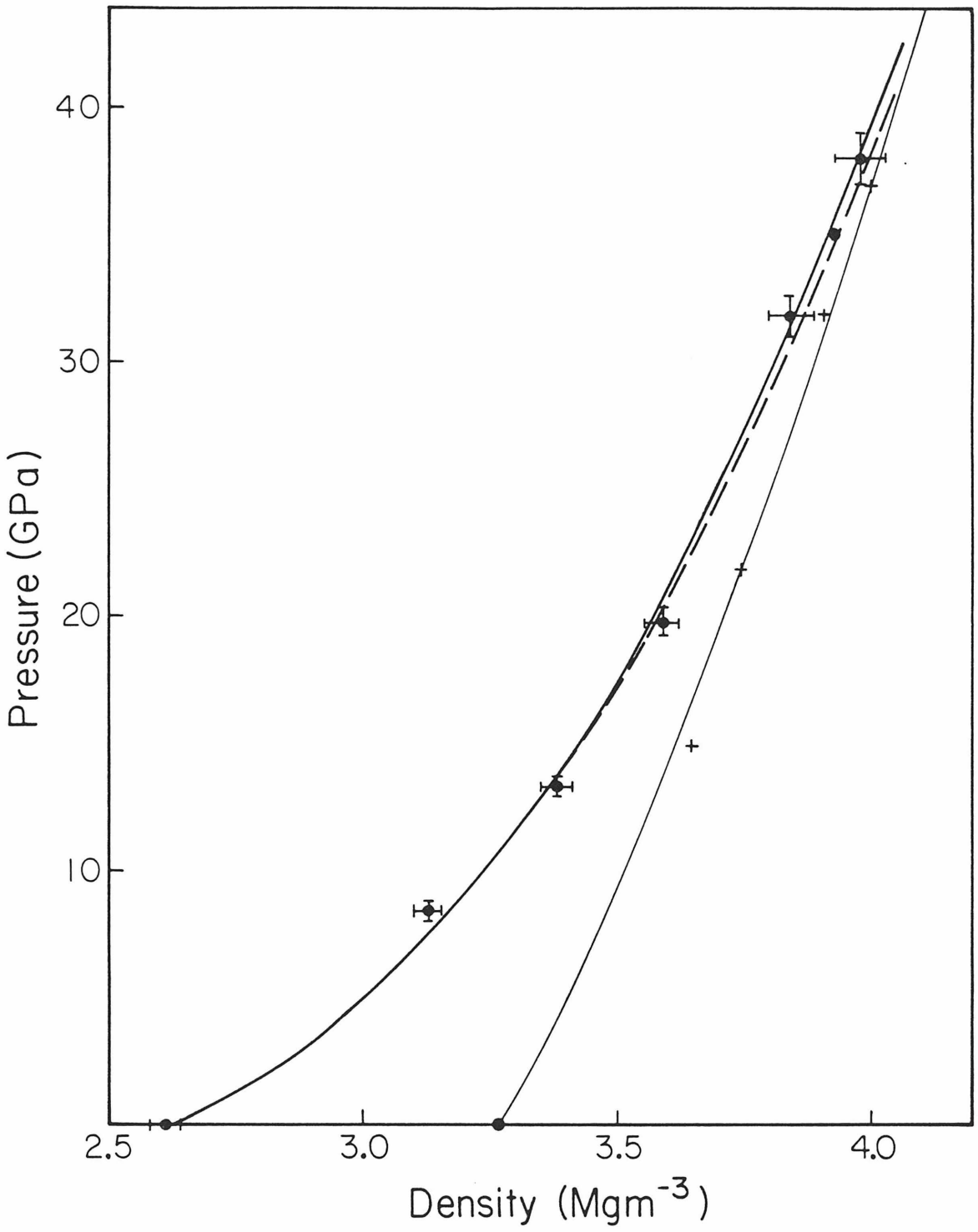

Figure 3

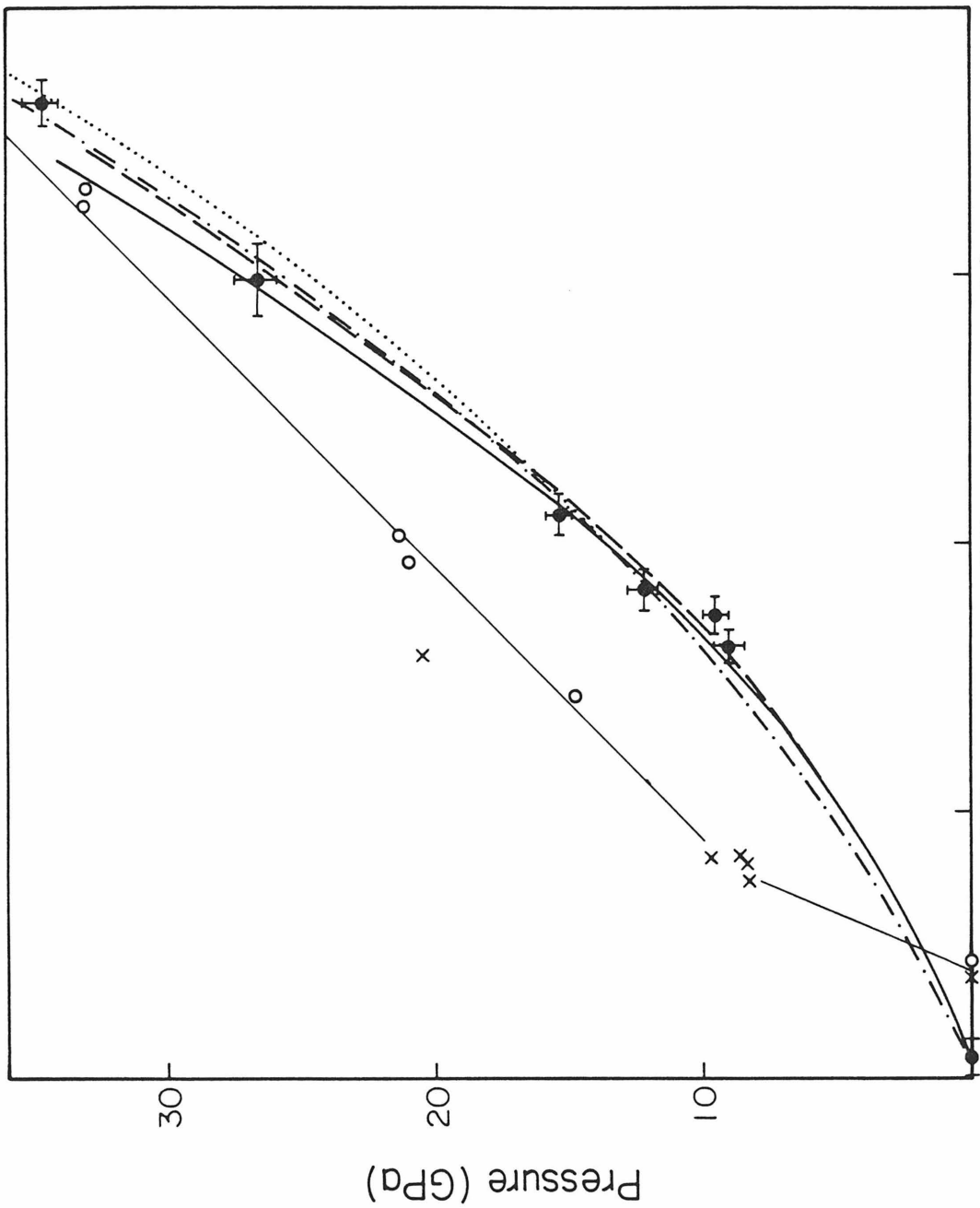

Figure 4

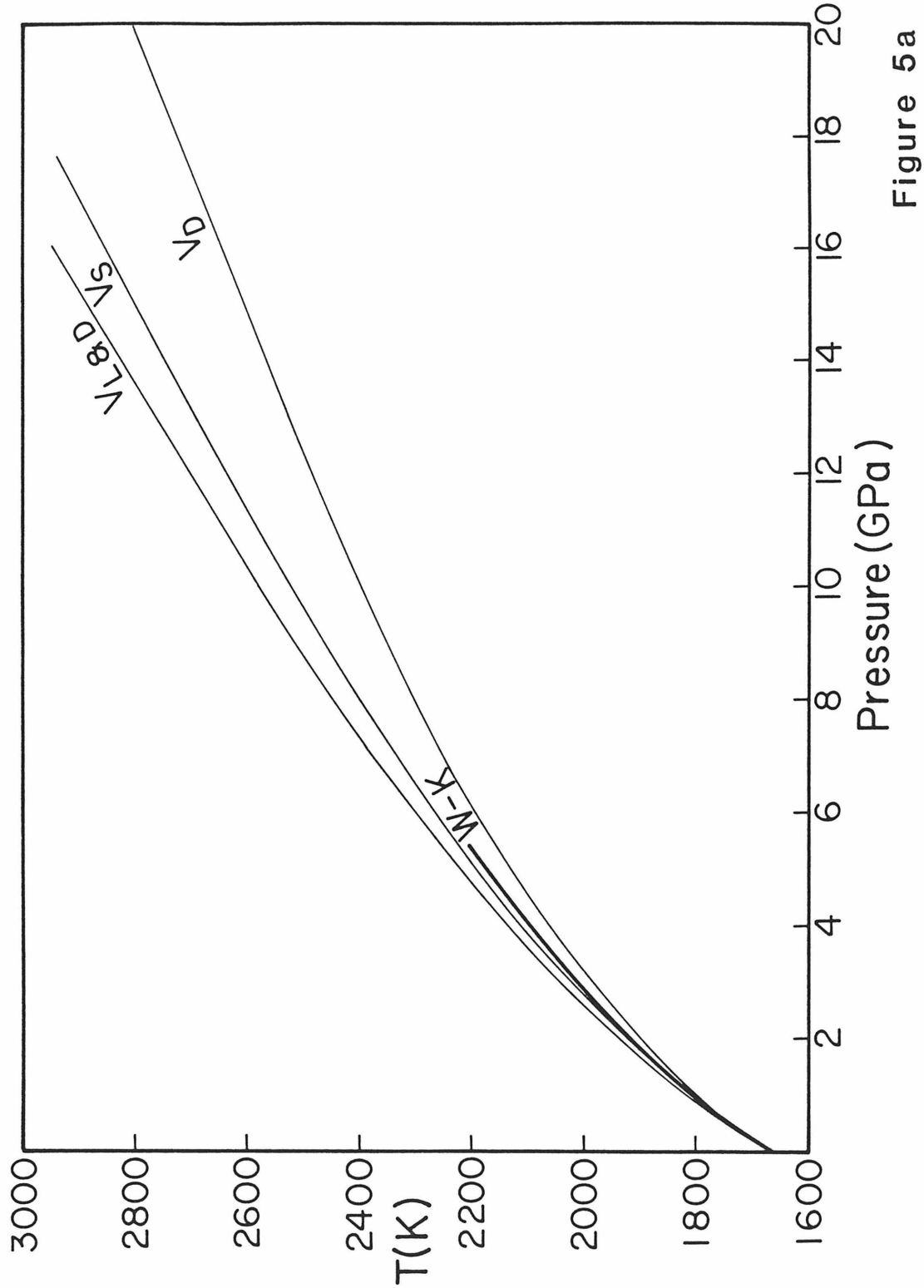
3000
2800
2600
2400
2200
2000
1800
1600
T(K)
2
4
6
8
10
12
14
16
18
20
Pressure (GPa)
W-K
V1.8D Vs
VD

Figure 5a

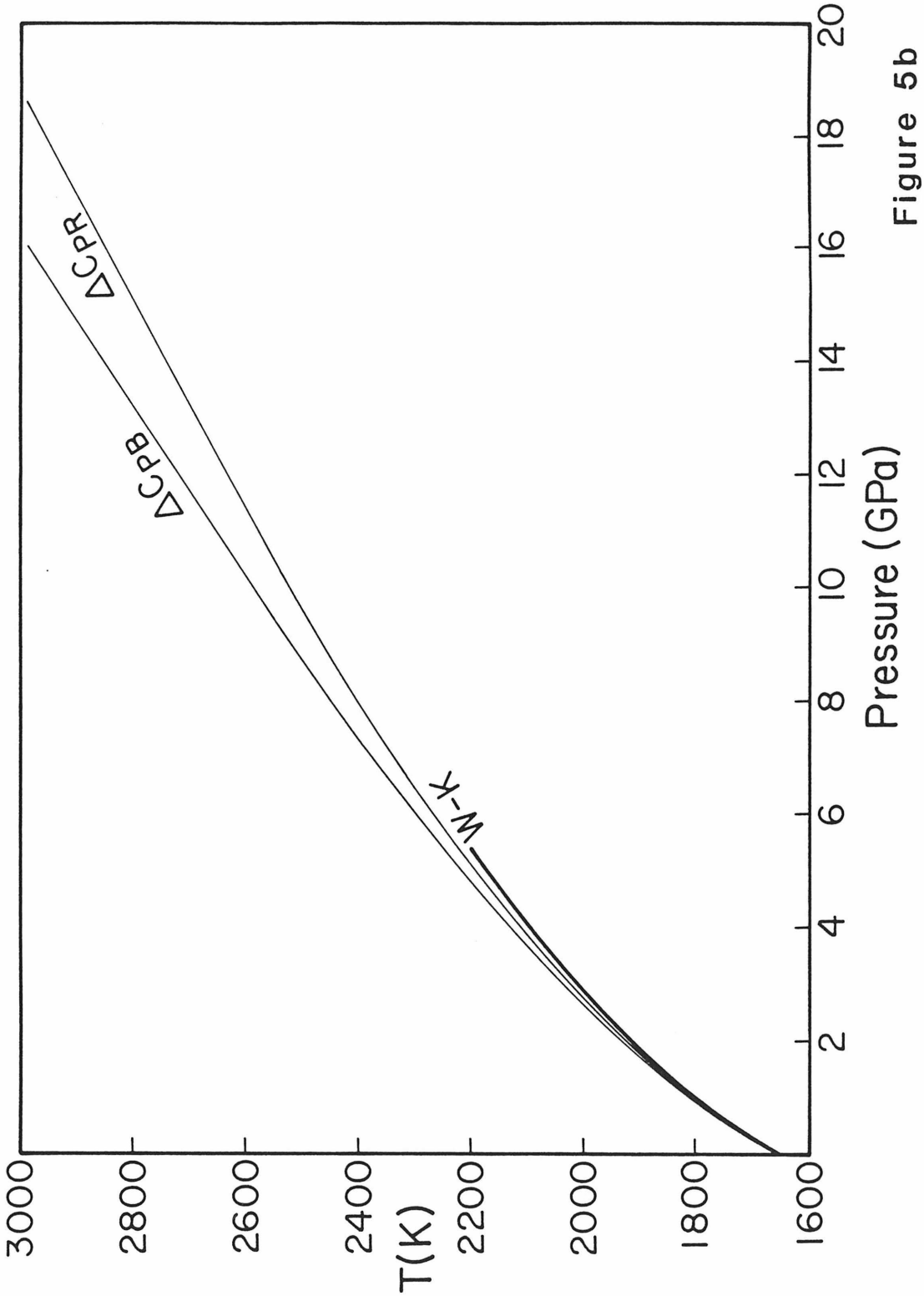
3000
2800
2600
2400
2200
2000
1800
1600
T(K)
2
4
6
8
10
12
14
16
18
20
Pressure (GPa)
ΔCpR
ΔCpB
W-K

Figure 5b

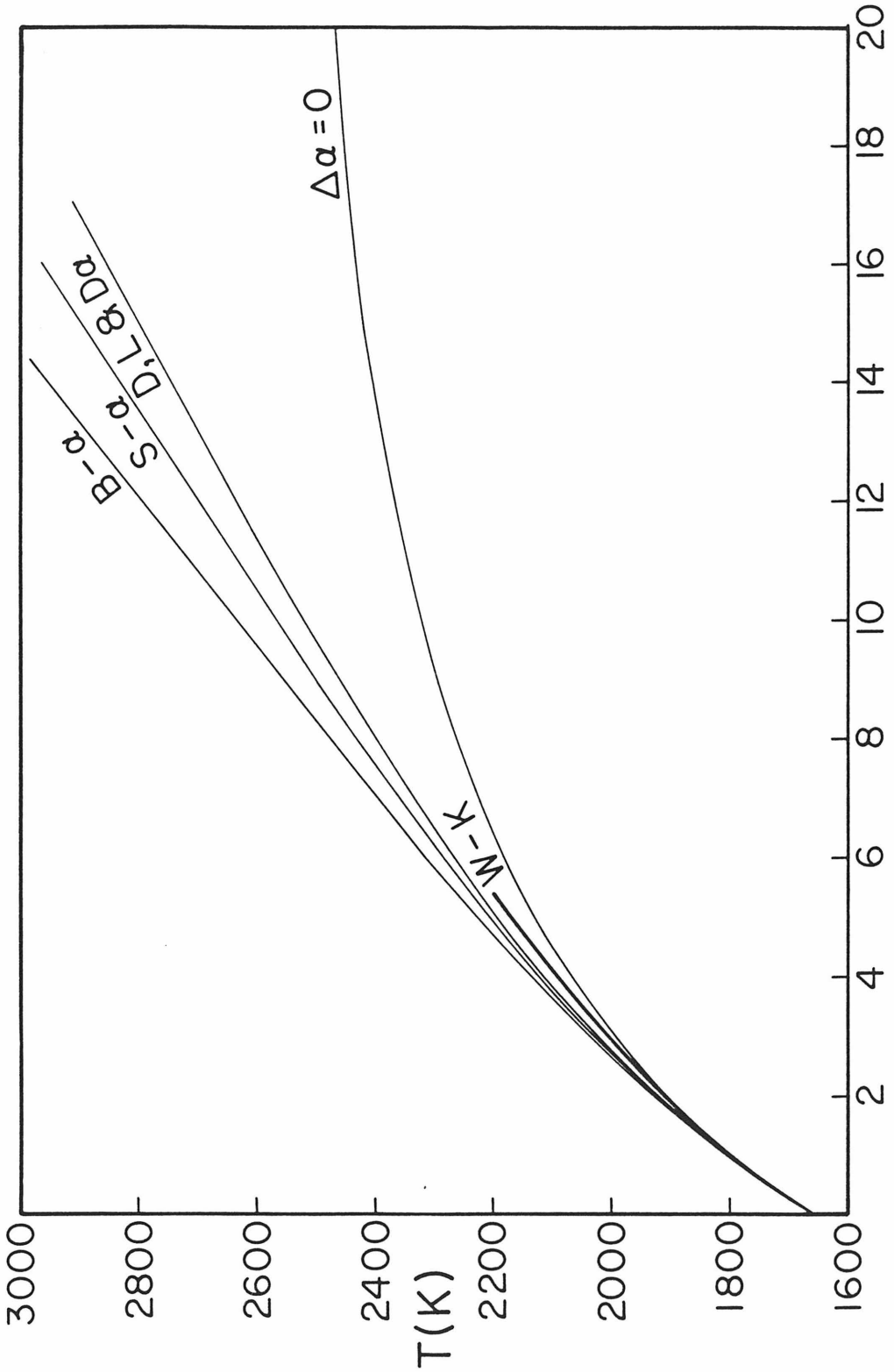
3000
2800
2600
2400
2200
2000
1800
1600
T(K)
2
4
6
8
10
12
14
16
18
20
Pressure(GPa)
B-a
S-a'D'1.8Da
Δα=0
W-K

Figure 5c

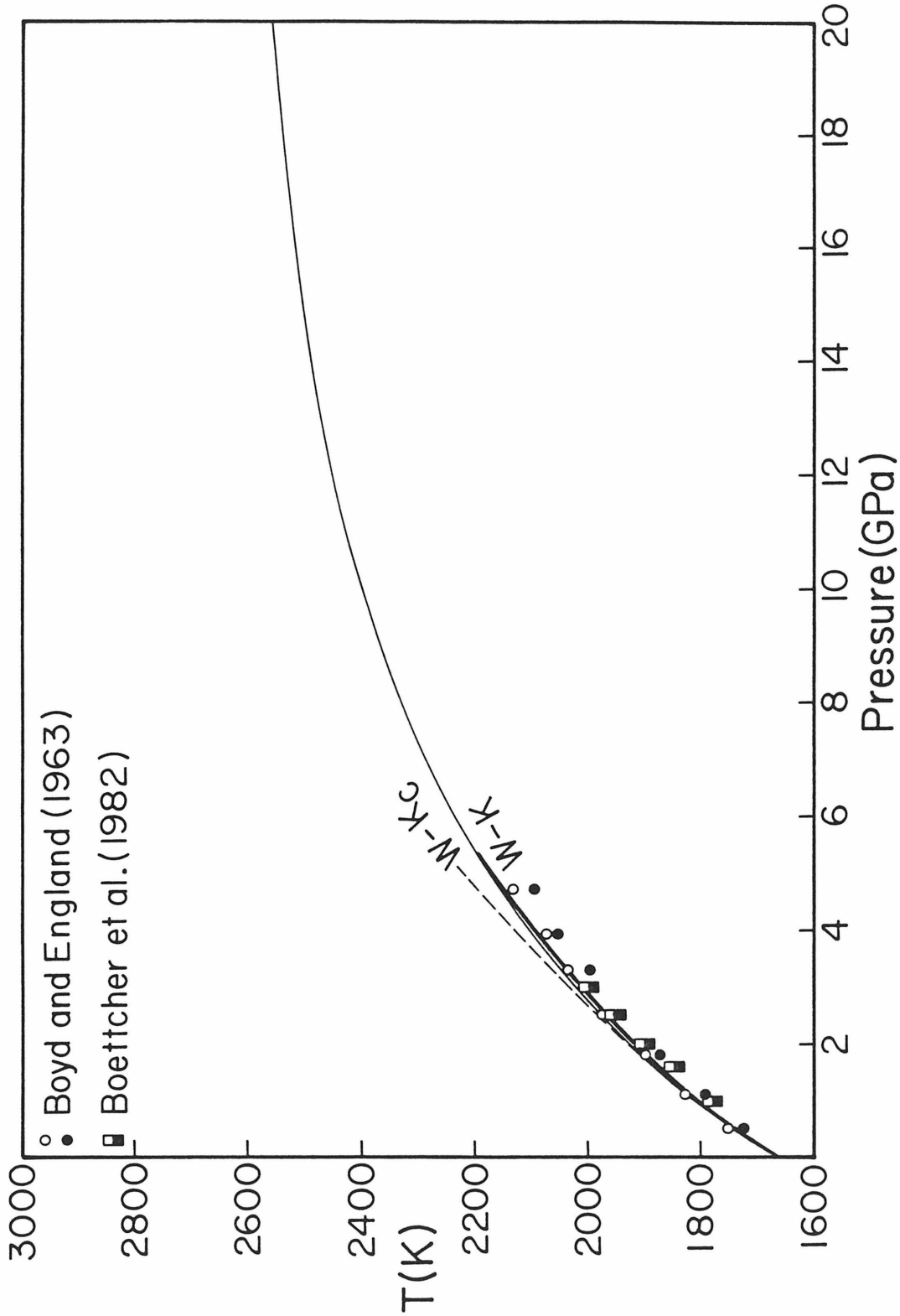
Boyd and England (1963)
Boettcher et al. (1982)
W-K
W-Kc
T(K)
Pressure(GPa)
3000
2800
2600
2400
2200
2000
1800
1600
2
4
6
8
10
12
14
16
18
20

Figure 5d

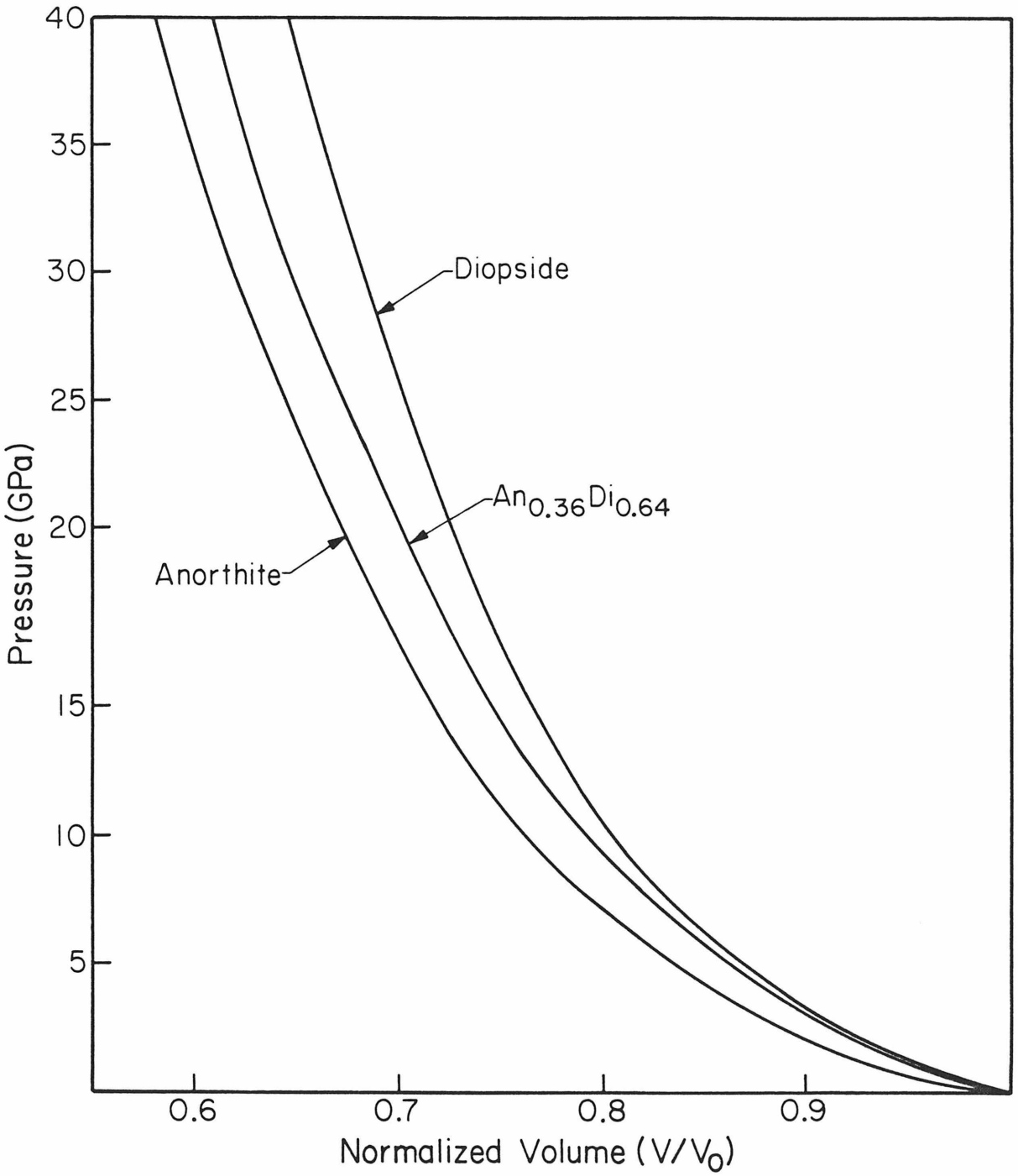
40
35
30
25
20
15
10
5
Pressure (GPa)
Diopside
$An_{0.36}Di_{0.64}$
Anorthite
0.6
0.7
0.8
0.9
Normalized Volume (V/V_0)

Figure 6

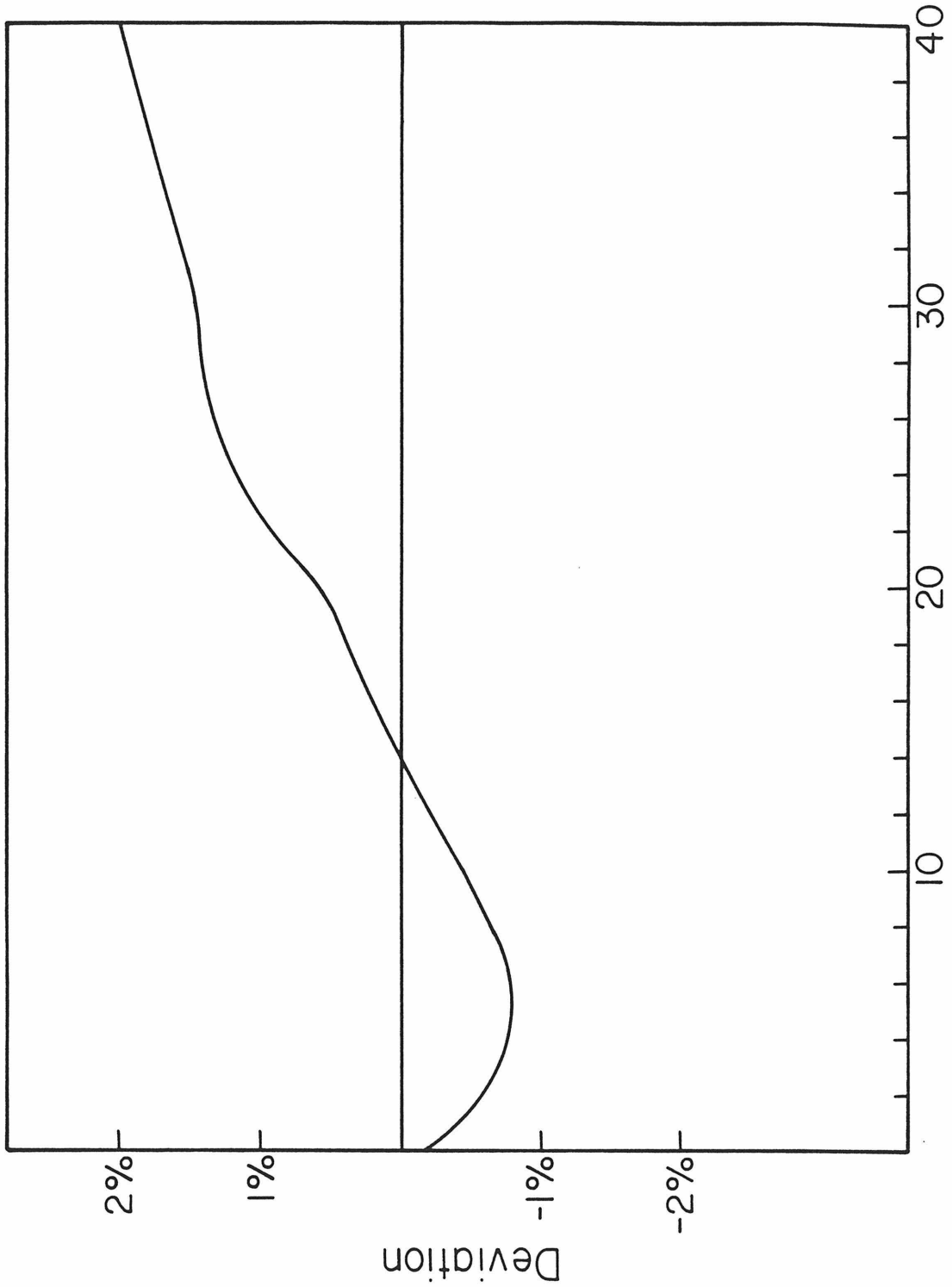

Figure 7

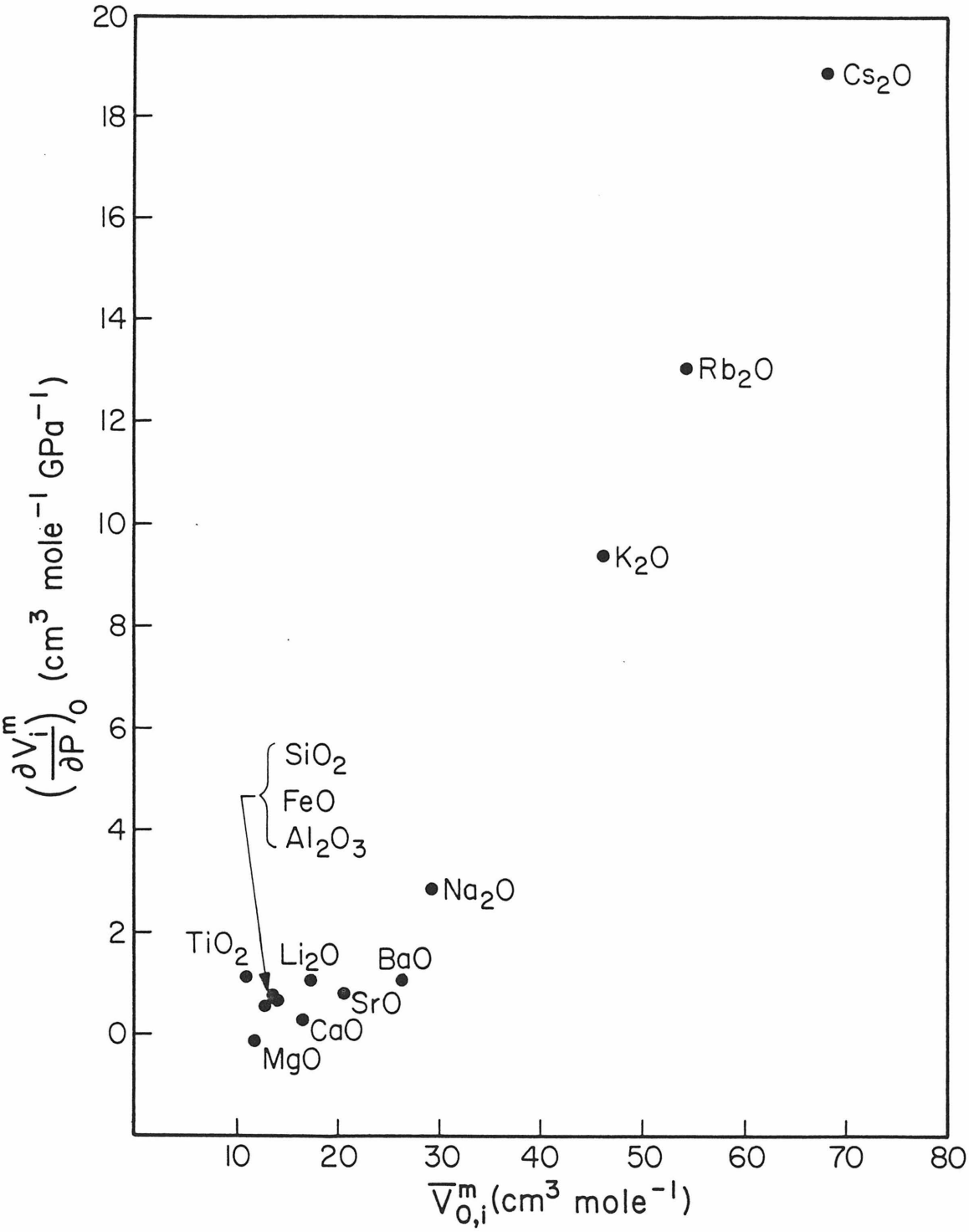
20
18
16
14
12
10
8
6
4
2
0
10
20
30
40
50
60
70
80
$\left(\frac{\partial V_i^m}{\partial P}\right)_o$ (cm^3 mole^{-1} GPa^{-1})
$\overline{V}^m_{o,i}$(cm^3 mole^{-1})
Cs_2O
Rb_2O
K_2O
Na_2O
SiO_2
FeO
Al_2O_3
TiO_2
Li_2O
BaO
SrO
CaO
MgO

Figure 8

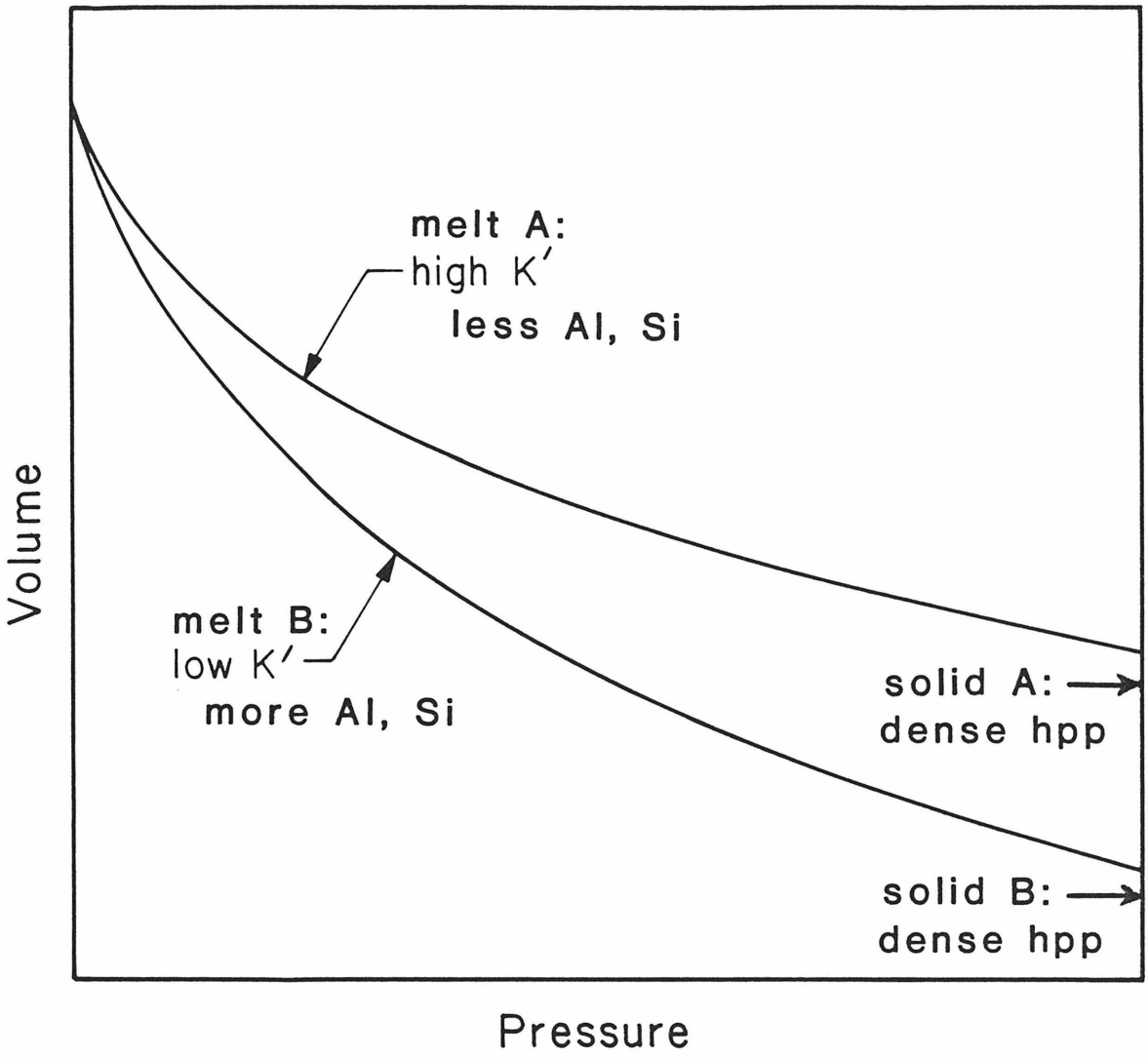
melt A:
high K′
less Al, Si
melt B:
low K′
more Al, Si
solid A:
dense hpp
solid B:
dense hpp
Volume
Pressure

Figure 9

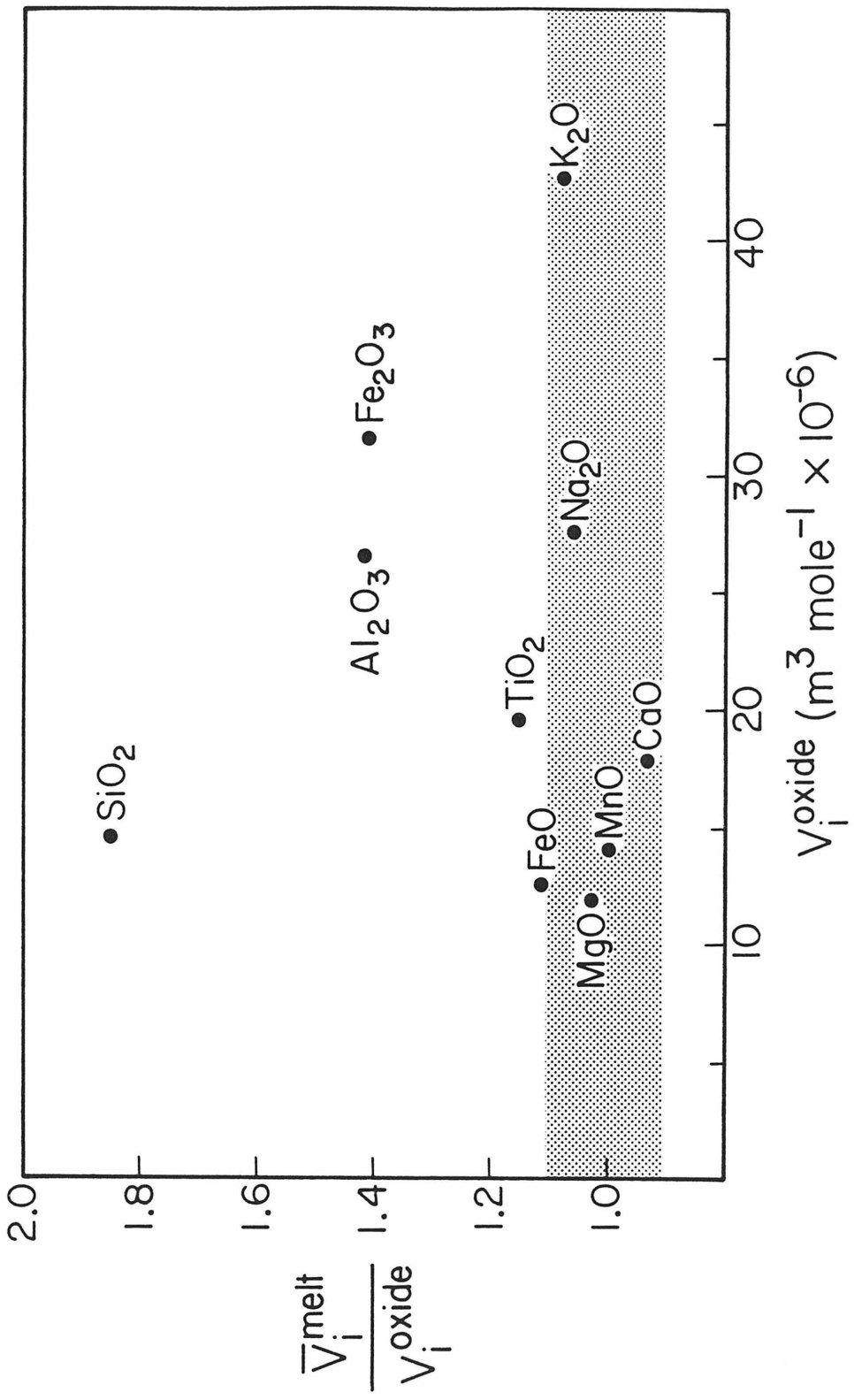
2.0
1.8
1.6
1.4
1.2
1.0
$\frac{\bar{V}_i^{melt}}{V_i^{oxide}}$
10
20
30
40
V_i^{oxide} (m^3 $mole^{-1}$ $\times 10^{-6}$)
SiO_2
Al_2O_3
Fe_2O_3
TiO_2
FeO
MgO
MnO
CaO
Na_2O
K_2O

Figure 10